PROPERTIES OF ROMAN BRICKS AND MORTARS USED IN SERAPIS TEMPLE IN BERGAMA

A Thesis Submitted to
the Graduate School of Engineering and Sciences of
İzmir Institute of Technology
in Partial Fulfillment of the Requirements for the Degree of

MASTER OF SCIENCE

in Architectural Restoration

by
Özlem ASLAN ÖZKAYA

July 2005
İZMİR

We approve the thesis of **Özlem ASLAN ÖZKAYA**

Date of Signature

---------- **22 July 2005**

Assoc. Prof. Dr. Hasan BÖKE
Supervisor
Department of Architectural Restoration
İzmir Institute of Technology

---------- **22 July 2005**

Assoc. Prof. Dr. Başak İPEKOĞLU
Co- Supervisor
Department of Architectural Restoration
İzmir Institute of Technology

---------- **22 July 2005**

Assist. Prof. Dr. S. Sarp TUNÇOKU
Department of Architectural Restoration
İzmir Institute of Technology

---------- **22 July 2005**

Assist. Prof. Dr. Engin AKTAŞ
Department of Civil Engineering
İzmir Institute of Technology

---------- **22 July 2005**

Assoc. Prof. Dr. Başak İPEKOĞLU
Head of Department of Architectural Restoration
İzmir Institute of Technology

Assoc. Prof. Dr. Semahat ÖZDEMİR
Head of the Graduate School of Engineering and Sciences

ACKNOWLEDGEMENTS

I would like to express my gratitude to Assoc. Prof. Dr. Hasan Böke and Assoc. Prof. Dr. Başak İpekoğlu for their supervision, guidance and care throughout this study.

Moreover, I am much indebted to Assoc. Prof. Dr. Hasan Böke for his helps during the collecting samples and carrying out the experimental study in the Material Conservation Laboratory.

My deepest thanks are due to my dear friends, Res. Assist. Elif Uğurlu and Res. Assist. Kerem Şerifaki for their friendship and helps in the Material Conservation Laboratory during this study.

I am also grateful to my friends, Işıl Talu and Sevinç Çulcu for her friendship and moral support.

Special thanks are due to staff of the Centre for Materials Research of the Institute for the XRD, SEM and mechanical analyses.

Finally, I am indebted to my family and my husband for their support and patience and tolerance during this study.

ABSTRACT

Serapis Temple, which was constructed in the Roman Period and reached our present time, is one of the most important monuments of the world heritage. We must hand over this monument to next generations. This requires the identification of the characteristics of original construction materials and their deterioration problems for preventive measures.

In this study, characteristics of bricks, mortars and plasters used in the Serapis Temple have been determined in order to have the necessary information of the characteristics of the intervention materials, which will be used in the conservation works of the temple. For this purpose, Roman, Byzantine and intervention bricks, mortars and plasters were collected for the laboratory analysis.

Several analyses were carried out to understand their basic physical properties, microstructural features, and mineralogical and chemical compositions.

Experimental results of the study indicated that Roman and intervention bricks are low dense and high porous. Raw materials used in their manufacturing were calcium poor clays and their firing temperatures did not exceed 900ºC.

Roman and Byzantine mortars and plasters are stiff, compact, low dense and high porous materials. They have high compressive strength values. But, intervention mortars are not stiff and compact and they have very low compressive strength.

The mortars used during the late restoration works (1940) were manufactured by using lime and cement. Due to the use of cement, they contain a high amount of soluble salts compared to the Roman and Byzantine ones.

The results of this study indicated that intervention materials should be compatible with the original materials and they will not give any damage to the original ones. This requires knowing about both the composition and physical properties of original materials as well as the problems of deterioration.

ÖZET

Roma döneminde Bergama'da inşa edilmiş olan Serapis Tapınağı (Kızıl Avlu) günümüze kadar ulaşmış önemli dünya kültür varlıklarındandır. Tapınağın korunarak gelecek kuşaklara aktarılması ancak, yapıyı oluşturan malzemelerin bozulmasına yol açan kaynakların kontrol altına alınması ve özgün malzemelerinin özelliklerinin bilinerek, koruma çalışmalarında bunlarla uyumlu çalışacak malzemelerin kullanılması ile mümkün olabilir.

Bu çalışmada, Serapis Tapınağı'nın inşasında ve sonraki dönem eklerinde kullanılan tuğlaların, harçların ve sıvaların özellikleri o dönemlerin malzeme teknolojisini belirleme amacına yönelik olarak incelenmiştir.

Bu kapsamda, toplanan tuğla, harç ve sıvaların; temel fiziksel ve mekanik özellikleri, ham madde kompozisyonları, puzolanik aktiviteleri, mineralojik, kimyasal ve hidrolik özellikleri laboratuvar analizleri ile belirlenmiştir.

Yapıda kullanılan tuğlaların; düşük yoğunluklara ve gözenekli bir yapıya sahip oldukları, üretimlerinde ham madde olarak, düşük miktarlarda kalsiyum içeren kil kullanıldığı ve pişirilme sıcaklıklarının 900 ºC'yi geçmediğini tespit edilmiştir.

Roma ve Bizans dönemi harç ve sıvaları yüksek basınç dayanımlarına sahip, düşük yoğunlukta ve gözenekli malzemelerdir. Buna karşılık, 1940'lı yıllardaki onarımlarda kullanılan harçlar mekanik özelliklerini tamamen yitirmiştir.

Roma ve Bizans dönemi harçları hidrolik özelliğe sahiptir. Harçlarda, aynı mineralojik ve kimyasal özelliklere sahip doğal puzolanik agregalar kullanılmıştır. Bizans harçlarında, doğal pozzolanların yanısıra, puzolanik tuğla kırıkları da kullanılmıştır. Bizans dönemi harçlarında, neden pozzolanik tuğla kırıkları, doğal pozzolanlarla birlikte kullanıldığı açıklanamamasına rağmen, bu kullanım, Bizans harçlarının Roma harçlarından ayırt edilmesini sağlamaktadır.

1940'lı yıllarda yapılan restorasyon çalışmalarında kullanılan harçlar, kireç ve çimento kullanılarak üretilmiştir. Çimento kullanımı nedeniyle bu harçlar mekanik özelliklerini yitirmişlerdir.

Bu çalışmanın sonucu, onarım malzemelerinin özgün malzemelerle uyumlu ve özgün malzemeye zarar vermeyecek özellikteki malzemelerden seçilmesi gerektiğini göstermiştir.

TABLE OF CONTENTS

LIST OF FIGURES

Figure **Page**

LIST OF TABLES

CHAPTER 1

INTRODUCTION

1.1. Subject and Aim of the Study

The statement in the Venice Charter dated 1964 "…*People are becoming more and more conscious of the unity of human values and regard ancient monuments as a common heritage. The common responsibility to safeguard them for future generations is recognized. It is our duty to hand them on in the full richness of their authenticity...*" stresses that the original characteristics of historical buildings can only be preserved through the protection of their original materials.

This requires the identification of the characteristics of the historical construction materials and the problems of deterioration they are in. Use of wrong materials in the restoration of historical buildings leads to rapid deterioration in the whole building and its construction elements, causing lost of their historical, documental and esthetical values. The materials used in restorations are mostly selected without carrying out a research and without determining what problems those materials may cause in the short and long-term.

The most important thing to be considered in the conservation works of the historical buildings is that intervention materials that should be compatible with the original material and which will not give them any damage in the long-term should be selected. This requires knowing about both the composition and physical properties of original materials as well as the problems of deterioration.

In this study, the properties of the Roman bricks and mortars used at the Serapis Temple, located in Bergama, have been examined. Both the monumental characteristics and its original building materials that have been mostly preserved had an effective role in choosing the Roman Period structure, Serapis Temple. This structure was also an important example in the view of comparison of the materials used in the Byzantine and Roman Period while converting the temple into a church. The degree of compatibility of

bricks and mortars used in the restoration of the temple, in the 1940s, in conserving the monument with the original ones, made the choice of this temple more important.

The objective of this study is to determine:

The main characteristics of original and repair materials used in the past and the characteristics of the materials that will be used in the future restoration works.

1.2. Limits of the Study

This study started by collecting sample materials used in the temple in different periods in order to determine the properties of them through laboratory analyses.

After reading the written documents and performing a visual examination of the monument, the places where the samples would be obtained, were determined and samples were collected where reached. The samples which had enough size to characterize the properties of the materials used in the temple were collected from the parts where insignificant deteriorations were observed.

In order to give as little damage to the monument as possible a limited number of samples were collected. Although, the study was carried out on limited samples, similar results were obtained from the same period samples collected from different parts. In this respect, it is possible to say that the samples used in this study represent the original materials as used in the temple.

1.3. Method of the Study

The method used in this study consists of recognizing the structure of the temple, collecting the samples and experimental studies. Firstly, the written documents were examined, necessary observations were made and the structure was documented by the photos. Secondly, collecting the samples were done after determining the places where the samples would be collected and collecting the samples would give the least damage to the temple.

Finally, the experimental studies contained the laboratory studies done to determine basic physical and mechanical properties, raw material compositions, pozzolanic activity, soluble salts, their mineralogical and chemical compositions, microstructural and hydraulic properties of the collected samples.

In conclusion, the results of the laboratory studies were evaluated, discussed and compared with the results of other studies done on some historic buildings of the Roman and Byzantine periods.

CHAPTER 2

ROMAN LIME MORTARS AND BRICKS

In this section the characteristics of bricks and lime mortars used in Roman buildings are defined.

2.1. Roman Lime Mortars

Mortars, plasters and bricks made from mud and straw were used in the construction of the first collective settlements. Mud is known to have been used as a binding material in the Mesopotamia 10,000 years ago (B.C). Mud mortars and plasters are produced through a mixture of clay, silt, sand, water and straw depending on the place of use. (Pearson 1992, Caron and Lynch 1988)

Another binding material which was used in the preparation of mortars is gypsum ($CaSO_4 \cdot 2H_2O$). Four thousand five hundred years ago from today, the Egyptians had constructed the pyramids by sliding the stone blocks weighing 2 - 45 tons on gypsum (Snell and Snell 2000). Gypsum is converted to hemihydrate ($CaSO_4 \cdot 0.5 H_2O$) by heating at approximate temperatures of 135 – 175 °C. This material, which converts to gypsum when mixed with water, had been used as a binder material.

The data on when lime ($Ca(OH)_2$) started to be first used in constructions is not so clear. However, lime is known to have been used by the Mayas, one of the oldest civilizations, as a construction material. From Ancient Greece, Roman and the succeeding periods to the discovery of cement, lime was the most basic and common binding material used in the construction of buildings (Cowper 1988). The written documents relating to the use of lime can be found in the Roman sources. The Romans had built their first concrete structures by using lime (Vitruvius 1960).

The raw material used in making lime is limestone. Limestones are consist of calcium carbonate ($CaCO_3$). Calcination temperatures of such stones are between 750-850 °C (Boynton 1980). In the calcination process, calcium carbonate converts to calcium oxide (Reaction 1). Their product is called as ‘quicklime’.

$$CaCO_3 + heat \rightarrow CaO + CO_2 \quad (1)$$

In the ancient times, the calcination of lime stones used to be done in kilns made of stone or bricks. Such kilns used to be burned after piles of wood and lime stone were put in them. Those kilns used to be left to cool after burning for a day or two, and then quicklime would be taken out from the lower part of the kiln. In spite of the fact that burning those kilns required ability and experience, criminals were generally used in running the lime kilns during the Roman period (Krumnache 2001).

Quicklime reacts with water and then converts to calcium hydroxide ($Ca(OH)_2$) (Reaction 2). This product is called 'lime'.

$$CaO + H_2O \rightarrow Ca(OH)_2 + Heat \quad (2)$$

Since the Roman and succeeding periods, it is known that lime has been used after having been left to rest for years without any contact with air. As the waiting period gets longer, its plastic quality increases (Cowper 1988; Rodriquez-Navarro et al. 1988). In the Roman Period, it was asserted that lime was to be used after waiting at least 3 years (Peter 1850). However, as a result of over-consumption of lime during the Augustan Period, this condition seemed to be ignored (Adam 1989). Recent analyses have shown that hydraulic lime was not used at all in the buildings of the Roman Period. This shows that pure limestones were preferred in the preparation of lime (Adam 1989).

The carbonation of lime is done with the carbon dioxide in the air (Reaction 3). As a result of this process, there seems to be an increase of 35 % in weight and 12 % rise in volume (Moorehead 1986).

$$Ca(OH)_2 + CO_2 \rightarrow CaCO_3 + H_2O \quad (3)$$

Lime mortars and plasters are produced by mixing lime and aggregates, which increases the ability to withstand pressure by preventing the formation of cracks in mortars and plasters. Aggregates also speed up the carbonation by leading to form porosity (Holmes and Wingate 1997). While preparing the lime, it was known that the Romans paid attention to the fact that the lime to be used was to be well-slaked, and that

the aggregates were to be clean and have flat sides (Peter 1850). Some Roman mortars used to be prepared by mixing lime and aggregates in a large bowl with a little amount of water using a wooden or iron stick to beat. During this beating process, lime and aggregates stick to each other better and the voids between the aggregates are filled with lime. This mixture is used after leaving it to rest for at least 3 years (Peter 1850).

Aggregates can be classified as materials that can react (pozzolan) and as materials that do not react with lime (inert) (Lea 1940). Inert aggregates are available in some stone mines, streams and seas whereas pozzolanic aggregates are materials made up of active silicates and aluminates which enable the mortars and plasters to harden under water through a reaction with lime. These materials can be studied in such groups as natural and artificial (Lea 1940).

Natural pozzolans are generally volcanic in origin (Lea 1940). The mortars used in some works of art of the ancient Greek Period are known to have been prepared using volcanic tuff brought from Santorini Island. Also, the mortars of many Roman Period structures were prepared with pozzolans brought from Pozzuoli near the Volcano Mt.Vesuvius. Of those structures, the most important are the Pantheon and Collesium in Rome (Cowan 1997).

On the other hand, baked materials, such as bricks and tiles were used as artificial pozzolan in the mortars and plasters of many Roman structures. Those mortars and plasters are hydraulic and were known as Cocciopesto in the Roman Period (Massazza and Pezzuoli 1981). The Romans used these types of mortars and plasters as a rendering exposed to severe environment conditions at a very humid ground level, usually in foundations, where the water table was high or used for thermal baths. These types of mortars were commonly used in structures such as cisterns, wells, aqueducts and baths of the Byzantium, Selcuk and Ottoman Periods because of their hydraulic properties (Akman et al. 1986, Böke et al. 1999, Güleç and Tulun 1996).

Near the end of the Roman Empire, brick-lime mortars were also used in the joints of the load-bearing facing walls. The thickness of the joints was increased together with the dimension of the aggregates containing crushed bricks. This type of mortar can be called conglomerate rather than mortar.

It is possible to present a summary of the mortar compositions used in the Roman Period as in Table 2.1 (Adam 1989).

Table 2. 1. The mortar compositions of the Roman Period

Binding Agent	Aggregate	Water
1 part of lime	3 parts of quarry sand	15 to 20%
1 part of lime	2 parts of river sand	15 to 20%
1 part of lime	2 parts of river sand and 1 part broken tile fragments	15 to 20%
1 part of lime	2 parts of pozzolana	15 to 20%

The features of the mortars used in the Roman structures have been examined in various studies. The mortars used in the foundation of Collesium were studied by Franco Massazza and Mario Pezzuoli (Massazza and Pezzuoli 1981). In that study, it was found that the aggregates containing leucitite had been used in the mortars, and that those aggregates were also used in road stone pavements in the Roman Period. It was found that the mortars had hydraulic characteristics because the aggregates - used as fine aggregates - contained pozzolanic properties. It was also put forward that the mortars were compact, and that the aggregates and lime bound well. As the samples were small in size, a series of hardness tests were done on mortars and their hardness were found to be 3-60 kg/cm^3.

The mortars used in Sagalassos, which was a Roman City, were studied in order to prepare new mortars for repair. The mortar samples were taken from the structures and water-related structures. Limestone, volcanic tuff and lava were generally used as aggregates in the mortars. On the other hand, crushed ceramics was used in the water-related structures. It was found that pure limestones mined from the environs of Sagalassos were used in making lime. In that study, it was asserted that lime was prepared using the dry slaking technique. Dry slaking is the technique, in which lime (CaO) is combined with a minimum amount of water necessary to alter all lime present in portlandite (Degryse et al. 2002). In the mortar samples taken from Tournai Cathedral, which belongs to the Roman Period, it was found that humid sand was mixed with quicklime using the dry slaking method, and that it had hydraulic qualities (Elsen et al. 2004).

When the mortars taken from the city walls of Pavia of the Roman Period were examined, it was seen that calcite aggregates had been commonly used. It was also

found that aggregates containing mica, biotite, and muscovite as well as calcite had been used in the construction of these walls (Riccard et al. 1998).

The Roman mortars used in Domitilla Catacombs (Spain) are known to have been prepared using volcanic dust and lime. In these mortars, the ratio of aggregate binder range from 0.5:1 to 1.1:1. Aggregate grain sizes are also variable, and the mortars have high porosity values (42%) (Sánchez-Moral et al. 2004)

In some of the mortars taken from the Roman structures excavated in the Negev Desert in Israel, it was found that they were formed using a mixture of lime and gypsum. Such studies revealed that wood ash was added into the lime as a pozzolan (Meir et al. 2005).

Some studies showed that the mortars used in the antique Roman baths, which were found in Ankara, were quite homogenous, and that aggregates containing quartz and plagioclase were used in their manufacturing process. In some mortars, it was seen that crushed brick pieces were also used as aggregate (Güleç and Tulun 1997).

2.2. Roman Bricks

In the production of bricks, natural raw material sources containing quartz, feldspar and clay are used. Of these raw materials, clays provide the plastic quality (gives the shape), feldspars reduce the melting temperature whereas quartz forms the porosity as a filling material. The bricks are produced through the processes of mixing the raw materials with water after being sifted, shaping, drying and baking. When the clays are baked at the temperatures of 450-900 °C based on their type, their crystal structures are collapsed and then turn to amorf structures made up of silicate and aluminate (He et al. 1995). At higher temperatures, some stable minerals such as mullite and kristobalite are formed (Lee et al. 1999).

The physical features of bricks made in the past seem to show differences from those used today depending on the preparation techniques and heating temperatures. Bricks in today's world are molded by means of vacuuming and they are heated at high temperatures homogenously. Hence, they have less porosity than those of the past and have greater mechanical properties.

Baked bricks were first used in Mesopotamia for a long time for water tight constructions, such as water troughs or pipes, or for more vulnerable parts of the

buildings, such as the frames of openings or the facings of large monuments (Adam, 1989). Greeks and Romans used the bricks much later as tiles and roof decorations for waterproof covering and as protection for the ends of the roof timbers.

Kilns for baking bricks were identical to those used for pottery except in size. The kiln can be circular or oblong and was partly located under the ground, which conserves heat and makes loading and unloading the material easier. The lower part is the combustion chamber. The heating chamber is covered by a brick vault with holes. The upper level is the charge chamber containing the bricks or tiles. In small-sized kiln, there is no loading door and the vault is constructed by raw materials of bricks which are destroyed when burning is complete. The top of the charge chamber is open to provide an air current for the fire.

The burning time depends on the size of the kiln, atmospheric conditions and the type of fuel used. The temperature in the charge chamber can be estimated as 800 °C near the internal shelf and 450 °C near the upper exit. Hence, the upper layer of bricks is usually discarded.

Another method of burning is burning in a stack, which requires piling up the baked bricks within one or several combustion chambers in which the fire is controlled directly.

Roman bricks were mostly longer and wider, but sometimes thinner than modern ones (Cowan, 1997). It is reported that brick sizes were up to 500 by 300 mm. Thickness ranged as low as 12mm, and thin bricks were easier to bake without warping or cracking. The bricks used for concrete works of art were frequently cut diagonally. This was called ‘opus testaceum’.

The most important Roman buildings constructed by brick were built in Rome. They are; Castra practoria, Domus Aurea, Internal masonry of Collesium, the major buildings of Trajan, whole townscape of Ostia (in the second century), The Pantheon, the Amphitheater Castrense (3th century), and the great building works of Diocleatin. This list is related to the city of Rome only.

2.3. The Serapis Temple

2.3.1. Historical Research

According to the data derived from the archeological excavations in the City of Pergamon (modern Bergama), it was found that the city walls were built in 7th century B.C., and based on this information it is understood that urbanization had started at that period. Pergamon had witnessed domination by the Persians, Alexander the Great, the kingdoms of Frigia, Trachia and Selevkos, the Roman and Byzantium Periods. When the Byzantium domination came to an end in 1302 A.D., Karasioğulları Emirate took over control, and later the control of the city was taken over by the Ottomans soon after 1341.

The Serapis Temple, which was built in Pergamon, is the largest Egyptian-style temple structure in the land of Hellenistic and Roman. The primary reason why it is an Egyptian-style structure is that the Egyptians had regarded Isis and Serapis as main Gods, and besides, this belief was not restricted to Egyptians mythology, but rather it had spread out of this country as well. Of the Egyptian Gods who were also worshiped in Anatolia, Isis and Serapis were the first. The importance those gods were given by the Anatolian people was proved by the temples which they had built for them. Such temples had been built not only in Pergamon, but also in Ephesus, Priene, Kyme, Stratonikaia amd Miletos (Kemertaş 2000).

Isis temples were called Iseum. The Isis Temple in Pompei gives us a general idea about those temples. The Isis Temple, which was built in the place of a temple destroyed in the earthquake in 63 B.C., was surrounded with a high wall. The main temple was located in the centre. It had a rectangular shape and there was a platform in the last section of it, on which a statue of the goddess and worship-related cupboards had been put. There was an altar out in the courtyard. In the internal courtyard in a corner was a rectangular-shaped building in which there was a cellar. It is predicted that this building had been used for examining the new participants and for the ceremonies. People used to enter the other saloons through the portic. These saloons are thought to have been used for meetings and conferences (Arseven 1994).

Isis temples had been built in the Hellenistic style. For these temples, on the one hand, small Isis statues made in Europe, altars and tools for sacrifice had been used, and

on the other hand, original Egyptian statues had been brought. Religious functionaries/practitioners had not hesitated at all to sell the old pieces of their temples (Wissowa et al. 1914, Kemertaş 2000).

The temples built for Serapis were called Serapeion and there were many temples; however, the two temples in Egypt were the best-known. One of them is located nearby Sakkaraon on the west bank of the Nile. The main gallery of this temple was used as a cemetery of bulls in 1400 B.C. and its additional rooms had been built during the period of Ramses the Second. The second Serapeion temple, which was built for Serapis, is the biggest and the most famous one in Alexandria. Ptttolemoios Soter the First (323 – 285 B.C.) had chosen Serapin as the official god of Egypt and had gotten Architect Parmeniskos to construct it (Kemertaş 2000).

Hellenistic and Roman temples were regarded as the houses of gods and as a protection for cult statues. In the temples of Eygptian gods, there is an enterance to a certain point, and for this reason, there is a need for a larger internal space. Some ceremonies and official parades required a larger temple space (Kemertaş 2000).

In the 2nd century A.D., changes began to appear in temple plans. This was the beginning of the formation of Byzantium basilicas. The interior space for those participating in ceremonies had been kept larger. There was less use of faceted stone constructions and they began to be replaced by constructions made of mortar. Wooden roofs began to disappear. Cambered roofs began to cover brick structures (Kemertaş 2000).

The Serapis Temple is thought to have been constructed in the 2nd Century during the Hadrianus Period. Hadrianus, during his own period (A.D. 117 – 138), had encouraged the construction of roads and establishment of new cities in Anatolia and provided financial support for the repair or construction of official buildings and temples; thus, the City of Pergamon looked like a construction site during the period of Hadrianus (Radt 2002).

Based on the cult and historical data, this temple is said to have been constructed in the first half of the 2nd Century A.D. and was dedicated to three Alexandria gods (Radt 2002).

In Pergamon, which became a center of bishopric during the Byzantium Period, The Serapis Temple had been converted to a church dedicated to St. Jean. This church is one of the seven churches of Christianity (Atilla and Öztüre 2001).

The Serapis Temple is thought to have been used for a very long time. Although it is not clearly known when it was last used, it is highly probable that it was abandoned during the Arab attacks in the 7th Century. During the Turkish Period, it had been completely abandoned and its materails had been used in the buildings constructed around it. Also, in early 17th Century, one of the columns of the church was brought and used in the construction of Sultan Ahmet Mosque (The Blue Mosque) in Istanbul (Deubber 1977).

The two tower-like round structures on the northern and southern sides of the church seem to have been better preserved in comparison with the main building. Of these structures, the one in the north is being used as a mosque at present, and the one in the south as a depot of the museum for the ancient works of art. The two courtyards lying in the direction of The Red Courtyard were revealed during the excavations in 1930s (Radt 2002).

Figure 2. 1. A gravure belonging to the Serapis Temple from the second volume of a book called "Constantinople and the Scenery of the Seven Churches of Asia Minor" published in 1836 in London (Atilla and Öztüre, 2001).

Figure 2. 2. A colour gravure of the Serapis Temple in 1840s (Atilla and Öztüre, 2001)

Figure 2. 3. South-east facade of the Serapis Temple (Photograph: Website of Ministry of Konak)

Charles Texier'nin 1849'da Paris'te yayımladığı "Descripsion de l'Asie Mineure" adlı kitabının 116. sayfasında yer alan "Bergama'da Bazilika" başlıklı gravür.

Figure 2. 4. A colour gravure of the Serapis Temple in 1840s (Atilla and Öztüre, 2001)

Figure 2. 5. South-west facade of the Serapis Temple at the present (2004)

Figure 2. 6. One of the circular tower-shaped structures situated in the south of the Serapis Temple used as the depot of ancient works of art of the museum today (2004)

Figure 2. 7. The other one of the circular tower-shaped structures situated in the north of the Serapis Temple used as the mosque today (2004)

2.3.2 Location of the Serapis Temple

Bergama is located on Bakırçay River Basin, the northern part of İzmir. It is surrounded by Kınık on the east, Dikili on the west, Aliağa on the south, Balıkesir and Manisa on the north. The surface is 1.688 km2.

Pergamon Serapis Temple is situated within today's town of Bergama and at the intersection of Kınık Road to Bergama (Figure 2.8).

Figure 2. 8. A view of the Serapis Temple in today's town of Bergama (2004)

2.3.3 Architectural Definition of Serapis Temple

Serapis Temple, the main structure has 60x26 m dimensions and is made up of two round structures on both sides with square atriums belonging to them and a large 100x200 m. atrium in front of this structure complex. The area that the structural complex covers is approximately 270 m. high and 100 m. wide (Figure 2.9). The height of the remaining part of the structure is 19 m at present (Radt 2002).

The main structure had been built of red bricks; and that is why the structure was called The Red Courtyard. The diameter of the monumental round stone structures on both sides are 12 m. Between the main structure and the round, structures on both sides are small atriums surrounded by 9x15 meter-wall (Trappmann 1970). The dimensions of the square atriums in front of the round tower structures are nearly 40x40m., and a line of columns was standing on one side of those atriums. The other three sides of the atriums were surrounded by galleries (Radt 2002).

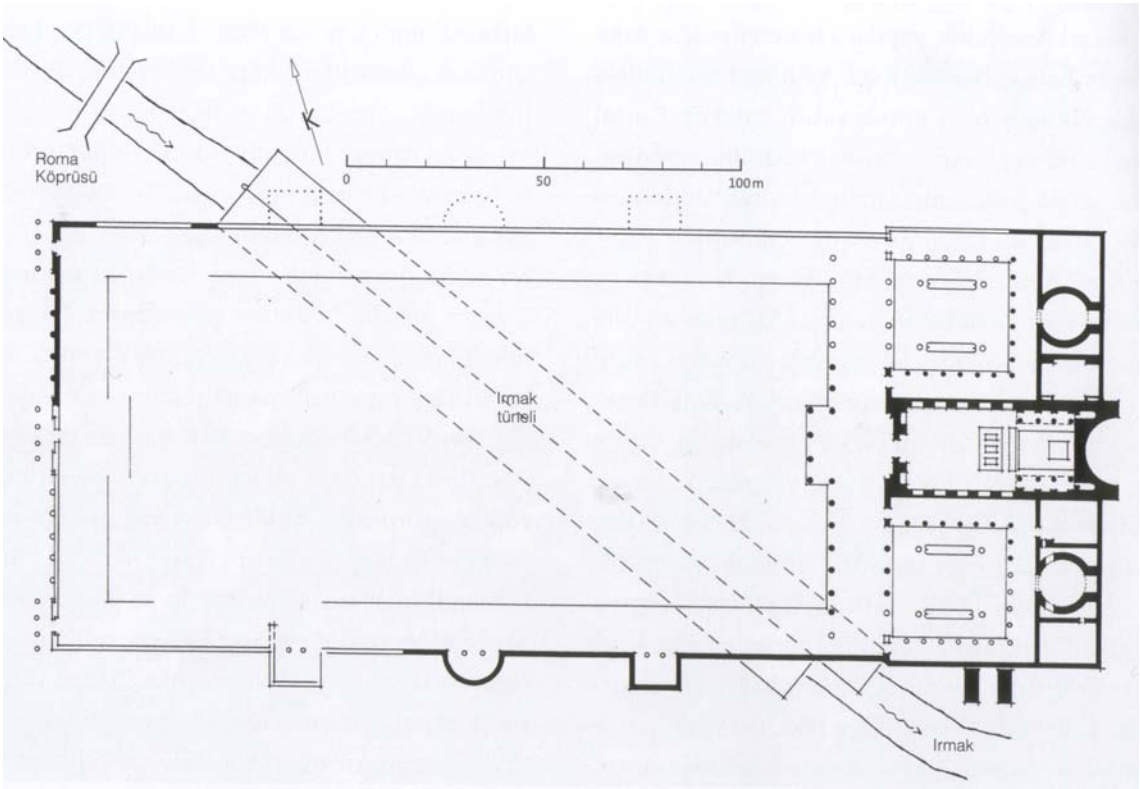

Figure 2. 9. Plan of the Serapis Temple compleks (Radt 2002)

The inner and outer parts of the whole temple structure, as well as, the round structures on its sides had been covered with marble plaques, and massive marbles had been used in the sections, such as door frames, which are important with respect to construction. The floors of all the buildings, galleries and the floor of the atriums in front of the round structures had been covered with marble plaques with motifs in various places (Radt 2002).

It is estimated that there was an open strongly-structured wooden roof skeleton carrying a marble tiled roof. In addition, it is thought that the roof coverings, including the round structures, were built using marble tiles (Radt, 2002).

The entrance to the main temple was through the atrium at the north-west front of the structure. The width of the door was over 7m, and its height was 14 m (Figure2.10). The door had been surrounded with heavy marble frames and there was a threshold over the door, which was made of a monolith marble weighing 70 tons and it is still sitting in its original place (Radt 2002).

Figure 2. 10. A view of the north-west elevation of the enterance to the Serapis Temple (2004)

The entrances to the round structures, which are very much alike, had atriums. These entrances were 11.5 m. high, and at the upper ends of the doors there were dual arches just like the door of the temple (Trappmann 1970).

The front section of the antique structure used to be lighted with windows, but the back section where the cult statue was situated was dim. The last part of the building was not apsis but was formed with a straight wall. At the deepest part of this wall was a platform which was 1.5m in the middle, 10 meter wide and 12 meter deep. Behind this platform was a round podest which was 1 meter high and 4.6 meter long. (Radt 2002).

The temple did not have any windows at the back. The lighting of the space inside was limited to two-thirds of the front section and to the section from the entrance to the cult podium where a lot of light enters. In this front section, the long walls on which there were 5 windows over large niches separating the lower parts into sections. The windows and the upper parts had an ending like an arch. There was also a niche on each wall facing the north-west on the two sides of the enterance, but there was no window over these niches. There was an architrave between the niches and the windows (Radt 2002).

Figure 2. 11. A view of the north-east and north-west elevation of the Serapis Temple (2004). (http://perso.infonie.be/parcours/pergame.html)

In the temple, there were passageways and a system made up of spaces which look like cellar warehouses and cistern. These were located partially under the atriums on the sides and partially under the buildings. On the sides of the round structure - both in the north and in the south -were cross- like vaults sitting on the columns and supporting the downward-sloping field. Narrow passageways, which extended as far as

underneath the atrium and the main temple, used to come out of these colums. A passageway under each atrium used to extend underneath the big wall pillars at the front of the Red Courtyard (Radt 2002).

When The Serapis Temple had been converted to a church, two walls, which were as high as a human and made of Horasan mortar mixed with stone pieces, had been built from the front to the back, extending to the corners of the abscissa (Figure 2.12). The abscissa itself, which could be seen from the entrance of the church, and the marble surrounding it had been built inside the old temple. The walls dividing the huge ancient place into three sections formed the base for the two lines of columns in the church. The foundation walls of the church were much higher than the ancient ground of the Red Courtyard. On the long walls of the Red Courtyard, repeating in equal distances, marble pales under andesite bands, which had been badly damaged due to fire, were among the additional structures built for the church. These used to support the ground of a gallery as a console (Radt 2002).

Figure 2. 12. Wall ruins belonging to early Byzantine period in the Serapis Temple. (Radt 2002)

Nothing can be perceived as a whole today relating to the porch which is in front of the structure complex, because a large portion of it is full of modern Bergama houses.

The atrium had been surrounded with high walls built with small faceted stones. From each wall, a small circle used to extend out. It is accepted that the atrium was surrounded by galleries with columns. The walls of the galleries and exedras had been covered with marble. The west front of the atrium wall had three doors with marble frames (Radt 2002).

In order to direct the Selinos River, ancient name, which flowed under the front atrium of the Serapis Temple, two tunnels had been built side by side with vaults, and they extended along the front atrium diagonally (Radt 2002).

The Director of Museum Osman Bayatlı carried out the restoration works especially of the southwest and south sections of the Serapis Temple, which are in danger, in the 1940s. The construction of a preservation-based wall was done using baked-clay tiles, which were specially made for this work. These restoration works had been given full support by the Regional Governor Kazım Dirik at the time (Figure 2.13-2.14) (Radt 2002).

Figure 2. 13. A view of the north-east elevation of the restoration sections of the structure carried out in 1940s in the Serapis Temple (2004).

Figure 2. 14. An interior view of the restoration sections of the structure carried out in 1940s in the Serapis Temple (2004).

The Serapis Temple, owing to its many features, was an unusual structure with respect to western Anatolia and its imperial period's architectural style. Of those unusual features, apart from the passageway systems as well as the details that resembled of Egypt, it is a fact the Red Courtyard is one of the few structures which had been totally built of brick in western Anatolia (Radt 2002).

CHAPTER 3

EXPERIMENTAL METHODS

The laboratory analyses of the bricks, mortars and plaster samples covered the determination of basic physical and mechanical properties, mineralogical and chemical compositions, raw material compositions, pozzolanic activities of aggregates and microstructural characteristics of the bricks, mortars and plasters.

3.1. Sampling

Brick, mortar and plaster samples were collected in 2004. The samples have been collected from the places which are possible to be reached and would be taken in a way that will create less damage to the structure.

Samples were collected from the walls of the Serapis Temple. The samples were labelled by the abbreviated name of the Roman brick (RB), intervention brick (IB) or original roman mortar (RM), intervention mortar (IM), original Byzantine lime plaster (BP) and sample number (1, 2, 3 ... etc.). The definitions of the collected samples are given as follows:

RB-1: Original Roman Brick collected from north-west elevations of the Serapis Temple (inside the Temple from 2 meters height above the ground) (Figure 3.1).

RB-2: Original Roman Brick collected from north-west elevations of the Serapis Temple (inside the Temple from 4 meters height above the ground) (Figure 3.2).

RB-3: Original Roman Brick collected from north-west elevations of the Serapis Temple (inside the Temple from 2 meters height above the ground) (Figure 3.2).

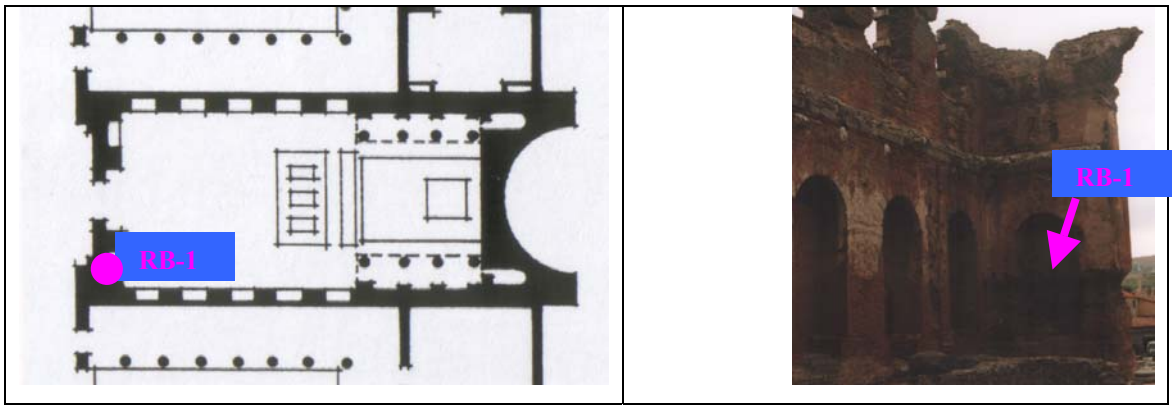

Figure 3. 1. Plan of the Serapis Temple (Radt 2002) and view from the north-west elevations (2004) showing where Roman brick sample (RB-1) was collected.

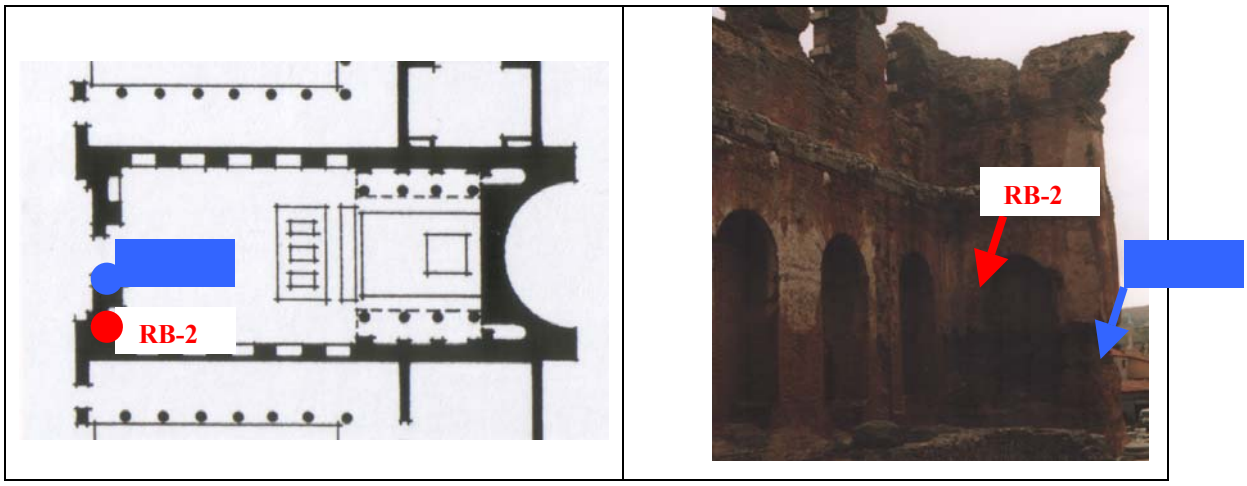

Figure 3. 2. Plan of the Serapis Temple (Radt 2002) and view from the north-west elevations (2004) showing where Roman brick samples (RB-2 and RB-3) were collected.

IB-1: Intervention Brick collected from south-west elevations of the Serapis Temple (from 60 centimeters height above the ground) (Figure 3.3).

IB-2: Intervention Brick collected from south-west elevations of the Serapis Temple (from 50 centimeters height above the ground) (Figure 3.3).

IB-3: Intervention Brick collected from north-east elevations of the Serapis Temple (inside the Temple, approximately 2.5 meters height above the ground) (Figure 3.4).

IB-4: Intervention Brick collected from south-west elevations of the Serapis Temple (approximately 1 meter height above the ground) (Figure 3.5).

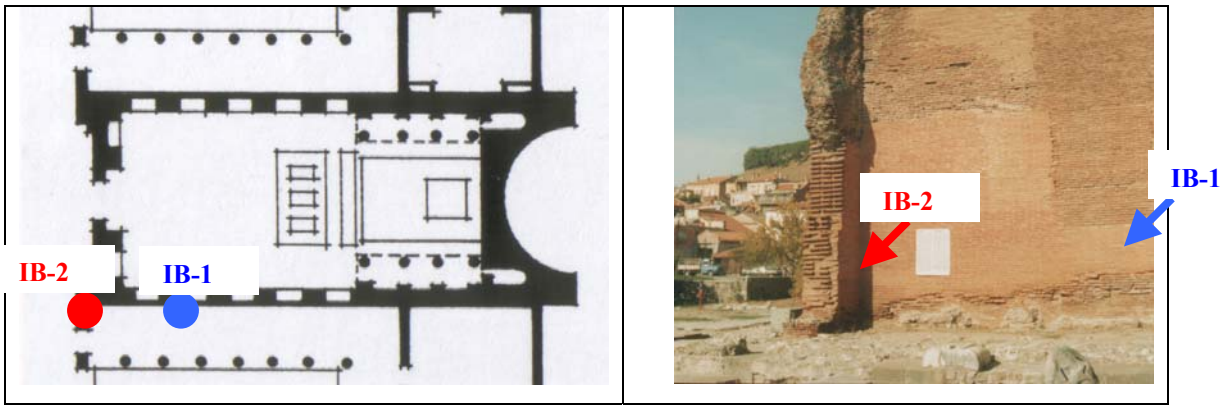

Figure 3. 3. Plan of the Serapis Temple (Radt 2002) and view from the south-west elevations (2004) showing where intervention brick samples (IB-1 and IB-2) were collected.

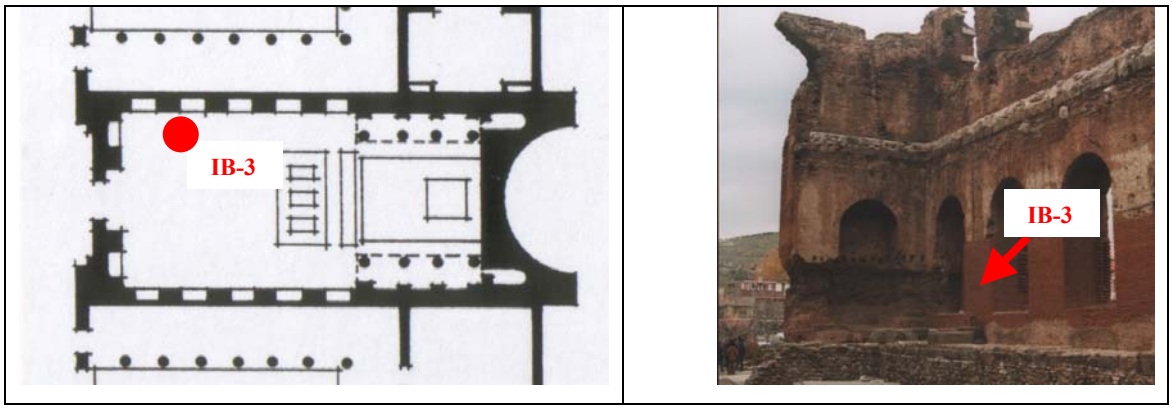

Figure 3. 4. Plan of the Serapis Temple (Radt 2002) and view from the north-east elevations (2004) showing where intervention brick sample (IB-3) was collected.

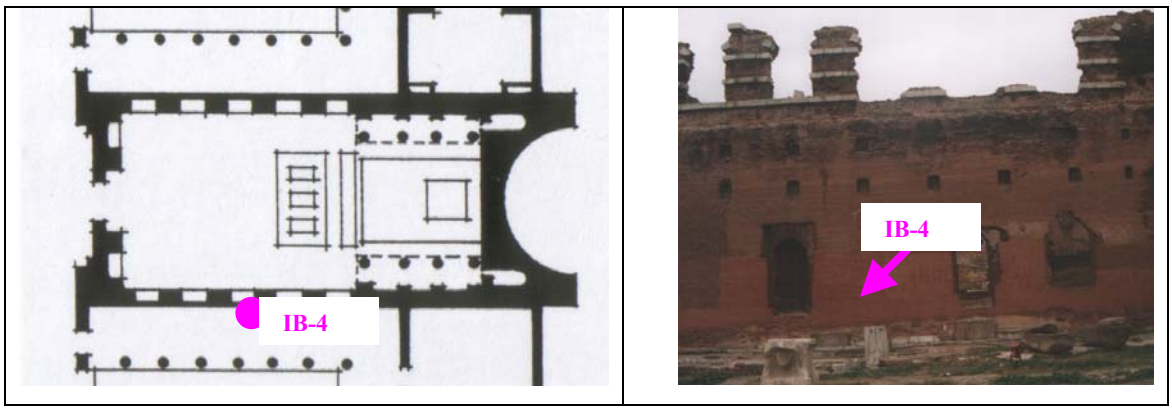

Figure 3. 5. Plan of the Serapis Temple (Radt 2002) and view from the south-west elevations (2004) showing where intervention brick sample (IB-4) was collected.

RM-1: Roman lime mortar collected from north-west elevations of the Serapis Temple (inside the wall, from 3 meters height above the ground) (Figure 3.6).

RM-2: Roman lime mortar collected from south-east elevations of the Serapis Temple (inside the stairs, approximately 6 meters height above the ground) (Figure 3.7).

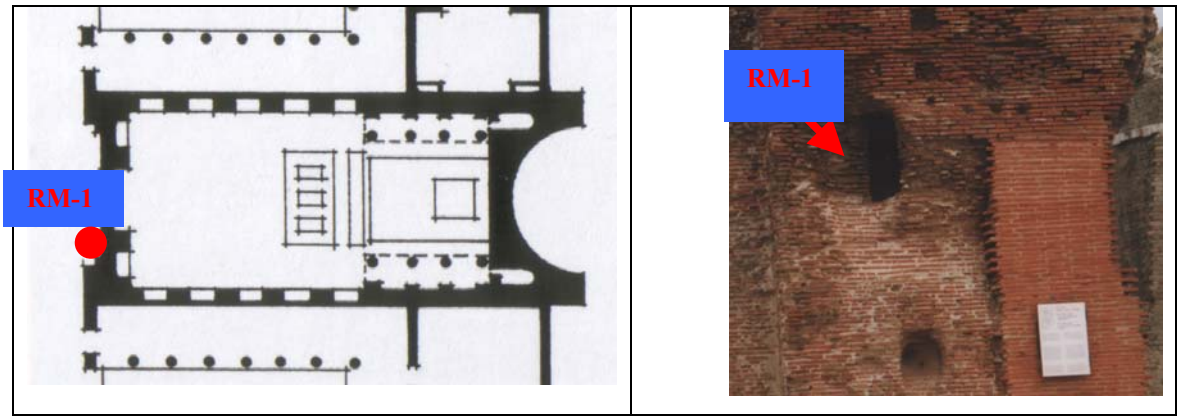

Figure 3. 6. Plan of the Serapis Temple (Radt 2002) and view from the northwest elevations (2004) showing where Roman mortar sample (RM-1) was collected.

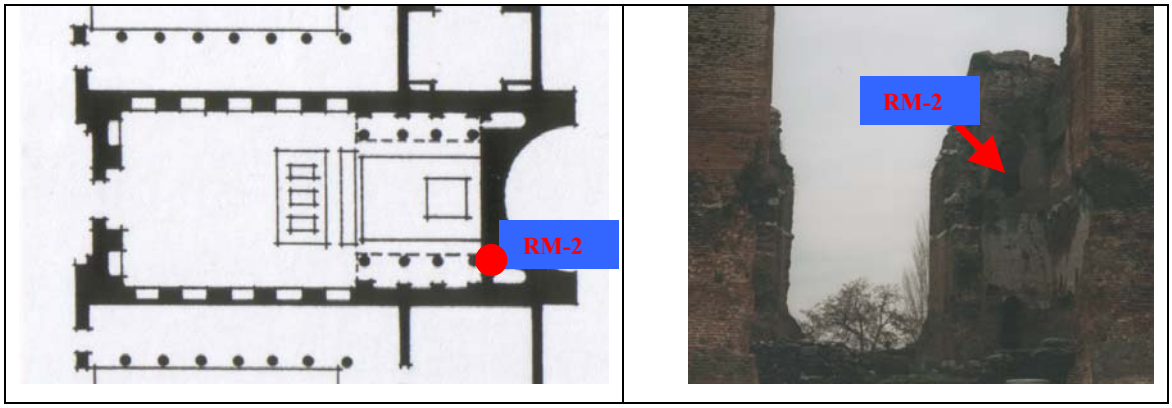

Figure 3. 7. Plan of the Serapis Temple (Radt 2002) and view from the south-east elevations (2004) showing where Roman mortar sample (RM-2) was collected.

BM-1: Byzantine brick–lime (horosan) mortar collected from the courtyard wall. (Figure 3.8).

BP-1: Byzantine Lime Plaster collected from south-west elevations of inside the Serapis Temple (approximately 2 meters height above the ground) (Figure 3.9).

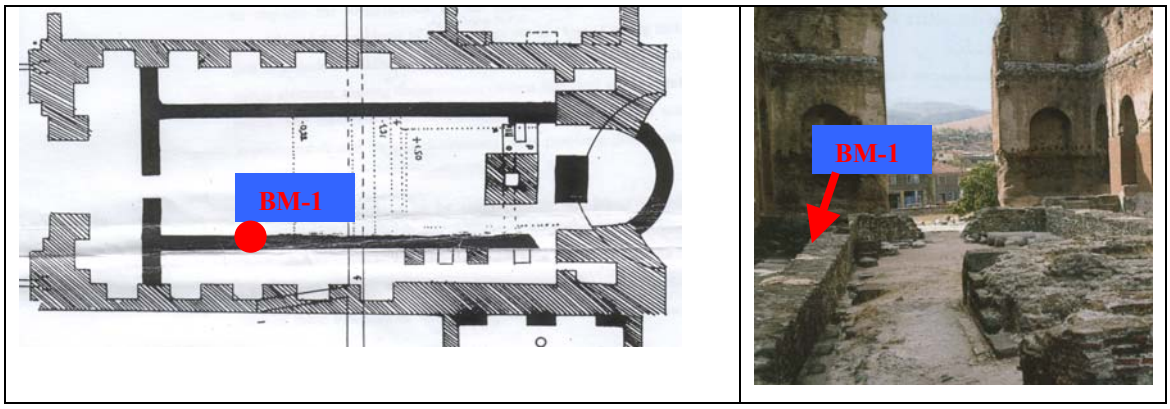

Figure 3. 8. Plan of the Serapis Temple (Kemertaş 2000) and view (Radt 2002) showing where Byzantine mortar sample (BM-1) was collected.

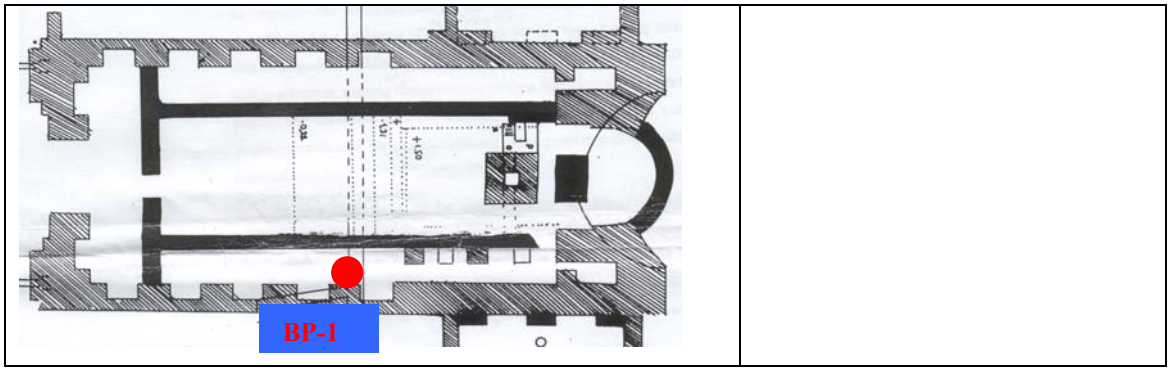

Figure 3. 9. Plan of the Serapis Temple (Kemertaş 2000) showing where Byzantine plaster sample (BP-1) was collected.

IM-1: Intervention Lime Mortar collected from south-west elevations of the Serapis Temple (from 50 centimeters height above the ground) (Figure 3.10).

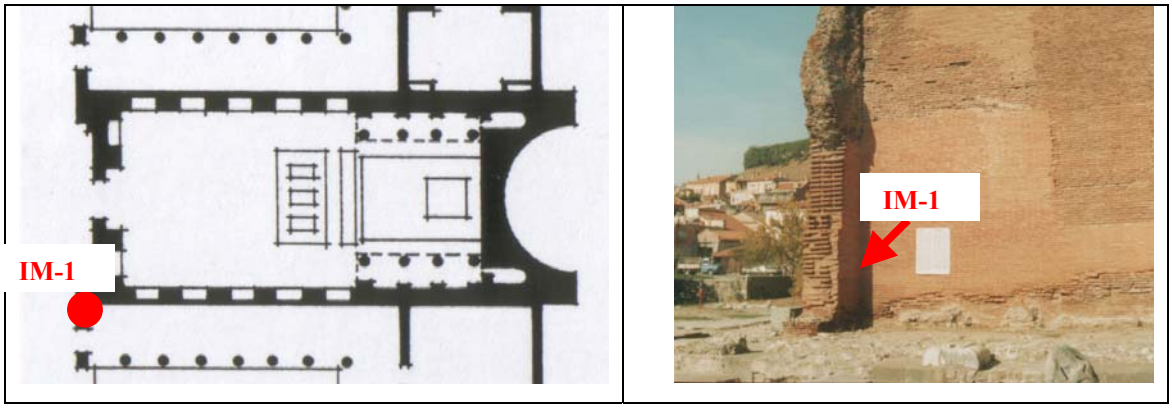

Figure 3. 10. Plan of the Serapis Temple (Radt 2002) and view from the south-west elevations (2004) showing where intervention mortar sample (IM-1) was collected.

IM-2: Intervention Lime Mortar collected from north-east elevations of the Serapis Temple (inside the Temple, approximately 2.5 meters height above the ground) (Figure 3.11).

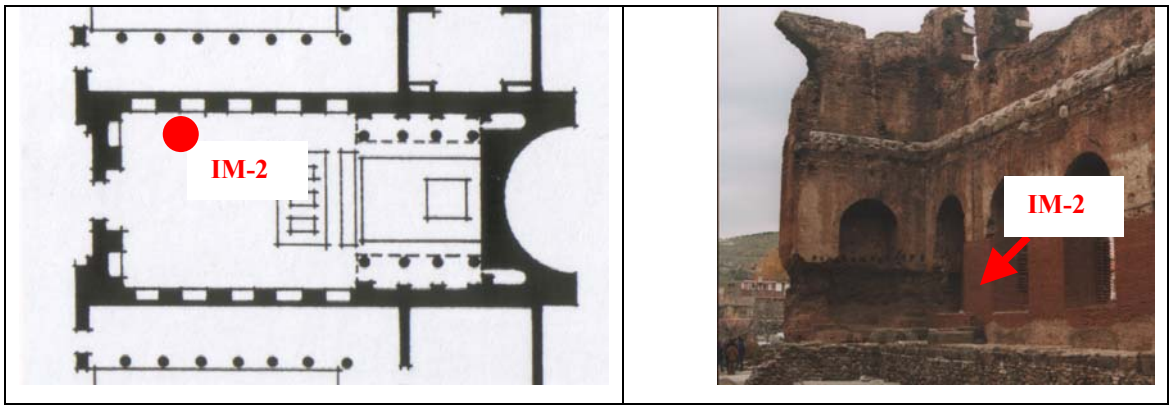

Figure 3. 11. Plan of the Serapis Temple (Radt 2002) and view from the north-east elevations (2004) showing where intervention mortar sample (IM-2) was collected.

IM-3: Intervention Lime Mortar collected from south-west elevations of the Serapis Temple (Figure 3.12).

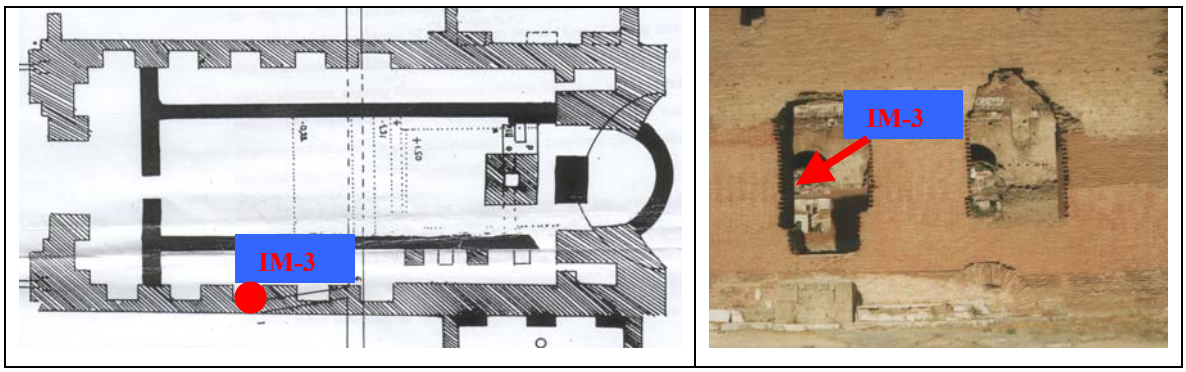

Figure 3. 12. Plan of the Serapis Temple (Kemertaş 2000) and view (2004) showing where intervention mortar sample (IM-3) was collected.

IM-4: Intervention Lime Mortar collected from north-west elevations of the Serapis Temple (from 50 centimeters height above the ground) (Figure 3.13).

IM-5: Intervention Lime Mortar collected from north-east elevations of the Serapis Temple (Figure 3.13).

IM-6: Intervention Lime Mortar collected from south-west elevations of the Serapis Temple (Figure 3.13).

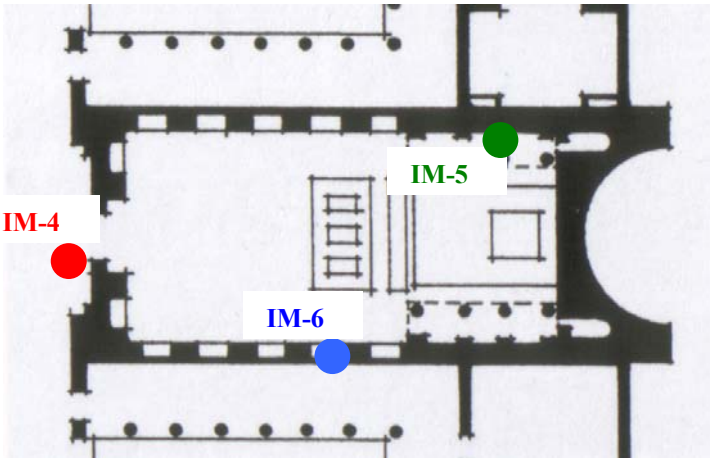

Figure 3. 13. Plan of the Serapis Temple (Radt 2002) showing where intervention brick samples (IB-4, IB-5 and IB-6) were collected.

Pictures of the collected samples:

Figure 3. 14. RB - 1

Figure 3. 15. RB - 2

Figure 3. 16. RB - 3

Figure 3. 17. IB - 1

Figure 3. 18. IB - 2

Figure 3. 19. IB - 3

Figure 3. 20. IB - 4

Figure 3. 21. RM - 1

Figure 3. 22. BM - 1

Figure 3. 23. BP - 1

Figure 3. 24. IM - 2

3.2. Determination of Basic Physical Properties

For the determination of basic physical properties, the samples were dried in an oven at 40 ^{0}C to constant weight. These weight measurements were recorded as the dry weights of the samples (m_{dry}).

The saturation of samples in water was carried out in a vacuum oven (Lab-line 3608-6CE Vacuum Oven). The weights of the water-saturated samples were recorded as saturated weights (m_{sat}). The weight of saturated samples was also measured in water and recorded as the Archimedes weight (m_{arch}) of the samples. All weights were measured with the sensitivity of 0.01g and they were used in the calculation of the porosity and density of the samples.

Porosity (P) is the fraction of the total volume of a porous material occupied by pores or, more simply, the empty spaces or voids in the mass. Porosity is expressed by the percentage of volume and calculated by the following formula (RILEM 1980, Teutonico 1986) :

$$P(\%volume) = [(m_{sat} - m_{dry})/(m_{sat} - m_{arch})] *100$$

where,

m_{sat} : saturated weight (g)

m_{dry} : dry weight (g)

m_{arch} : the weight of the sample in water (g)

Apparent Density (D_a) is the ratio of the mass to the apparent volume of the sample expressed in g/cm^3 and calculated by the following formula :

$$D_a\ (\ g/cm^3\ ) = (m_{dry})/(m_{sat} - m_{arch})$$

Real Density (D_r) is the ratio of the mass to the real (or impermeable) volume of the sample expressed in g/cm^3 and calculated by the following formula :

$$D_r\ (\ g/cm^3\ ) = (m_{dry})/(m_{dry} - m_{arch})$$

3.3. Determination of Drying Rate

Brick and mortar samples of approximately 100-150g and 40x40x45mm with prismatic shapes were prepared for this experiment. Samples were first dried in the oven at 35 ^oC to constant weight. Then, their dry (m_{dry}) and saturated weights in distilled water under vacuum were determined by using an AND HF-3000G balance. Following their weight measurements in saturated state (m_{sat}) they were left for drying. The weight loss of the samples was followed by weight measurements (m_{wet}) at certain time intervals such as 15-30-60 minutes, 1-2-3-16-24 hours and 2-3-4 days subsequently.

The drying rate is indicated as the density of vapor flow rate (g) evaporated from the surface of the sample and it is calculated as a function of average moisture content

for each time span versus surface area of the sample by using the following formula (RILEM, 1980):

$$(g) = M / A^* t$$

where,

(g) : density of flow rate (kg / m^2. s)

M : moisture content of the sample (kg) at the time t

A : total surface of the area of the prismatic test specimen (m^2)

t : time span (second)

M (moisture content of the sample) is found by the use of dry, wet and saturated weights of samples:

$M = (m_{wet} - m_{dry}) / (m_{sat} - m_{dry})$

where,

m_{sat} : saturated weight (kg)

m_{dry} : dry weight (kg)

m_{wet} : wet weight (kg) at a certain time

The results have been expressed in diagrams as the percentage of the weight loss versus time, and density of water vapor flow rate versus time.

3.4. Determination of Uniaxial Compressive Strength

The determination of Uniaxial Compressive Strengths of bricks and mortars were measured by Shimadizu AG-I Mechanical Test Instrument.Samples were prepared by using a cutting machine (Discoplan-TS 372).

The lumps of collected samples were cut into pieces with prismatic shapes with the minimum thickness of 30mm (Figure 3.25).

Shimadzu AG-I Mechanical Test Instrument automatically computed, displayed and recorded test results using a software system. Maximum 15 kN force was applied with 1mm/min. speed. The strokes were recorded under loading. The relationship between the strokes and load by a graph was automatically displayed on the test condition monitor. This graph was composed of a curve whose peak point gave the

maximum force (F) under which the specimen failed. As a result, uniaxial compressive strenghts represented by **'σ'** were calculated by using this graph with the following formula:

$\sigma = F/A$

where;

F : Failure load (kN)

A : Area onto which loading was applied (mm^2)

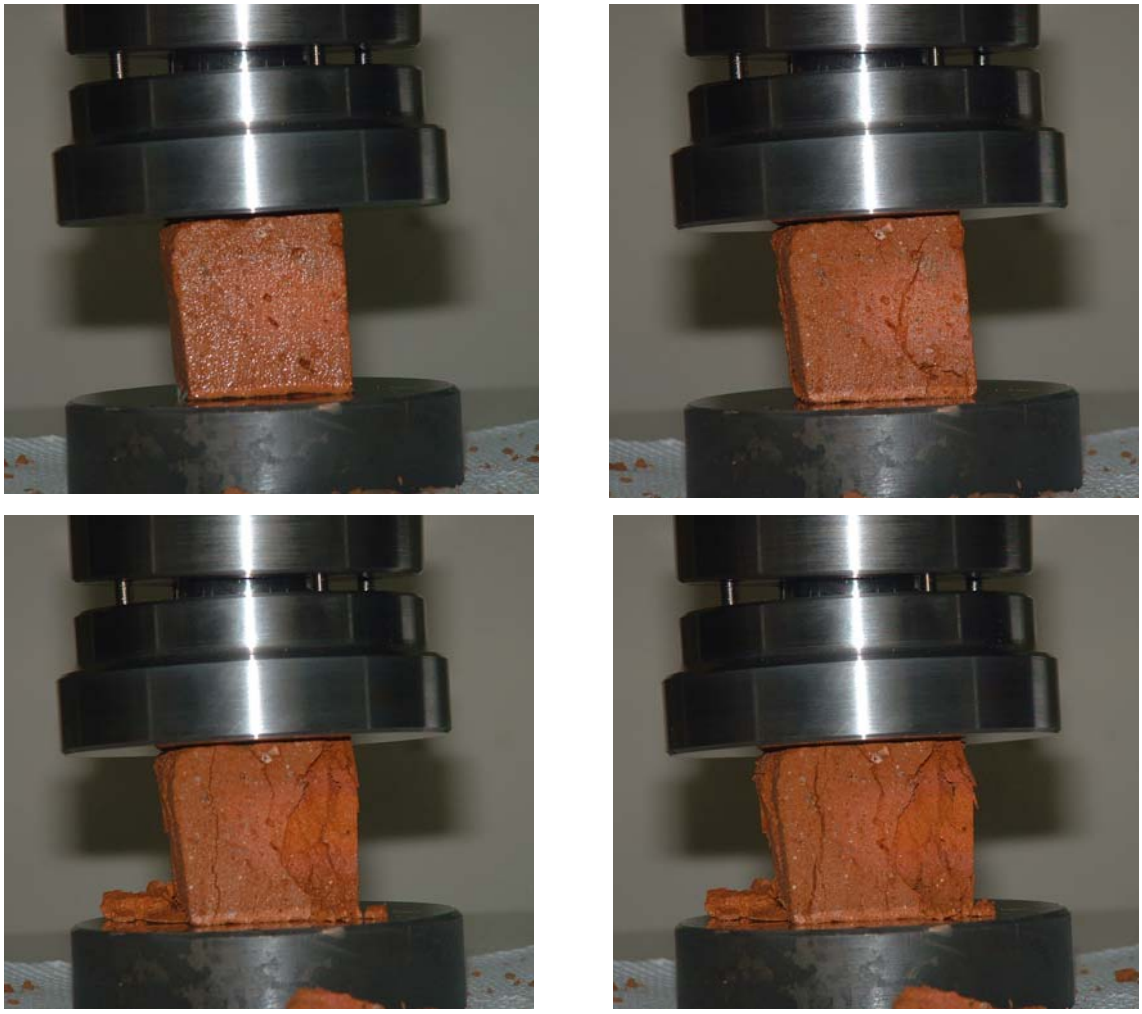

Figure 3. 25. Images showing how uniaxial compressive strength test was carried out.

3.5. Determination of Modulus of Elasticity

Modulus of elasticity is the rate of change of strain as a function of stress. It provides required information about how well a material can resist deformation under the action of external forces (Airapetov 1986). The modulus of elasticity (E) is formulated as follows:

$E = \text{Stress} / \text{Strain} = \sigma / \varepsilon = (\triangle F/A) / (\triangle l/l_o)$

where;

$\triangle F$: Failure load (kN)

A : Area onto which force was applied (mm^2)

$\triangle l$: Change in thickness of the sample along its vertical axis (mm)

l_o : Initial thickness of the sample (mm)

Stress (σ) is the ratio of force to the area where the force is applied. Strain (ε) corresponds to the change in thickness of samples under the action of the applied force (Airapetov 1986). When a compression force is applied onto a solid material, the force is transmitted through its body and causes it to become deformed along the direction of the applied force (Airapetov 1986). The decrease in thickness is denoted by $-\triangle l$. Here, the minus sign refers to contraction in dimension. This change in dimension is called strain and denoted by $\triangle l/l_o$ (Airapetov 1986).

Relationship between deformation and applied force is expressed by a stress-strain curve. Slope of this curve ($\tan\theta$) gives modulus of elasticity of that material (Airapetov 1986). Therefore, modulus of elasticity were calculated using the slopes of the stress-strain curves obtained from the results of the compression strength tests.

3.6. Determination of Raw Material Compositions of Mortars and Plasters

Lime-aggregate ratios and particle size distributions of the aggregates were determined in order to know the raw material compositions of mortars and plasters.

Amount of lime and aggregates were determined by dissolving the carbonated lime in mortars with dilute hydrochloric (HCl) acid (Jedrzejevska 1981, Middendorf and Knöfel 1986). Two dried pieces of each mortar (~10-30 g) were dissolved in 5% hydrochloric acid. Insoluble part was filtered, washed with distilled water, dried and

weighed (m_{insol}). Acid soluble and insoluble parts were calculated by the following formulae and expressed as percentages (Jedrzjevska).

Insoluble % = $[(M_{sam} – M_{agg}) / M_{sam}] \times 100$

Acid Soluble % = 100 – Insoluble %

where;

M_{sam} : Weight of the mortar sample

M_{agg} : Weight of the aggregates

Acid soluble ratio is not the exact ratio corresponding to lime ratio since both lime and calcareous aggregates that could be used in the mortars were dissolved in the solution of dilute hydrochloric acid. Therefore, lime/aggregate ratio was calculated by the formula as follows:

Aggregate % = (100 × Insoluble %) / [(Acid Soluble % × $M.W._{Ca(OH)_2}$) /$M.W._{Ca(CO_3)}$) + Insoluble %]

Lime % = 100 – Aggregate %

where;

$M.W._{Ca(CO_3)}$: Molecular weight of $Ca(CO_3)$ which is 100.

$M.W._{Ca(OH)_2}$: Molecular weight of $Ca(OH)_2$ which is 74.

3.7. Determination of Particle Size Distribution of Aggregates

Particle size distributions of the aggregates were determined by sieve analysis. The aggregates were passed through a series of sieves (Retsch mark) having the sieve sizes of 53µm, 125µm, 250µm, 500µm, 1180µm using sieve shaker (Retsch AS200). Subsequently, each of the particles retained on each sieve was weighed respectively and each of their percentages was calculated. Finally, their cumulative percentages were calculated.

3.8. Pozzolanic Activity Measurements by Electrical Conductivity

Pozzolanic Activity of fine aggregates (less than 53µm size) were determined by mixing them with saturated calcium hydroxide solution ($Ca(OH)_2$) with the solution

ratio of 5 g/200ml. In this analysis, at first, electrical conductivity of the saturated calium hydroxide was measured and then the decrease in the electrical conductivity of saturated calcium hydroxide with aggregate was recorded at the end of two minutes. Their difference (ΔEC in mS/cm) was used to express the pozzolanic activity of the aggregates. It was suggested that if the ΔEC was over 1.2mS/cm the aggregates have good pozzolanicity (Luxan et al., 1989).

3.9. Mineralogical, Chemical and Micro-Structural Analyses

Mineralogical compositions of bricks, mortars, plasters and aggregates used in the mortars and plasters were determined by X-ray Diffraction (XRD) analyses. The analyses were performed on powdered samples using a Philips X-Pert Pro X-ray Diffractometer.

Chemical compositions and microstructural properties of brick and mortar matrices, lime binder and aggregates were determined by Philips XL 30S-FEG Scanning Electron Microscope (SEM) equipped with X-Ray Energy Dispersive System (EDS) (Figure 3.26). EDS analysis was performed on the lime binder, aggregates, brick and mortar matrices, which were ground to a fineness of less than 53μm and then pressed into pellets, in order to determine their chemical compositions.

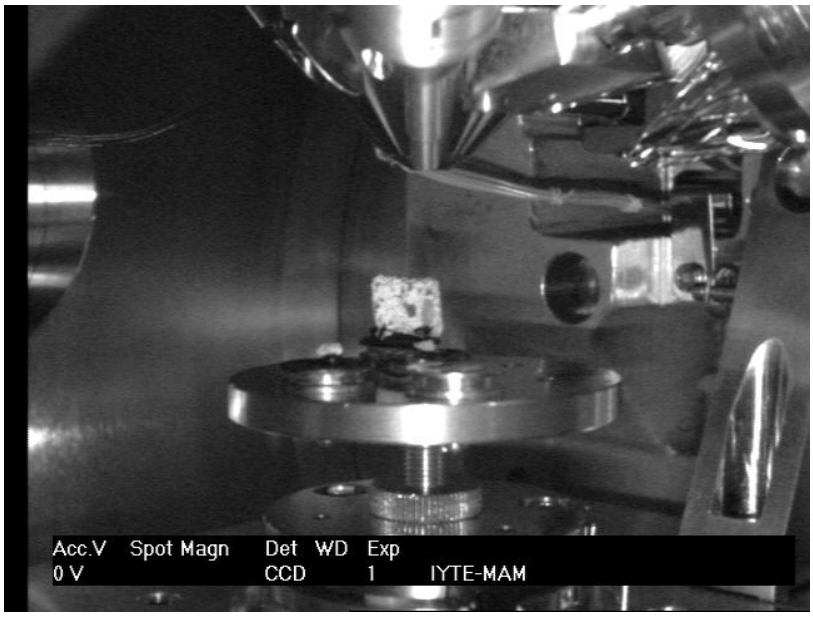

Figure 3. 26. Image of Philips XL 30S-FEG Scanning Electron Microscope

3.10. Determination of Hydraulicity of Mortars and Plasters by TGA

Thermogravimetric analysis (TG/DTG) was carried out on mortar and plaster samples by using Shimadzu TGA-21 in order to evaluate hydraulicity of the mortars and plasters. For this purpose, percent hygroscopic water, structurally bound water and carbon dioxide contents of the mortars and plasters were calculated. The thermogravimetric analysis was carried out in static nitrogen atmosphere at a temperature range of 30-1000°C with a controlled heating rate of 10°C/min.

3.11. Determination of Soluble Salts

Percent soluble salts in bricks, mortars and plasters were determined by an electrical conductivity meter (Black 1965). For this analysis, 1.00 g of finely-ground mortar and brick samples were mixed with 50 ml distilled water. After stirring, this mixture was filtered. Conductivity of the filtered solution was measured by the electrical conductivity meter (WTW MultiLine P3 pH/LF). Percentage of soluble salts within the sample was calculated using the following formula:

$$\text{Soluble Salts (\%)} = [(A \times V_{sol}) / 1000] \times [100 / M_{sam}]$$

where;

A = Salt concentration (mg/lt) = 640 x EC

EC= Electrical conductivity measured by electrical conductivity meter (mS/cm = mmho/cm)

640 = Constant

V_{sol} = Volume of the solution (ml)

M_{sam} = Weight of the sample (mg)

After the calculation of the percentage of soluble salts in the samples, anion parts of the soluble salts were determined by spot test (Black 1965, Arnold 1983, Teutonico 1988). Principle anions such as sulphate (SO_4^{-2}), chloride (Cl^-), nitrate (NO_3^-), carbonate (CO_3^{-2}), and phosphate (PO_4^{-3}) in the solutions were determined.

CHAPTER 4

EXPERIMENTAL RESULTS AND DISCUSSION

The main characteristics of the original and intervention materials used in the construction of the Serapis Temple are given in this section separately. Experimental study includes determination of the following properties of bricks, mortars and plaster:

- Basic Physical Properties of Bricks, Mortars and Plaster (Density, Porosity, Drying Rates)
- Basic Mechanical Properties of Bricks, Mortars and Plaster (Uniaxial compressive strength, Modulus of elasticity)
- Raw Material Compositions of Mortars (Lime-aggregate ratios of mortars, Particle size distributions of aggregates)
- Pozzolanic Activity of Bricks and Aggregates
- Mineralogical and Chemical Compositions and Microstructural Properties of Brick Matrices, Mortars Matrices and Plaster Matrices
- Hydraulicity of Mortars by TGA
- Analysis of Soluble Salts in Mortars (Percent soluble salts in mortars, Anion parts of soluble salts

4.1. Roman Bricks

Bricks are ceramic materials manufactured by heating raw materials containing clay, quartz, feldspats at temperatures between 600-1000 °C. Color, composition and mechanical properties of bricks depend on the raw materials, kiln environment, operators, temperature and firing process and nature of the temper (quartz, carbonates, shards, grounded fired clays) (Cardiano et al. 2004).

In this section experimental results of main physical, mineralogical, chemical and microstructural properties of Roman bricks are discussed in relation to these characteristics.

4.1.1 Basic Physical and Mechanical Properties of Roman Bricks

The Roman bricks used in the Serapis Temple contain very coarse rock and brick fragments(grog) (Figure 4.1). The porosity values of the Roman bricks were in the range of 32 – 35 % and their average value was 33 %. The real density values of them were 2.5 gr/cm^3. Their apparent density values ranged between 1.6 - 1.7 gr/cm^3 (Figure 4.2).

The density and porosity values of Roman bricks used in the temple are in the same range with other Roman bricks used in historic structures in Toledo, Spain and Sicily (Lopez-Arce and Garcia-Guinea 2004, Cardiano et al. 2004).

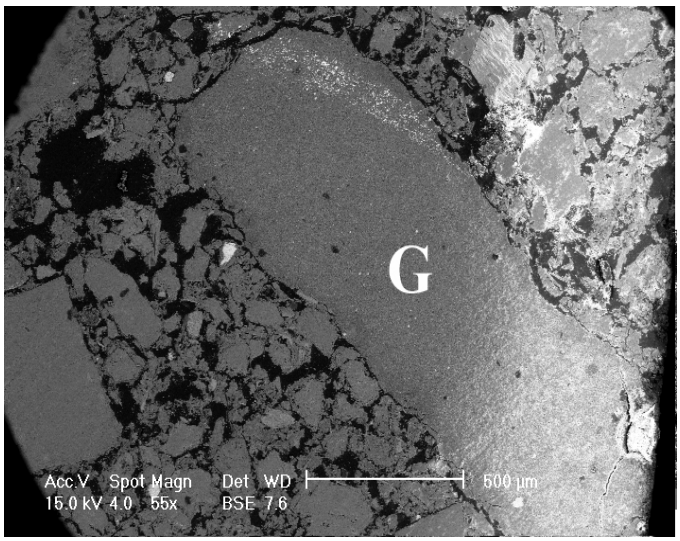

Figure 4. 1. BSE (back-scattered electron) image of a grog particle in the brick (G: Grog)

The drying rate of the bricks was found by following the loss in the weight of the water saturated brick samples versus time. Drying rate characteristics (Figure 4.3) have shown that 50~% adsorbed water in the pores of the bricks rapidly evaporate

within 15 minutes. This can show that the bricks have a high percent of large pore sizes in their total porosity.

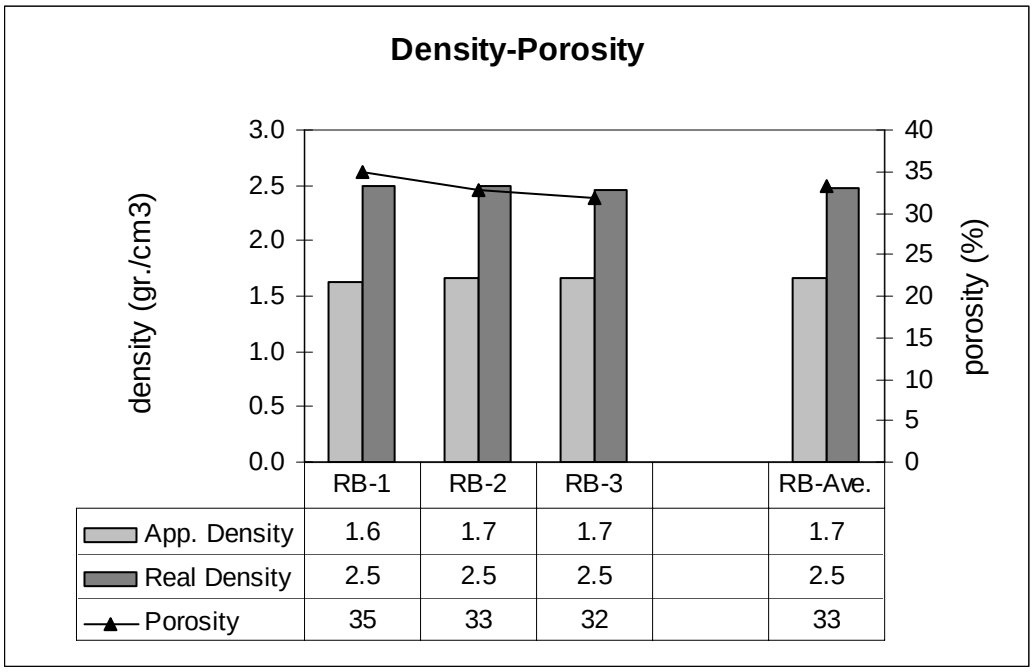

Figure 4. 2. % Porosity and density values of Roman bricks

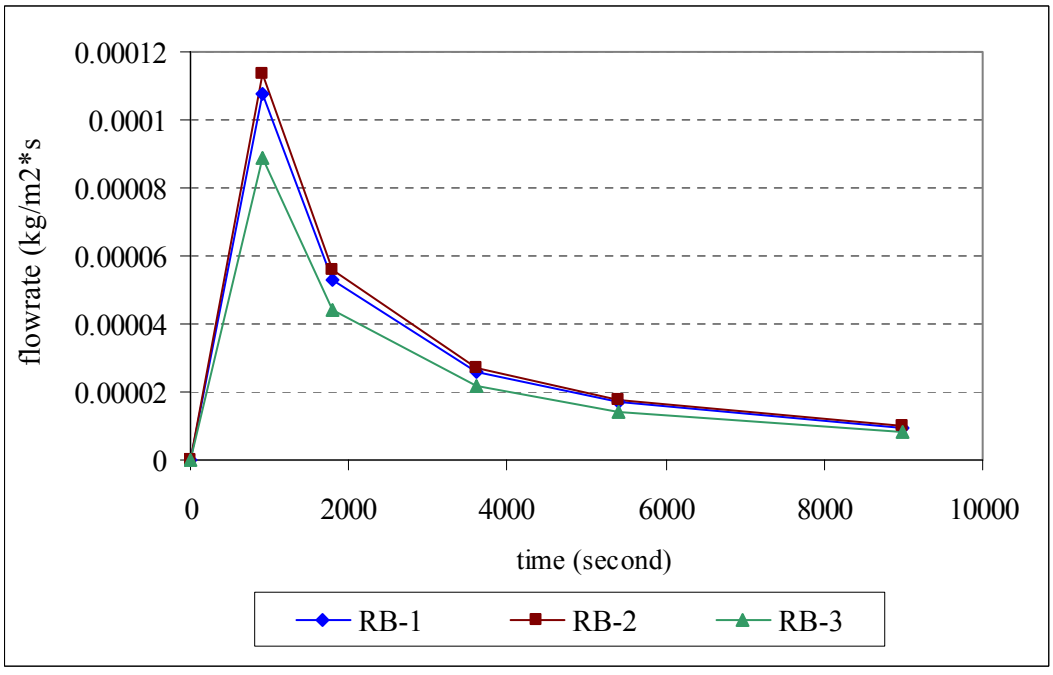

Figure 4. 3. Drying rates of the Roman bricks

Uniaxial compressive strength measurements were carried out on dry brick. Compressive strength values of the brick samples were 5.5 and 6.1 MPa. Modulus of elasticity values were 464.1 MPa and 422.9 MPa (Table 4.1). The similar values have also been found on the Roman bricks used in historic structures in Toledo, Spain (Cardiano et al. 2004, Lopez-Arce and Garcia-Guinea 2004).

Table 4. 1. Unixial Compressive Strength and Modulus of Elasticity values of roman bricks in dry states

SAMPLE	COMPRESSIVE STRENGTH (MPA.)	MODULUS OF ELASTICITY (MPA.)
RB-1	5.5 MPa	464.1 MPa
RB-3	6,1 MPa	422.9 MPa

4.1.2 Mineralogical and Elemental Compositions and Microstructural Properties of Roman Bricks

XRD analysis were carried out in powdered brick samples in order to determine mineralogical composition of the bricks and to predict their firing temperatures.

Quartz, albite, potassium feldspar, hematite and muscovite are the main observed minerals of the Roman bricks (Figure 4.4 - 4.6). To check the presence of any unhydroxylated clay minerals (like illite) seen around in d values 10 Å, the samples were heated at 900°C for 1 hour. After heating, the same peak was observed at 10 Å with the unheated ones. This shows that the all clay minerals are dehydroxylated during the baking process of bricks and the peak seen at 10 Å belongs to muscovite mineral (Figure 4.7).

When the calcite rich clay sources are heated, calcite, gehlenite, anorthite or diposide minerals can be observed in the XRD spectrum depending on the firing temperature (Cardiano et al. 2004). In the XRD spectrum of the Roman bricks, the peaks of these minerals were not indicated. This shows that calcium poor clays were used in manufacturing the Roman bricks (Sujeong et al.1999).

The presence of hematite formed at 850 °C in the calcium poor clays is the indicator of their firing temperature (Cardiano et al. 2004). The observation of hematite

peaks in the XRD spectrum of the Roman bricks show that the firing temperature of the bricks is nearly 850 °C. In addition, absence of mullite peaks in the XRD patterns shows the firing temperature did not exceed 900 °C (Sujeong et al.1999).

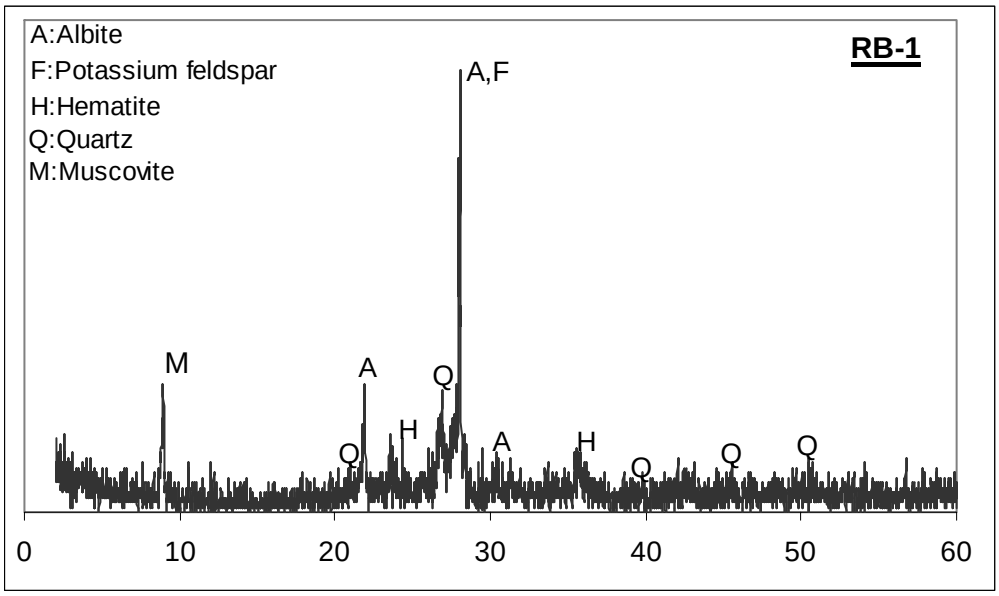

Figure 4. 4. XRD pattern of the Roman brick sample (RB-1)

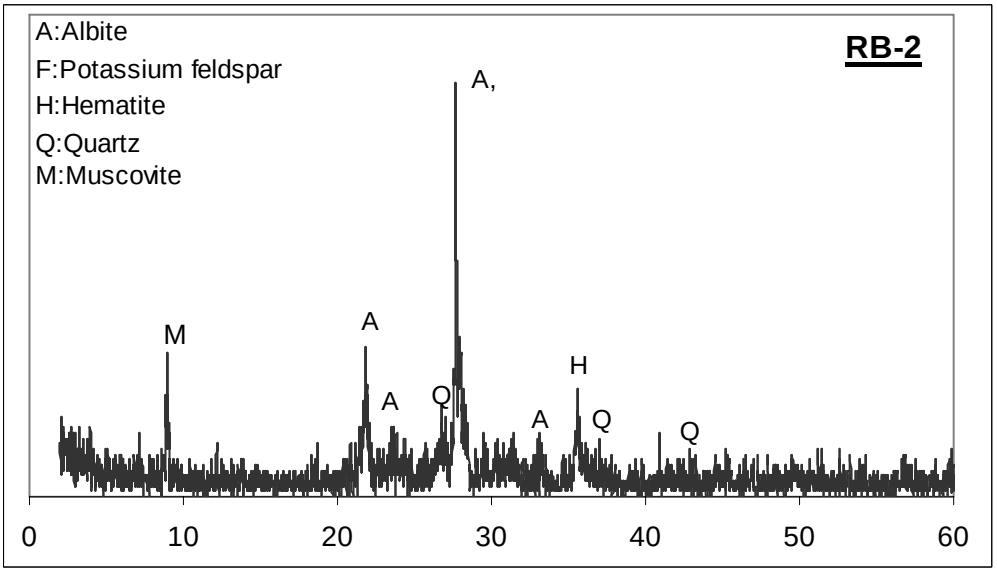

Figure 4. 5. XRD pattern of the Roman brick sample (RB-2)

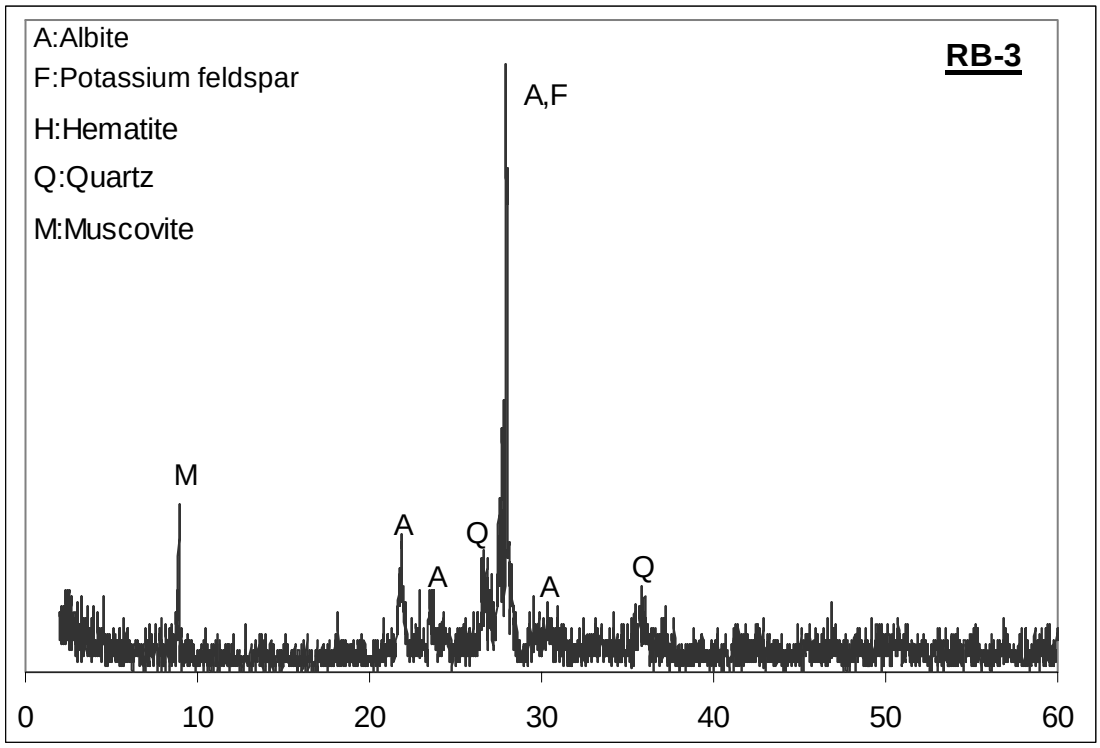

Figure 4. 6. XRD pattern of the Roman brick sample (RB-3)

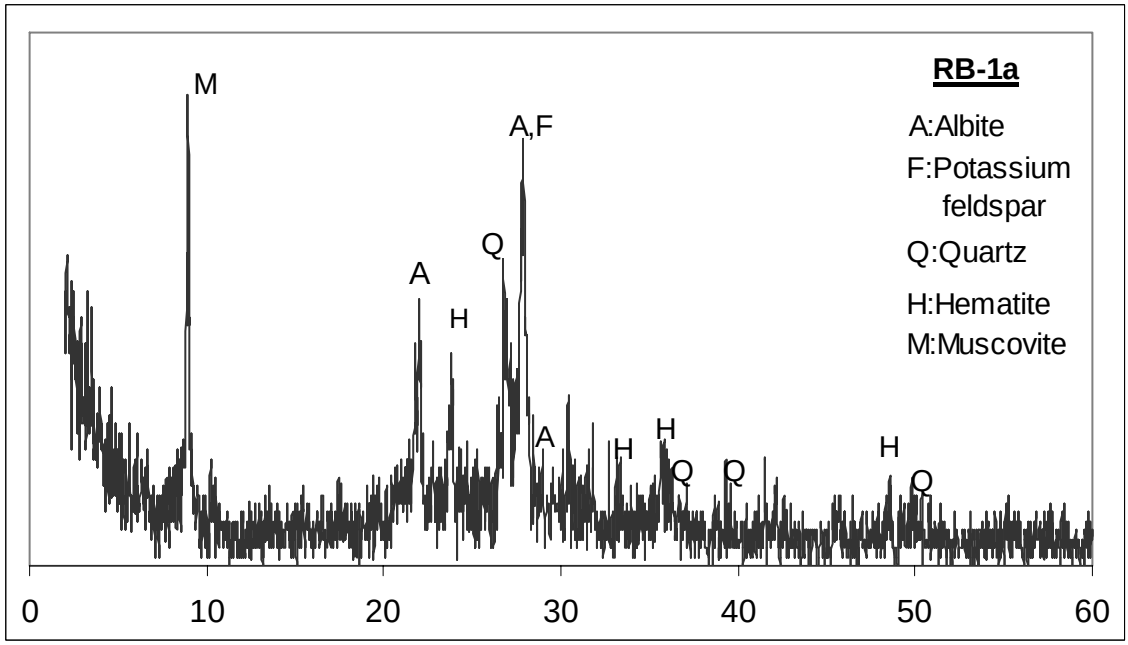

Figure 4. 7. XRD pattern of the heating at 900°C Roman brick sample of RB-1

The elemental composition of the original Roman bricks were determined by SEM-EDS analysis (Table 4.2). Elemental analysis results show that bricks contain high amount of SiO_2, Al_2O_3, and Fe_2O_3, and low amount of Na_2O, K_2O, MgO, and CaO. The presence of low amounts of Ca in their composition indicated that calcium poor clay had been used in the manufacturing of the bricks.

Table 4. 2. Elemental compositions of Roman bricks

SAMPLES	Fe_2O_3	Na_2O	MgO	Al_2O_3	SiO_2	K_2O	CaO
RB-1	11,4±2,3	2,4±0,3	3,9±0,1	17,6±0,3	57,5±2,7	3,3±0,5	3,8±0,4
RB-2	9,7±1,5	3,4±0,4	3,1±0,5	17,8±0,1	58,1±1,3	3,6±0,5	4,4±0,7
RB-3	11,2±2,4	3,0±0,4	4,0±0,5	17,0±0,4	56,0±2,1	4,6±0,4	4,2±0,4

Microstructural characteristics of the bricks were determined by SEM-EDS analyses. In the BSE image of the bricks matrices glassy phases were not observed (Figure 4.8). This indicates that the bricks had been heated at low temperatures. Heating bricks at high temperatures (900 °C and over) results in damage in their amorph structures and leads to formation of high temperature products such as mullite, crystoballite. In XRD patterns, the absence of mullite and crystoballite peaks shows the temperature did not exceed 900 ºC.

Most of the grog pieces found in brick samples show similary elemental composition with the brick matrix, but some of the pieces have different chemical compositions (Figure 4.9-4.10). This shows that grog particles were not always belonging to the original bricks.

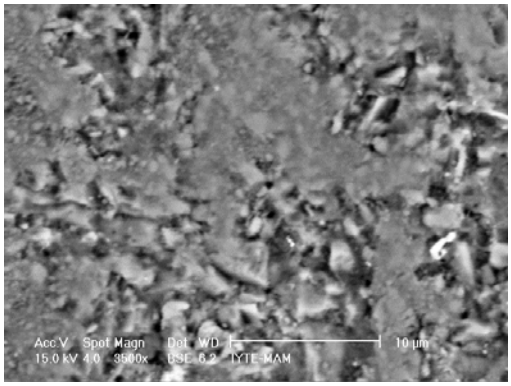

(3500x)

Figure 4. 8. BSE image of brick matrix (RB-1)

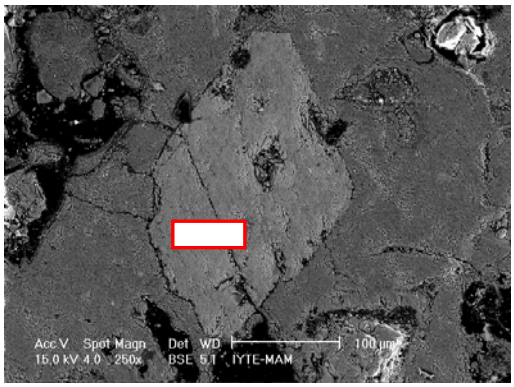

(250x)

Element	Wt %
O	47.58
Na	2.36
Mg	9.13
Al	4.85
Si	23.88
K	0.76
Ca	5.57
Fe	5.88

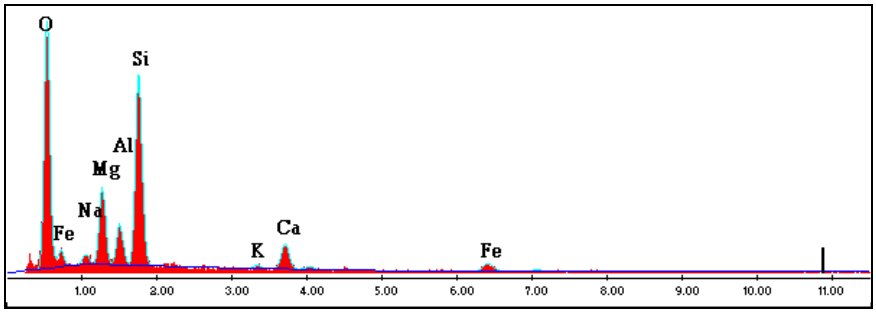

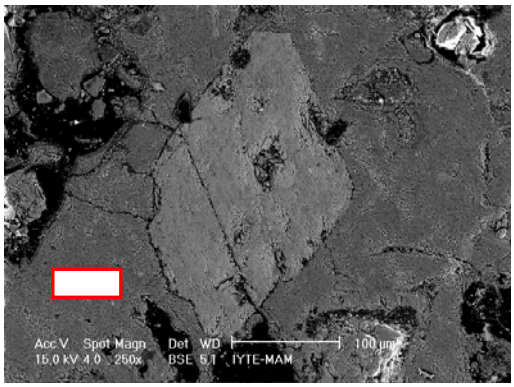

(250x)

Element	Wt %
O	52.67
Na	1.92
Al	6.95
Si	34.87
K	3.59

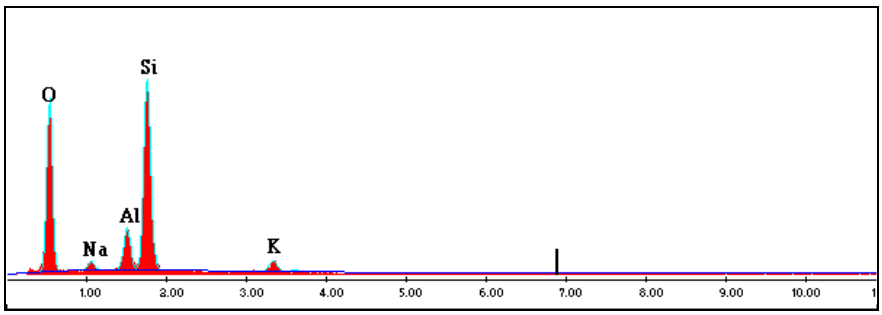

Figure 4. 9. BSE (back-scattered electron) images, EDX spectrums and elemental compositions (%) of a grog particle and brick matrices (RB-1).

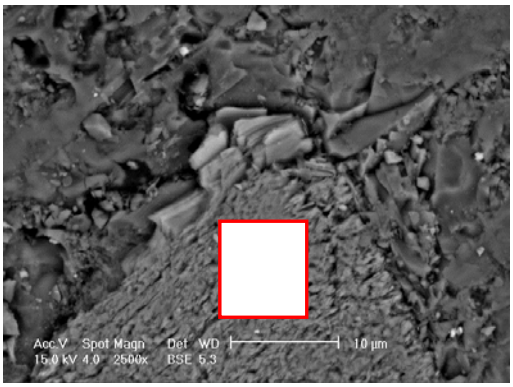

(2500x)

Element	Wt %
O	46.67
Mg	10.20
Al	8.04
Si	19.33
K	6.33
Ti	2.53
Fe	6.90

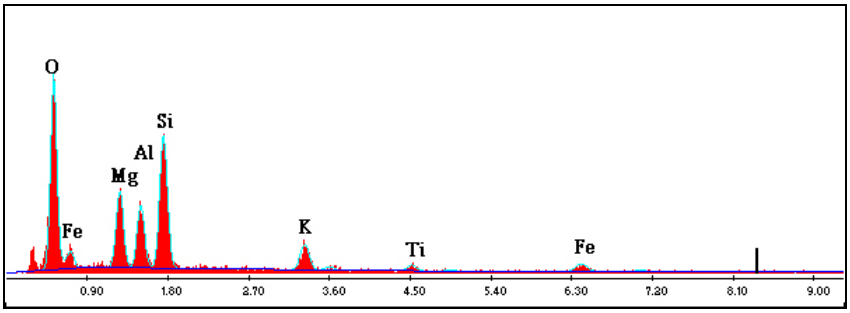

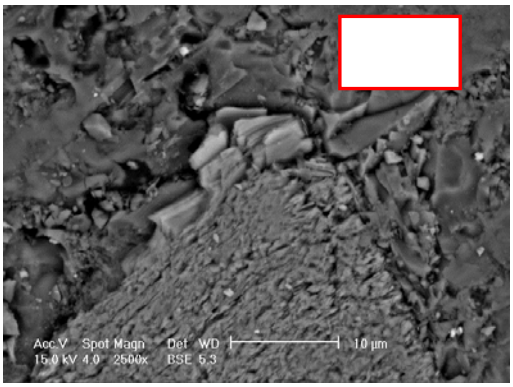

(2500x)

Element	Wt %
O	50.94
Na	2.45
Al	7.02
Si	35.41
K	4.17

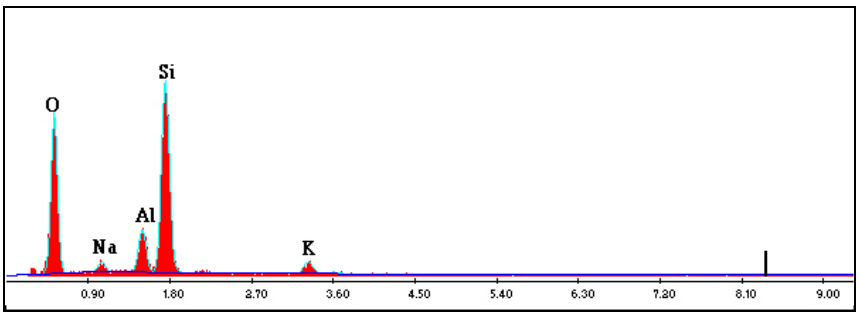

Figure 4. 10. BSE (back-scattered electron) images, EDX spectrums and elemental compositions (%) of a grog particle and brick matrices (RB-1).

Quartz, feldspar and hematite are the main minerals found in the composition of the Roman brick (Figure 4.11). In these matrices, valuable metals such as platinum and copper have been observed in trace amount. These elements are found together with elements such as silicon and iron (Figure 4.12-4.19). This indicates that raw material used in the Roman brick manufacturing sources contain valuable metals.

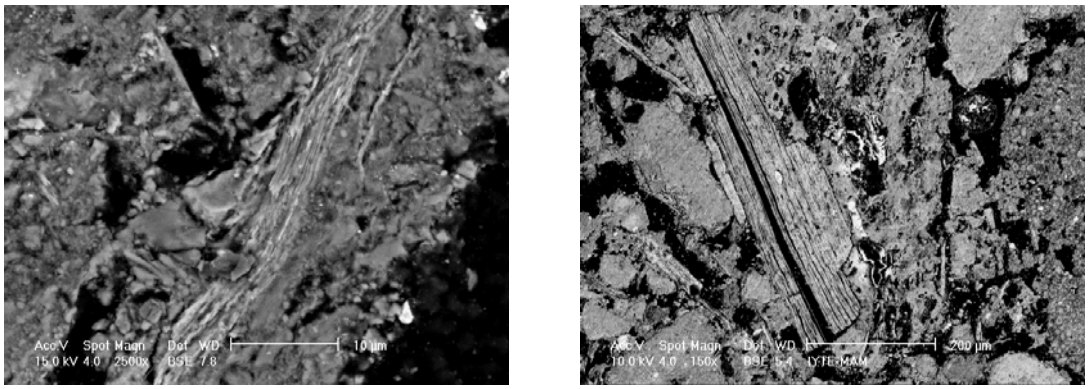

(2.500x) (150x)

Figure 4. 11. BSE images of quartz and feldspar crystals in the Roman brick matrix (RB-1)

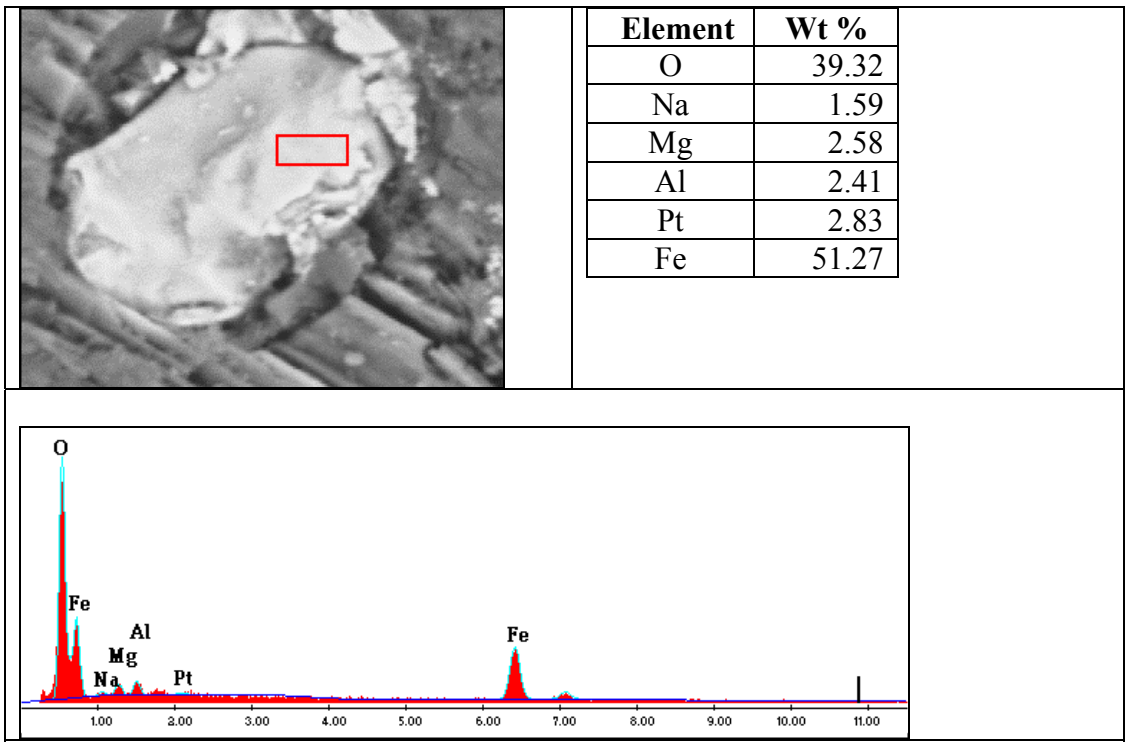

Element	Wt %
O	39.32
Na	1.59
Mg	2.58
Al	2.41
Pt	2.83
Fe	51.27

Figure 4. 12. EDX spectrum of iron and platinum containing particle in the brick matrices (RB-1)

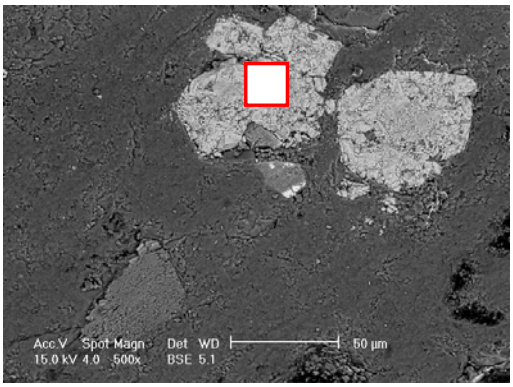

(500x)

Element	Wt %
O	40.86
Na	1.01
Mg	1.27
Al	2.53
Si	4.28
Pt	7.95
Ti	2.05
Fe	40.05

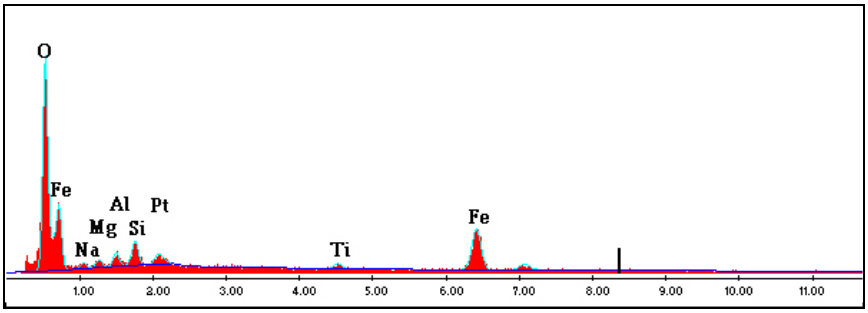

Figure 4. 13. BSE (back-scattered electron) images, EDX spectrums and elemental compositions (%) of a tiny particle platinum containing high amount of Iron (RB-1)

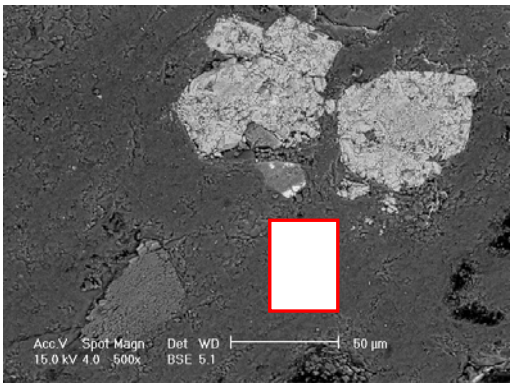

(500x)

Element	Wt %
O	52.24
Na	2.37
Mg	0.69
Al	7.19
Si	33.83
K	3.68

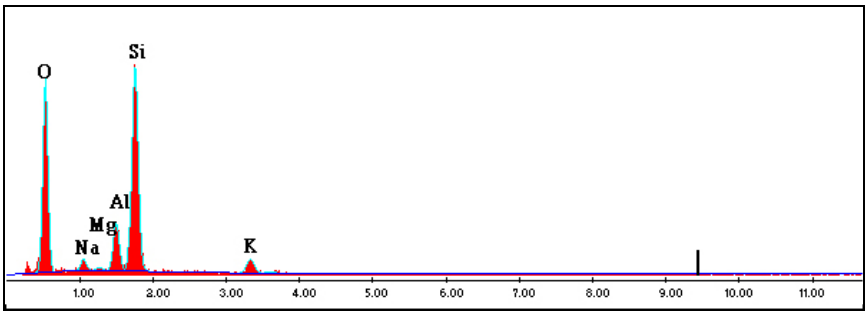

Figure 4. 14. BSE (back-scattered electron) images, EDX spectrums and elemental compositions (%) of brick matrix.(RB-1)

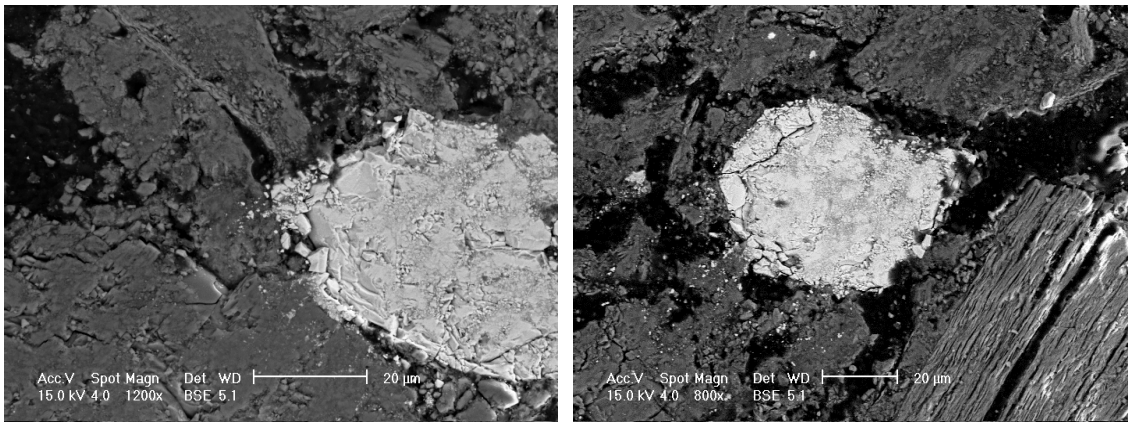

(1.200x) (800x)

Figure 4. 15. BSE images of a tiny platinum particle containing silicon in the brick matrix (RB-1)

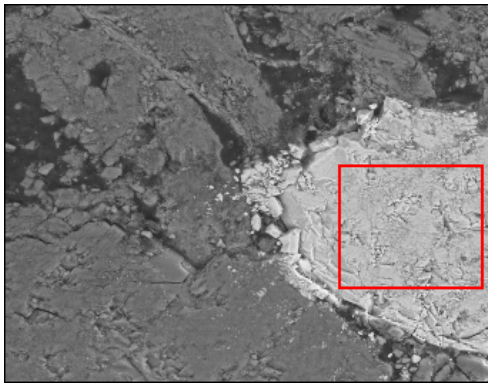

Element	Wt %
O	27.13
Al	0.59
Si	14.25
Pt	58.03

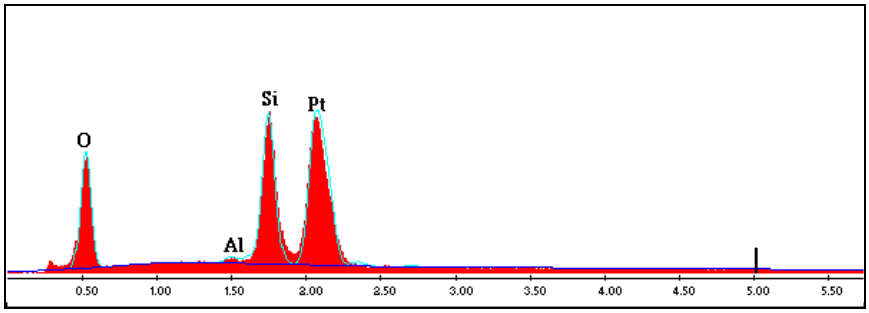

Figure 4. 16. EDX spectrum of the platinum containing particle. (RB-1).

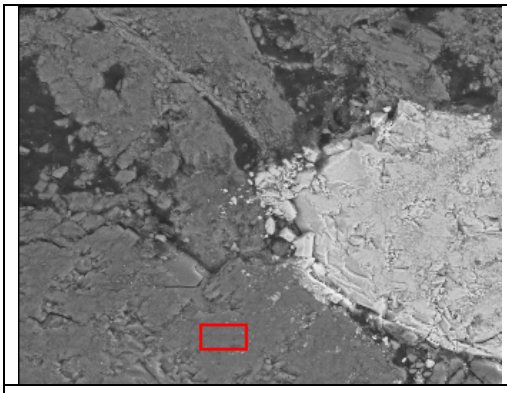

Element	Wt %
O	49.48
Na	5.88
Al	13.43
Si	25.80
K	1.27
Ca	4.13

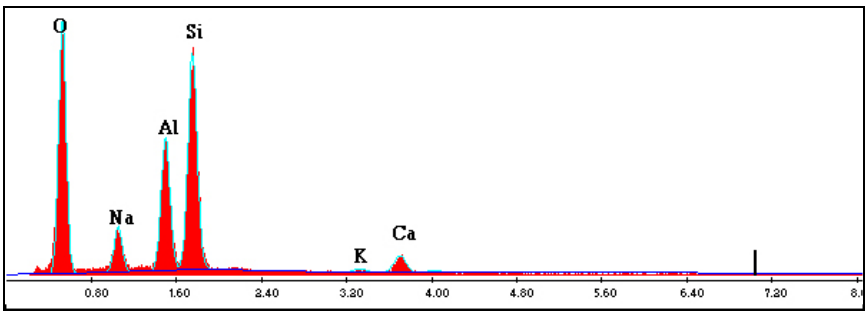

Figure 4. 17. Elemental composition of brick matrix. (RB-1)

Element	Wt %
O	32.11
Al	0.48
Si	13.03
Pt	54.38

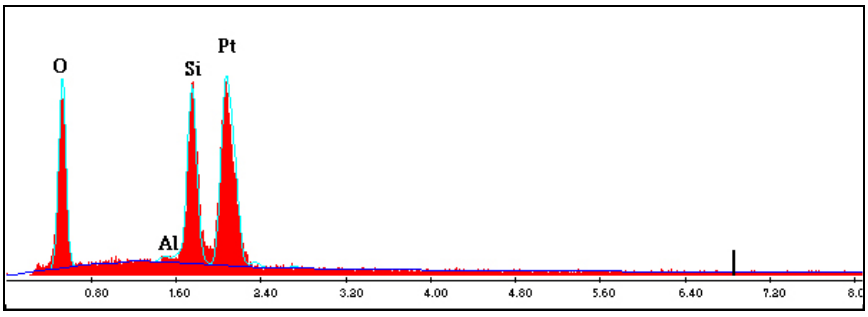

Figure 4. 18. EDX analysis of tiny platinum particle containing silicon (RB-1)

Element	Wt %
O	50.75
Na	3.04
Al	7.71
Si	34.82
K	3.69

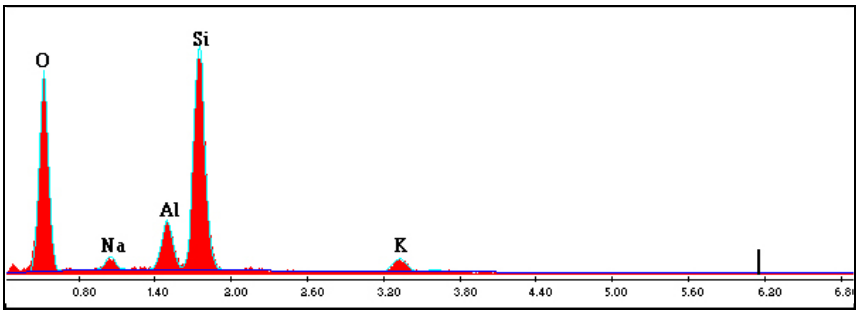

Figure 4. 19. Elemental composition of brick matrix (RB-1)

4.1.3 Pozzolanicity of Roman Bricks

Pozzolanic activities of bricks are found by measuring the electrical conductivity of saturated calcium hydroxide solution before and after the brick powders have been mixed. If the electrical conductivity difference values are higher than 1.2 mS/cm, they are thought to have good pozzolanic features (Luxan et al. 1989).

In the Roman bricks used in the construction of Serapis Temple, the values found were lower than that, which shows that these bricks did not have good pozzolanic properties (Figure 4.20). This may indicate that the raw materials containing clay minerals were not enough to produce high amounts of pozzolanic amorphous substances. Similar results were also observed in the bricks used in some historic structures (Baronia and Binda 1997).

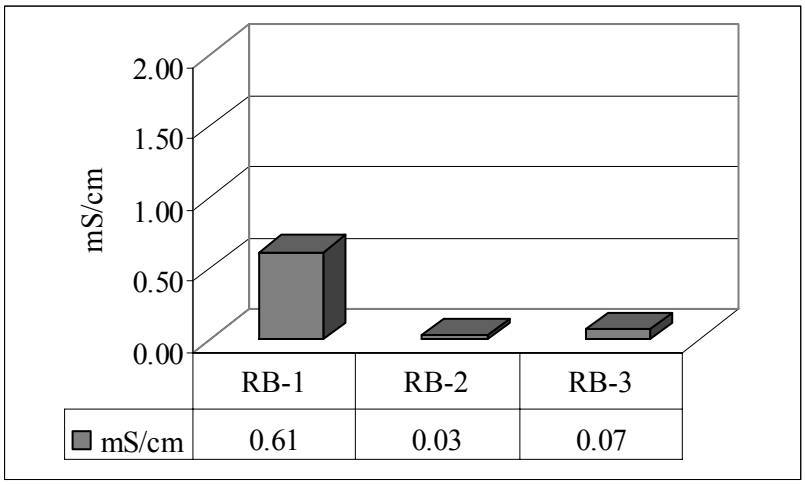

Figure 4. 20. Pozzolanic Activity values of Roman bricks.

4.2. Intervention Bricks

In order to find out the compatibility between the intervention bricks used in the restoration works at Serapis Temple in 1940s and the original Roman bricks, basic physical properties of these bricks, their mineralogical and chemical compositions as well as their micro-structural characteristics were identified.

4.2.1 Basic Physical and Mechanical Properties of Intervention Bricks

The intervention bricks have light brown color and fine textured matrix with some small grog particles (Figure 4.21).

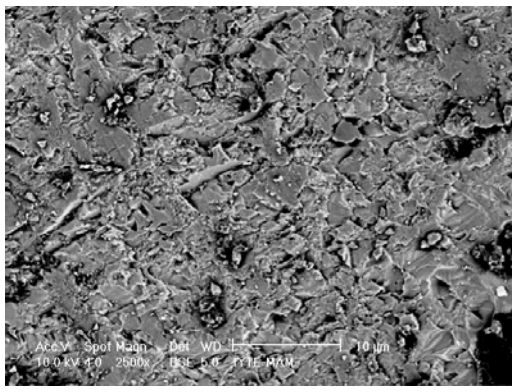

Figure 4. 21. BSE image of general texture of the intervention brick matrix (IB-4)

The porosity and density values of intervention bricks and original bricks found were nearly the same. The porosity values of intervention bricks ranged between 34 - 37 %, and the average value was 36 %. The apparent density values of intervention bricks varied between 1.5 - 1.6 gr/cm^3 , and the average value was 1.5 gr/cm^3. The real density values of intervention bricks varied between 2.3 - 2.4 gr/cm^3 and the average value was 2.4 gr/cm^3 (Figure 4.22).

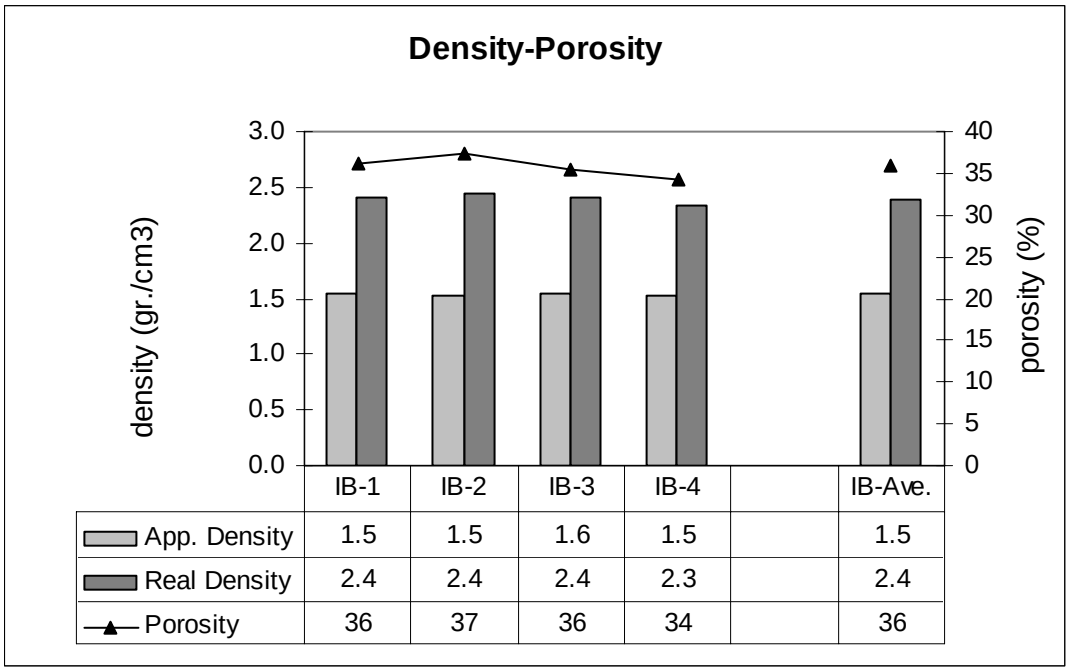

	IB-1	IB-2	IB-3	IB-4		IB-Ave.
App. Density	1.5	1.5	1.6	1.5		1.5
Real Density	2.4	2.4	2.4	2.3		2.4
Porosity	36	37	36	34		36

Figure 4. 22. % Porosity and density values of intervention bricks

Drying characteristics of the original and intervention bricks are similar. As the intervention bricks have a porous structure, fifty percent of the total water they absorbed evaporated in the first 15 minutes. Evaporation slowed dawn at the end of 6 days (Figure 4.23).

Their dry uniaxial compressive strength values were in the range of 4 – 9,7 MPa and their modulus of elasticities values were between 303.6 – 668.6 Mpa. These results show that the roman bricks and intervention bricks have nearly the same physical characteristics (Table 4.3).

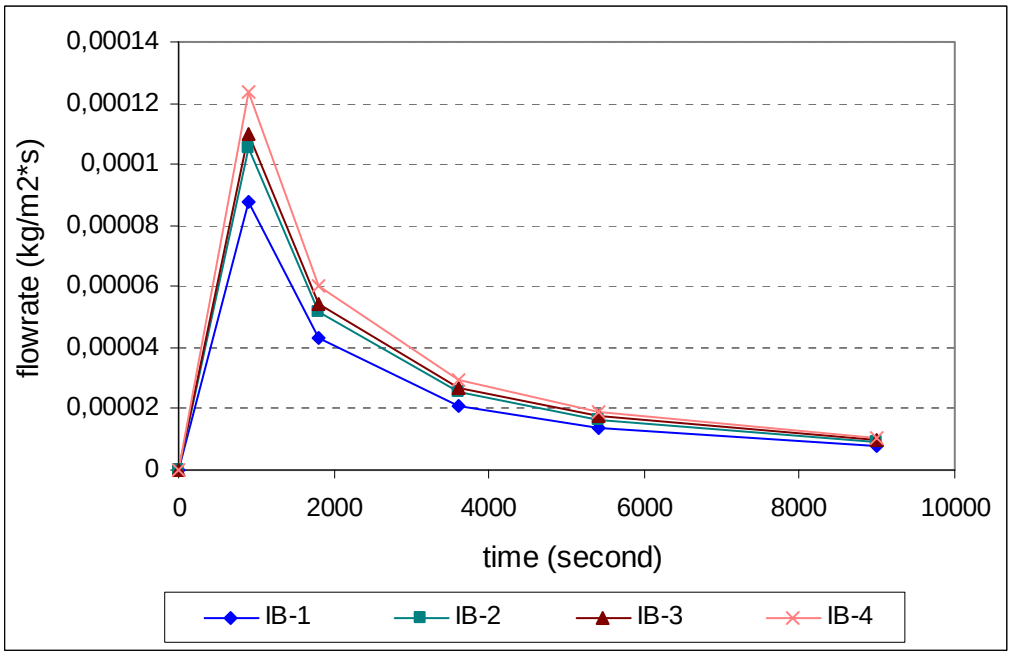

Figure 4. 23. Drying rates of the intervention bricks

Table 4. 3. Unixial Compressive Strength and Modulus of Elasticity values of intervention bricks in dry states

SAMPLE	COMPRESSIVE STRENGTH (MPA.)	MODULUS OF ELASTICITY (MPA.)
IB-1	9.7 MPa	668.6 MPa
IB-2	4 MPa	303.6 MPa
IB-3	8,8 MPa	495.2 MPa
IB-4	5.8 MPa	478.3 MPa

4.2.2. Mineralogical and Elemental Compositions and Microstructural Properties of Intervention Bricks

In the XRD patterns of the intervention brick samples, quartz, albite, potassium, feldspar, and hematite minerals have been observed (Figure 4.24 – 4.27). Absence of calcium -containing minerals in their XRD spectrum indicated that the used raw material sources were calcium poor clays. The absence of muscovite minerals in the intervention bricks may indicate that their raw material sources were not same with the

Roman ones. Presence of hematite peaks in the XRD spectrum shows that their baking temperature was over 850 °C. These results show that original Roman and intervention bricks had been baked at approximately the same temperatures.

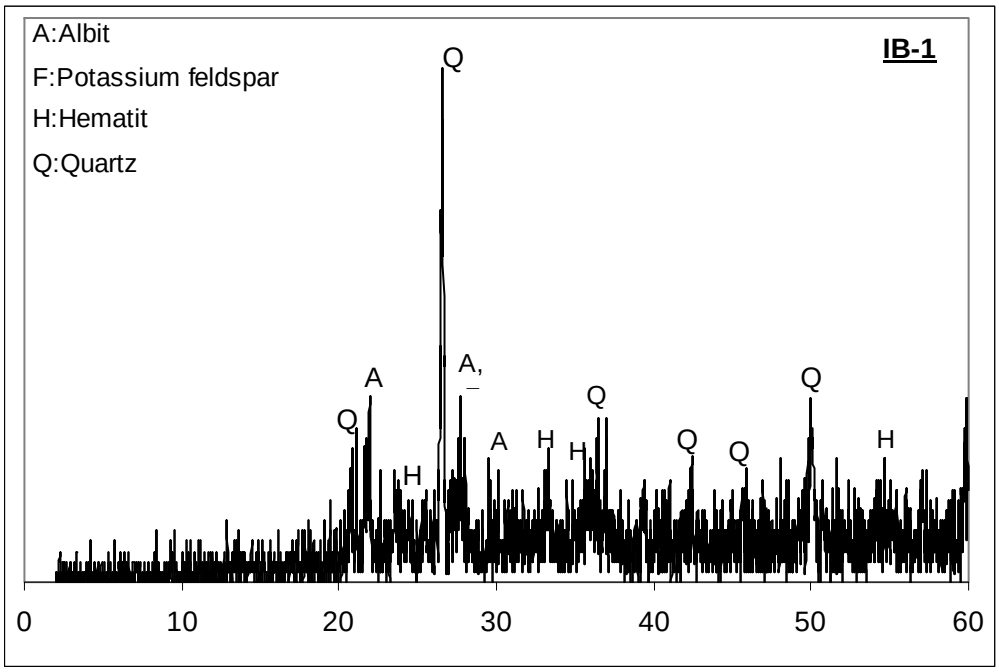

Figure 4. 24. XRD pattern of the intervention brick sample of IB-1

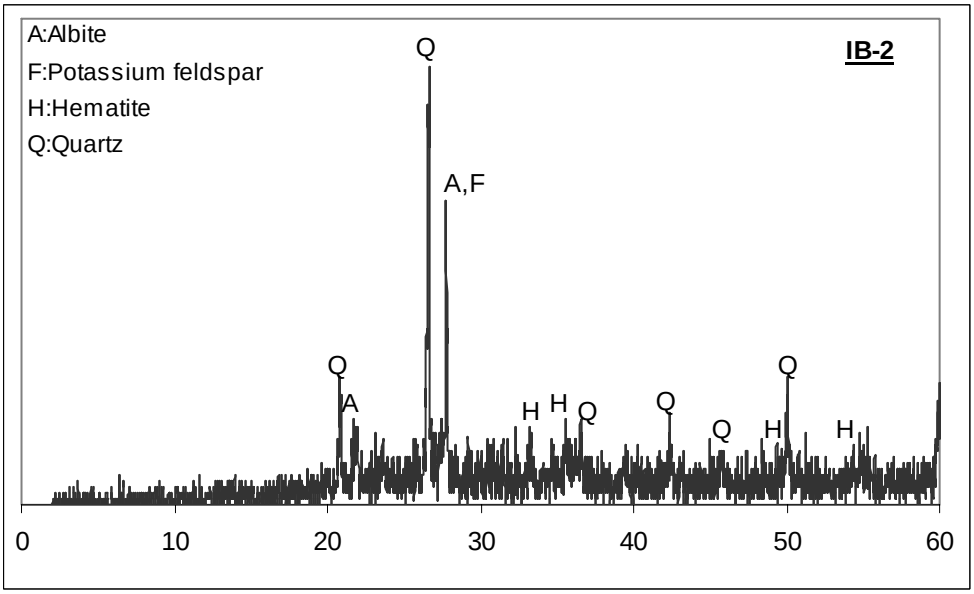

Figure 4. 25. XRD pattern of the intervention brick sample of IB-2

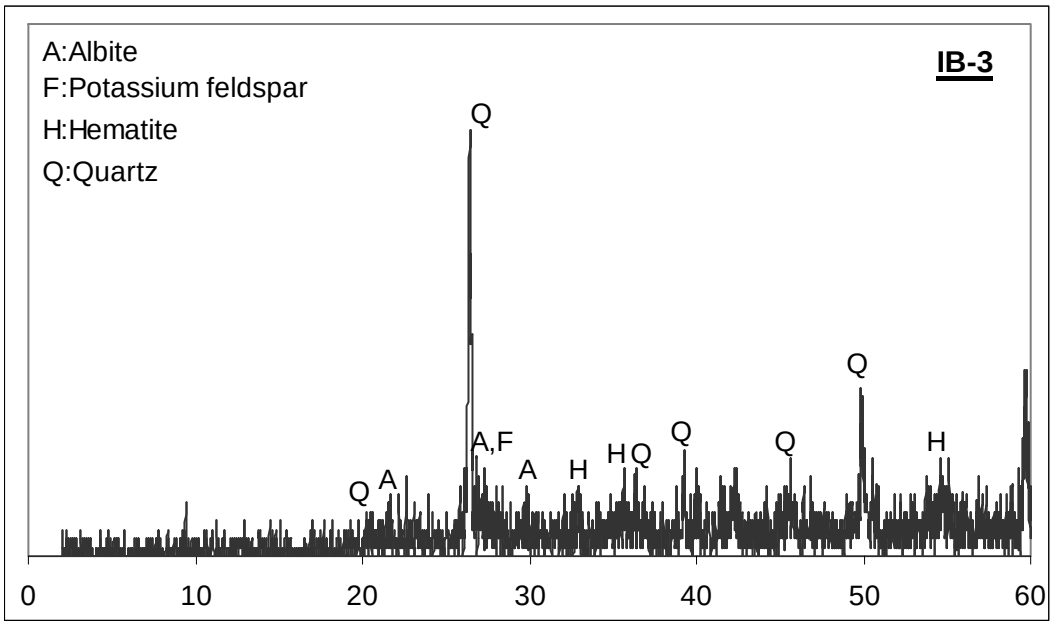

Figure 4. 26. XRD pattern of the intervention brick sample of IB-3

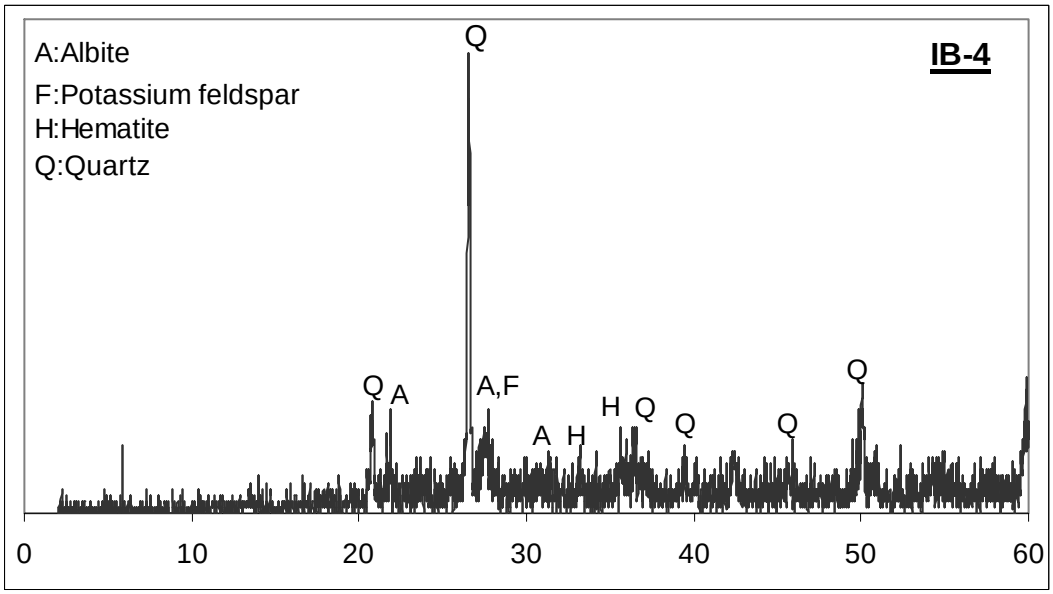

Figure 4. 27. XRD pattern of the intervention brick sample of IB-4

The elemental analyses of intervention bricks by EDS indicated that they were mainly composed of a high amounts of SiO_2, Al_2O_3, and moderate amount of Fe_2O_3 (Table 4.4). Their compositions are similar to those of Roman bricks. The presence of a small amount of calcium oxide indicates that calcium poor clays had been used in the preparation of the bricks. Quartz, albite and K-feldspar, which were found in XRD analyses, have been identified in the microstructures of the bricks, using the SEM-EDS

analyses (Figure 4.28 – 4.29). Glass-like structures were not indicated in the structure of intervention bricks, which shows that the bricks had been baked at low temperatures (<1000 °C) (Figure 4.30).

Table 4. 4. Elemental compositions of intervention bricks

SAMPLES	Fe_2O_3	Na_2O	MgO	Al_2O_3	SiO_2	K_2O	CaO
IB-1	9,8±1,5	1,9±0,4	2,6±0,3	20,4±0,3	59,7±1,8	3,7±0,6	2,0±0,1
IB-2	8,1±0,8	1,9±0,2	2,3±0,1	19,3±0,7	63,0±2,0	3,5±0,2	1,9±0,3
IB-3	11,3±2,0	2,2±0,3	2,8±0,3	20,9±0,2	57,3±2,0	3,9±0,4	1,6±0,1
IB-4	10,6±1,7	2,3±0,4	2,5±0,2	20,5±0,5	58,2±2,1	4,1±0,3	2,0±0,3

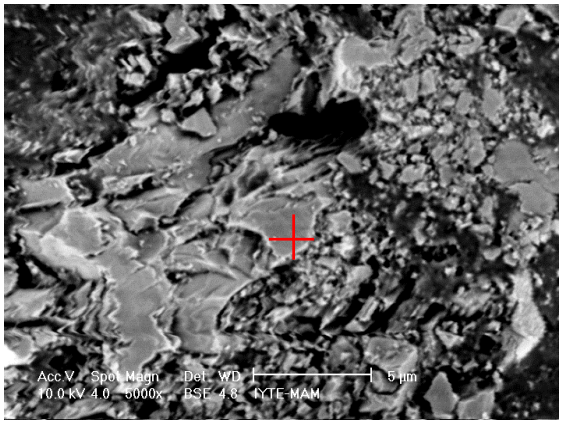

(5000x)

Element	Wt %
O	79.61
Na	1.56
Si	18.82

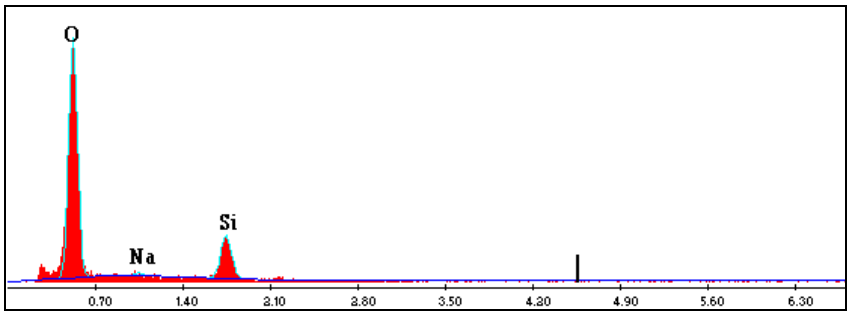

Figure 4. 28. BSE image, EDX spectrum and elemental composition (%) of quartz crystals in the intervention brick matrix. (IB-4)

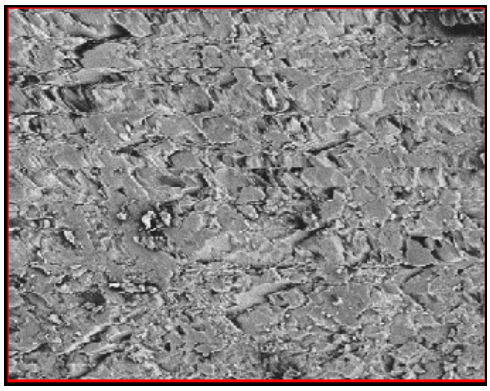

Element	Wt %
Na	10.73
Al	25.67
Si	63.60

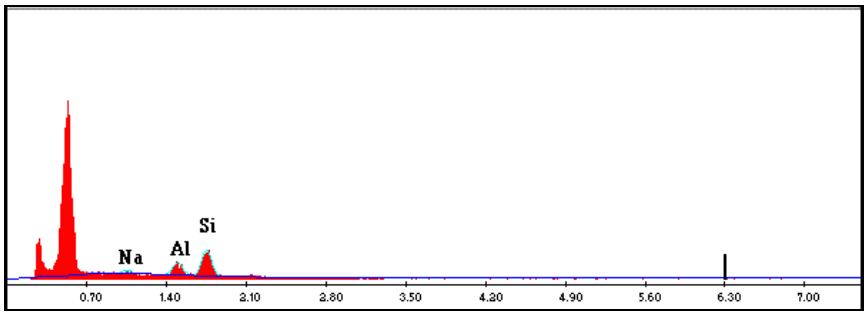

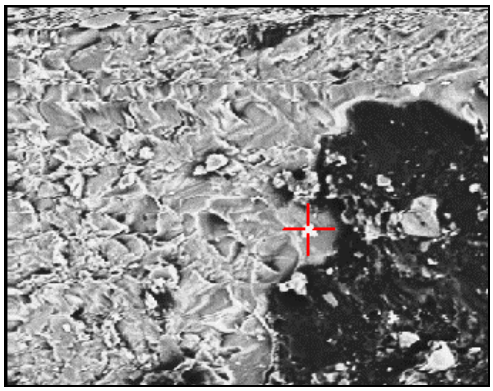

Element	Wt %
Na	8.81
Al	24.47
Si	66.72

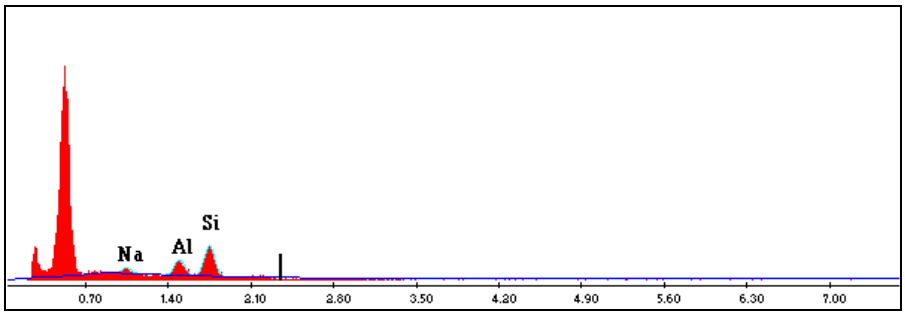

Figure 4. 29. BSE images, EDX spectrums and elemental compositions (%) of Albit crystals in the intervention brick matrix. (IB-4)

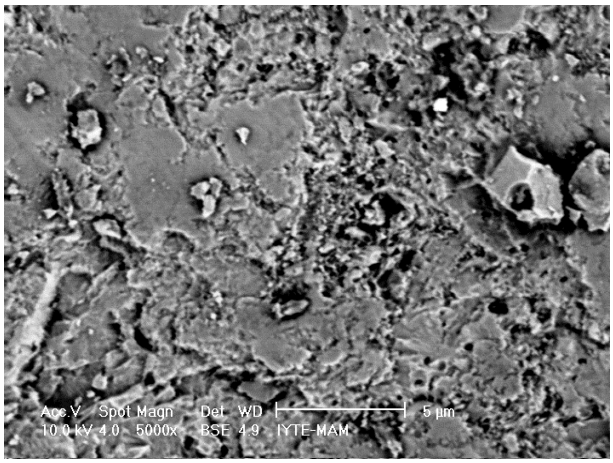

Figure 4. 30. BSE image of unglassy texture of the intervention brick matrix (IB-4)

4.2.3 Pozzolanicity of Intervention Bricks

The pozzolanic properties of the intervention bricks have been identified by the method used in Roman Period bricks, and it was found that the intervention bricks, just like Roman Period bricks, had low pozzolanic activity values (Figure 4.31).

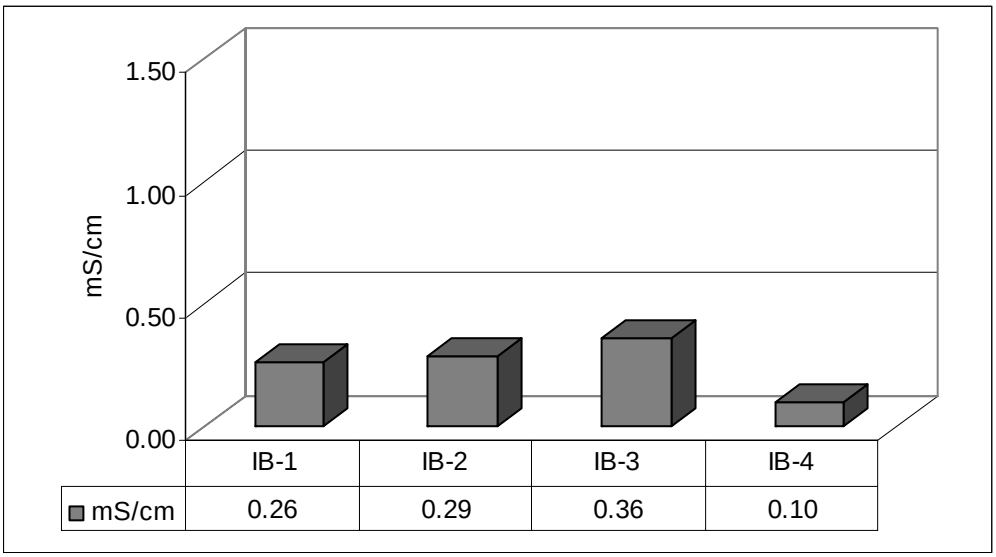

Figure 4. 31. Pozzolanic Activity values of intervention bricks

4.3. Roman Mortars

Romans generaly manufactured lime mortars by mixing lime with pozzolana to produce hydraulic mortars. In this study, the mortars used in the brick masonry of Serapis Temple have been investigated as to whether they are hydraulic or not.

4.3.1 Basic Physical and Mechanical Properties of Roman Mortars

Roman mortars have a stiff and compact appearance. Their porosity values were 34 and 38 % , and their average value was 36 %. The apparent density values of mortars were 1.5 gr/cm^3. The real density values of mortars were in the range of 2.3 - 2.5 gr/cm^3 , and their average value was 2.4 gr/cm^3. The results indicated that they are high porous and low dense mortars (Figure 4.32).

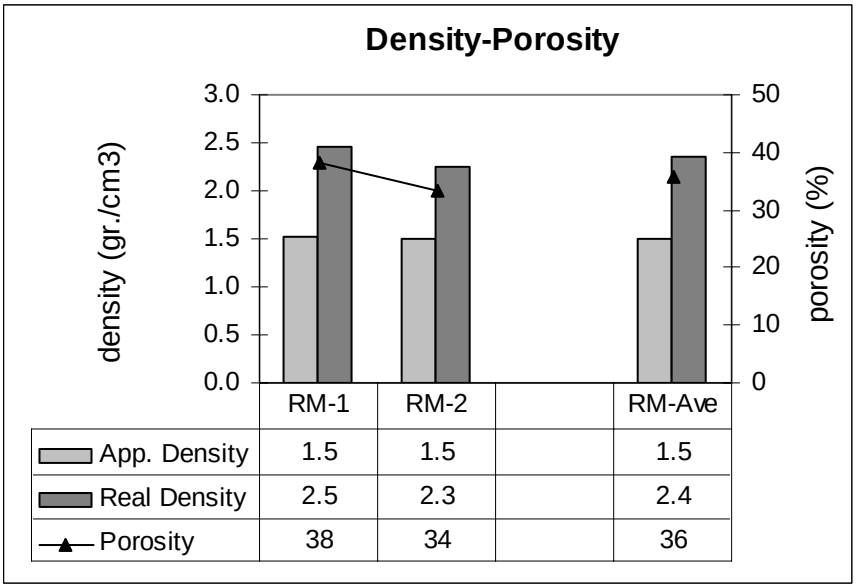

	RM-1	RM-2		RM-Ave
App. Density	1.5	1.5		1.5
Real Density	2.5	2.3		2.4
Porosity	38	34		36

Figure 4. 32. Porosity and density of Roman mortars

The drying rate of mortars shows that 50 % adsorbed water evaporated within 15 minutes. This indicates that they have a mostly macro porous structure (Figure 4.33). Their compressive strength value was 6,6 MPa and their modulus of elasticity was

630,6 MPa. (Table 4.5). These main physical properties of the mortars are similar with those of some Roman mortars (Güleç and Tulun 1997, Sánchez-Moral et al. 2004).

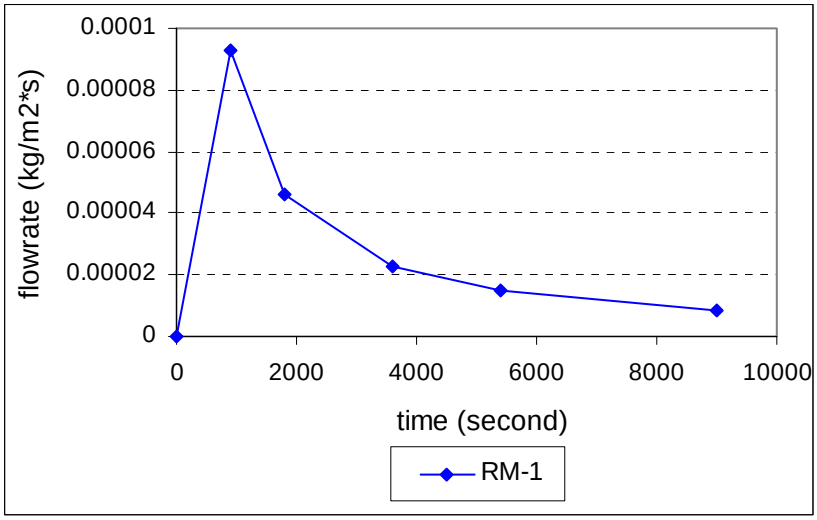

Figure 4. 33. Drying rates of the Roman mortar by weight loss versus time and surface area

Table 4. 5. Unixial Compressive Strength and Modulus of Elasticity values of Roman mortar in dry states.

SAMPLE	COMPRESSIVE STRENGTH (MPA.)	MODULUS OF ELASTICITY (MPA.)
RM-1	6.6 MPa	630.6 MPa

4.3.2 Raw Material Compositions of Roman Mortars

Lime/aggregate ratios of original Roman mortars were around 1:4 by weight (Figure 4.34 and Table 4.6). The aggregates with particle sizes greater than 1180 µm are composed the largest fraction of the total aggregates used in original Roman mortars. This largest fraction was about 38 % (Figure 4.35).

These values differed from lime percents of several mortars used in Roman period and other historic brick masonry mortars (Adam 1989, Böke et al. 2004, Çizer 2004, Tunçoku 2001).

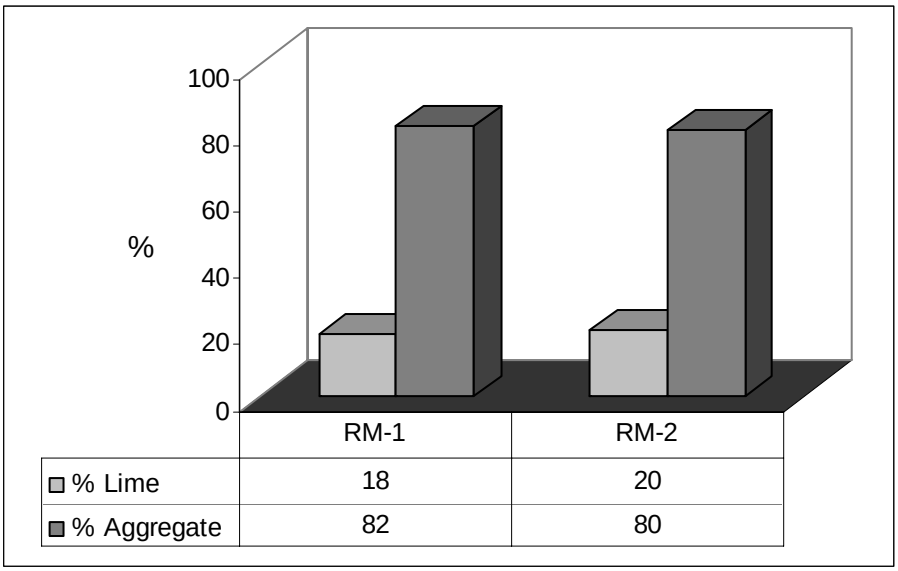

Figure 4. 34. Lime-Aggregate ratios of Roman mortars

Table 4. 6. Lime-Aggregate ratios of Roman mortars

Sample	Lime/aggregate ratio
RM-1	1 : 4,5
RM-2	1 : 4

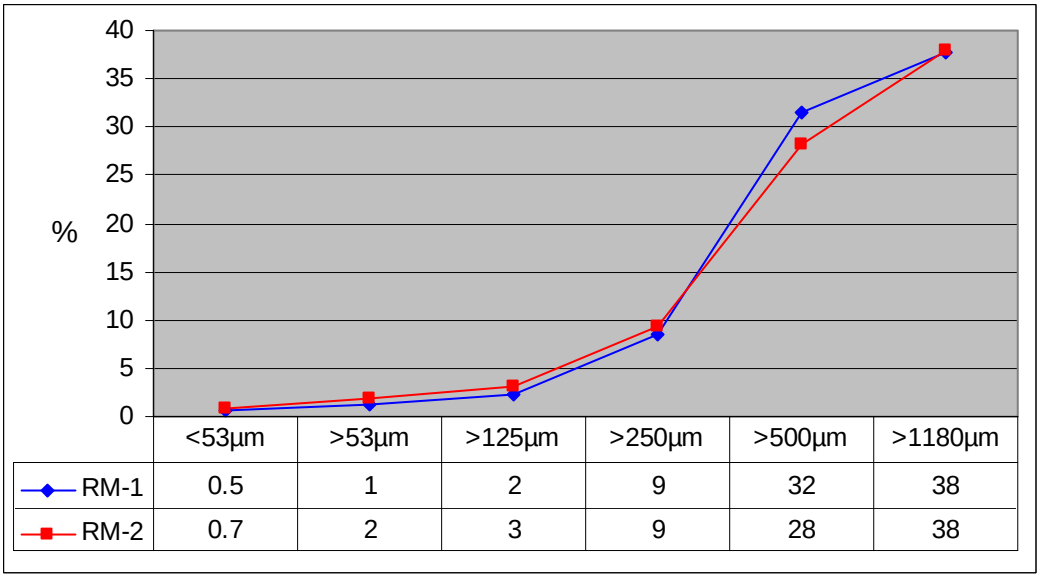

Figure 4. 35. Particle Size Distribution curves of the aggregates used in Roman mortars

4.3.3 Pozzolanic Activity of Aggregates of Roman Mortars

Hydraulic lime mortars were manufactured by mixing lime with either natural or artificial pozzolanas and have been used since ancient times. The Romans used generally natural pozzolana to produce hydraulic mortars. In this work, the pozzolanacity of the agrregates are determined whether to know if natural pozzolana were used or not in the brick masonry mortars of the temple.

Pozzolonic activities of the fine aggregates used in Roman mortars were found to be about 7 mS/cm (Figure 4.36). This show that the aggregates can be considered very good pozzolan which acquires a hydraulic character of the mortar.

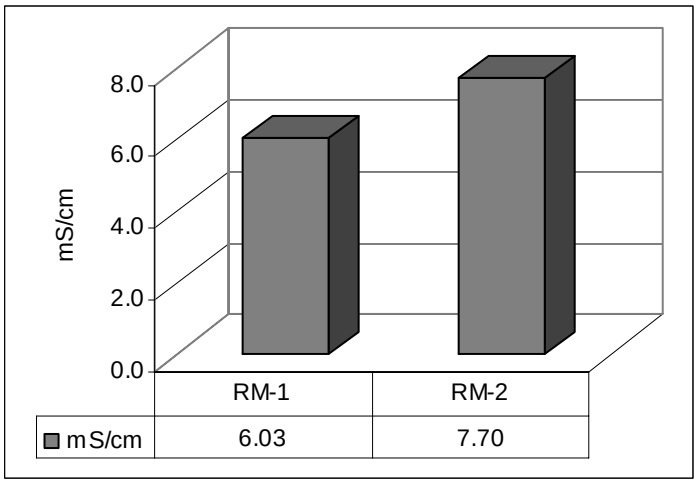

Figure 4. 36. Pozzolanic Activity measurements of fine aggregates of Roman mortars (less than 53 μm).

4.3.4 Mineralogical Compositions of the Mortar Matrices and Agregates

XRD patterns of the Roman mortar matrices showed that they were mainly composed of calcite and quartz (Figure 4.37 – 4.38). Calcite originated from carbonated lime while quartz from fine aggregates. Although the the pozzolanic characters of the aggregates were found by conductivity measurements, the expected peaks of calcium silicate hydrates and calcium aluminate hydrate were not observed. This may be due to their amorphous characters (Haga et al. 2002).

XRD patterns of fine aggregates used in the Roman mortars showed that they were composed of albite, K-feldspar and quartz. In their XRD patterns, a diffuse band between 20-30 degrees was observed. This band showed the presence of pozzolanic amorphous silica confirmed by pozzolanicity test is the natural pozzolanic materials which give hydraulic character of the lime mortars (Figure 4.39).

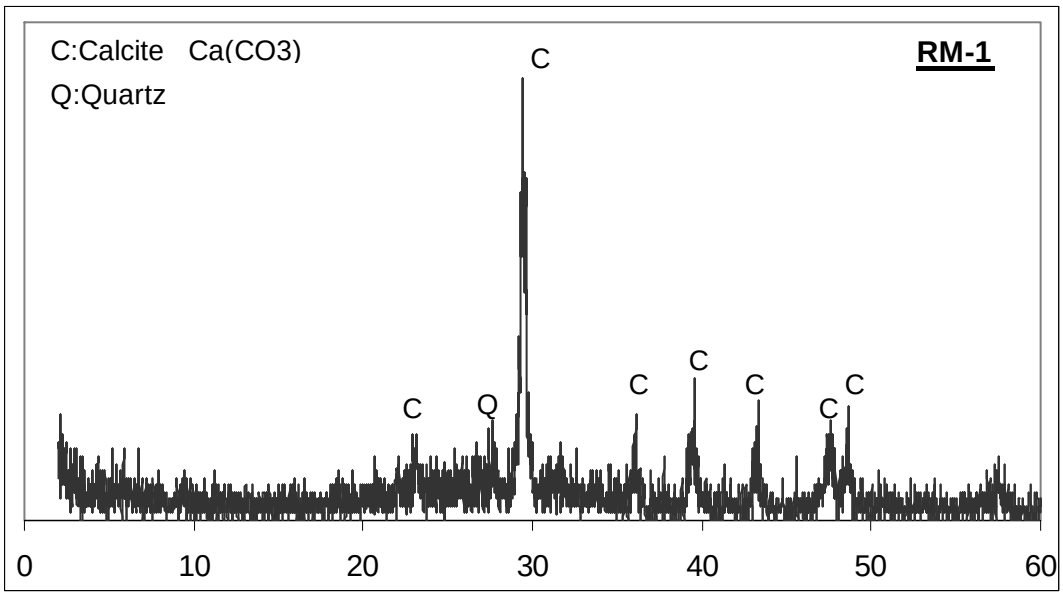

Figure 4. 37. XRD patterns of the Roman mortar matrices

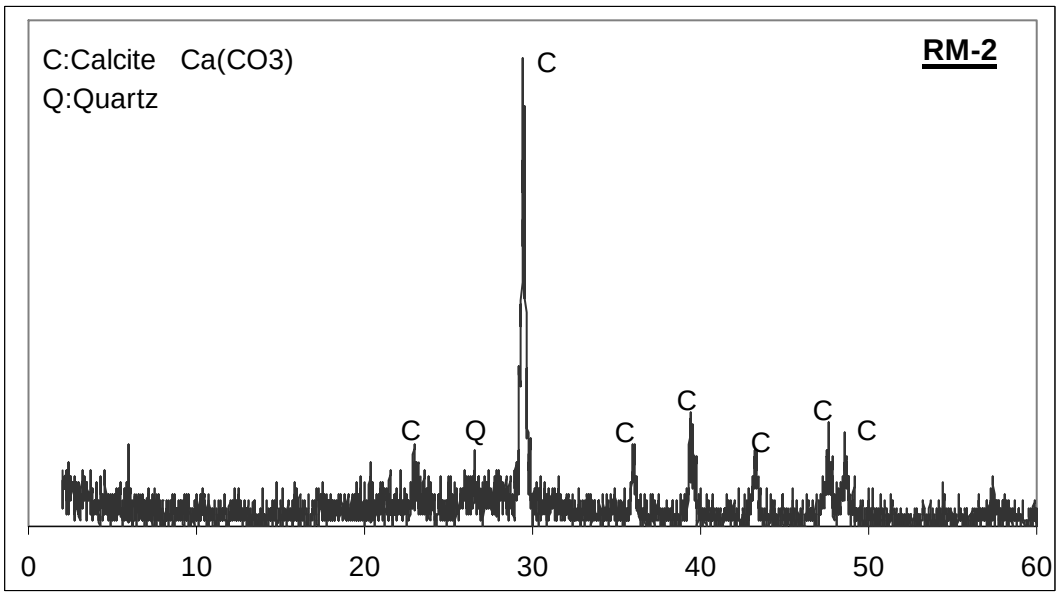

Figure 4. 38. XRD patterns of the Roman mortar matrices

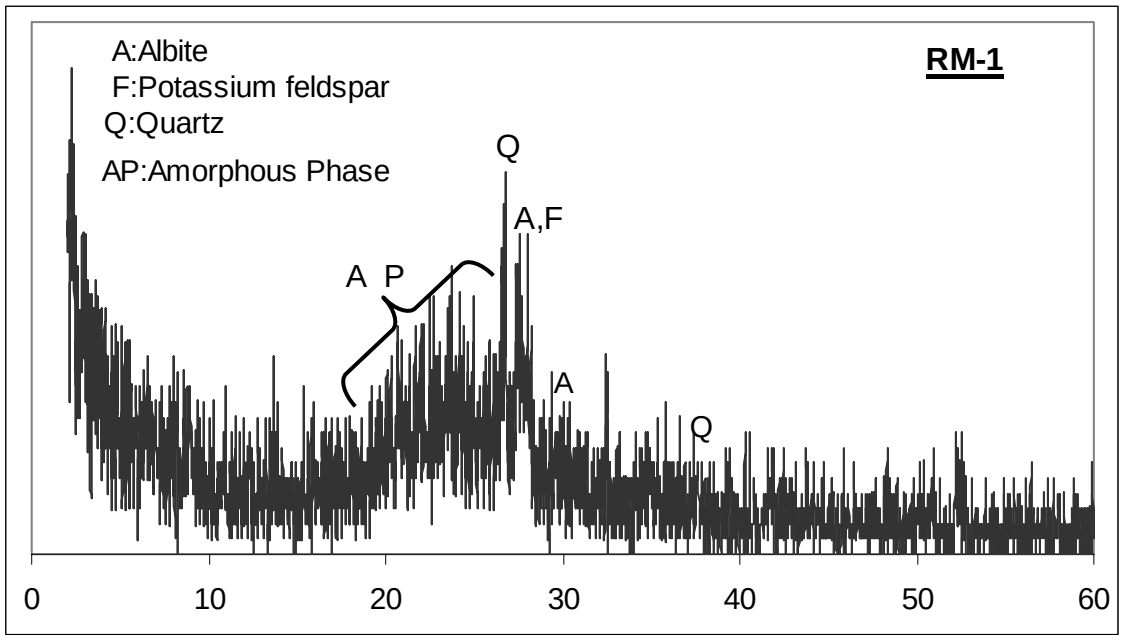

Figure 4. 39. XRD pattern of the fine aggregates used in Roman mortar

4.3.5 Elemental Compositions and Microstructural Properties of Roman Mortars

Roman mortars have a stiff and compact appearance. The cohesion between aggregates and lime is strong. Lime-aggregate interface is generally free from fissures and cracks (Figure 4.40-4.41).

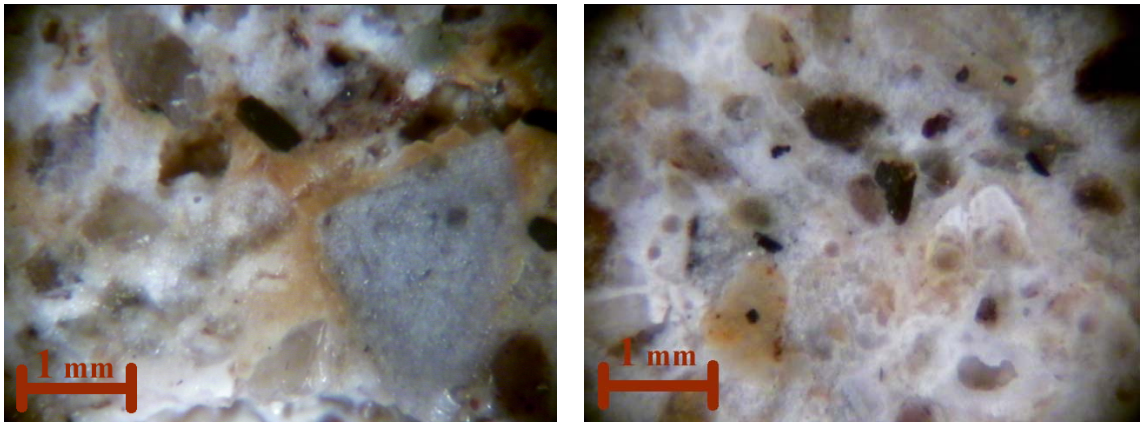

Figure 4. 40. Stereo microscope images showing good adhesion between aggregates and lime (RM-1).

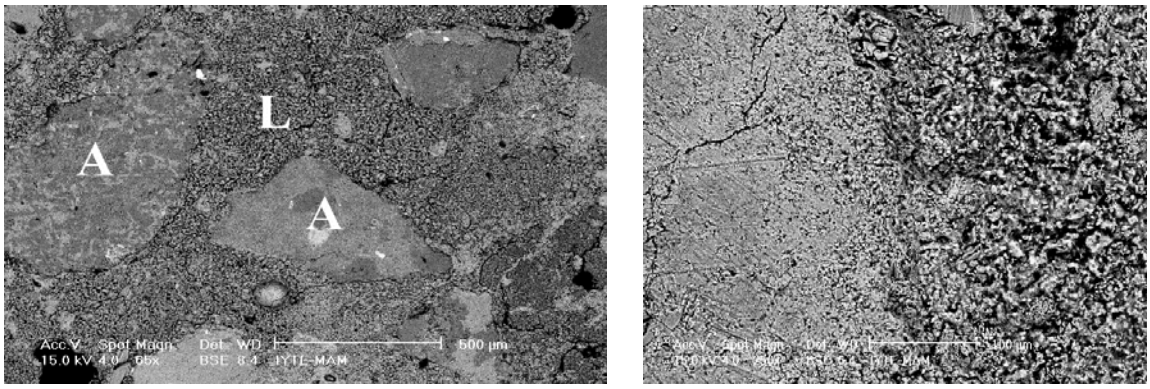

(65x) (250x)

Figure 4. 41. BSE images showing good adhesion between aggregates and lime (RM-1). A: Aggregate , L: Lime

The aggregates used in the mortars were very porous and mostly semi-rounded (Figure 4.42). They are mainly soft and easily granulated. They have mostly grey color. Their micropores are very fine and irregular (Figure 4.43). This fine porous structure gives good elasticity to the amorphous silica (Davraz and Gunduz 2004). Their SEM images show glassy phases in the amorphous pozzolanic aggregates (Figure 4.44). The glassy amorphous silica accelerates the formation of calcium silicate hydrates.

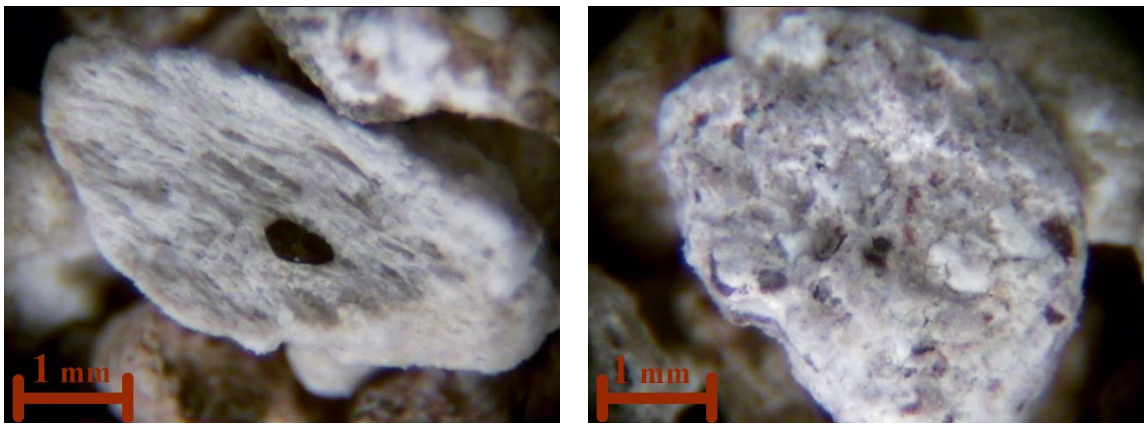

Figure 4. 42. Stereo microscope image of aggregates used in Roman mortar (RM-1)

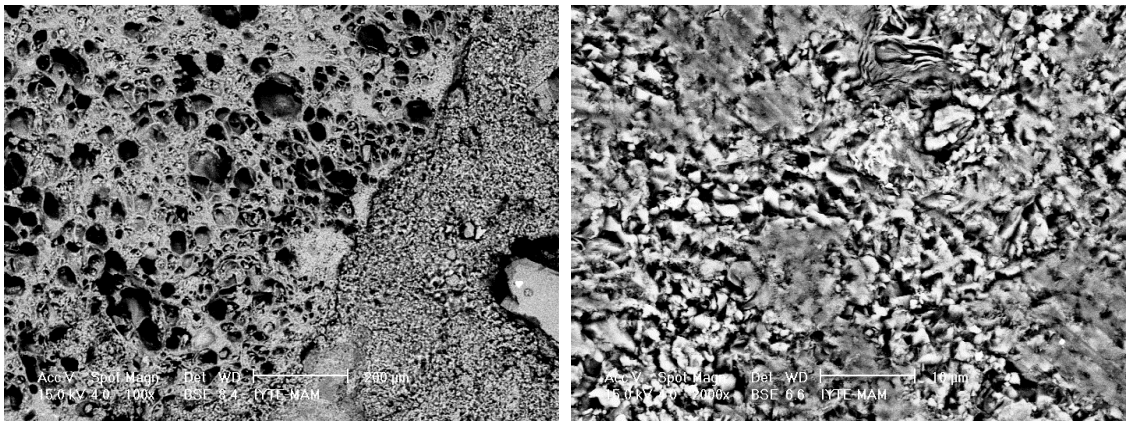

(100x) (2.000x)

Figure 4. 43. BSE images of very porous aggregates in the mortar matrix (RM-1)

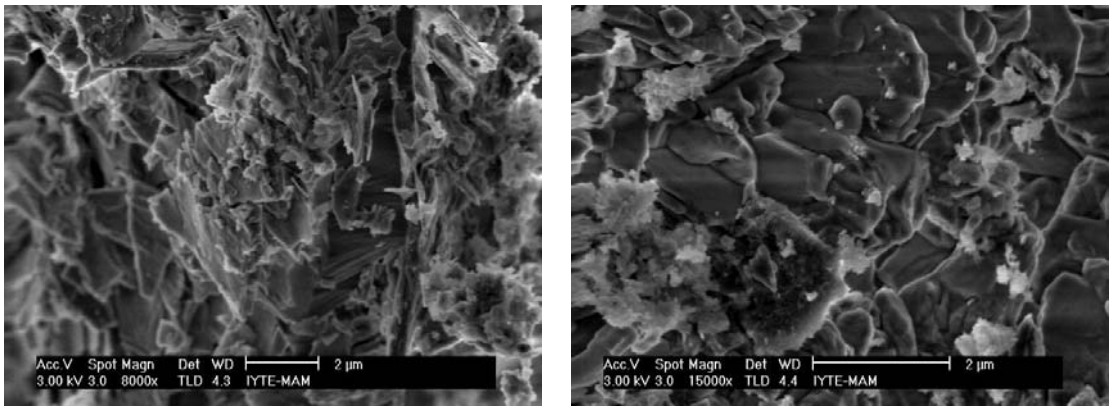

(8000x) (15000x)

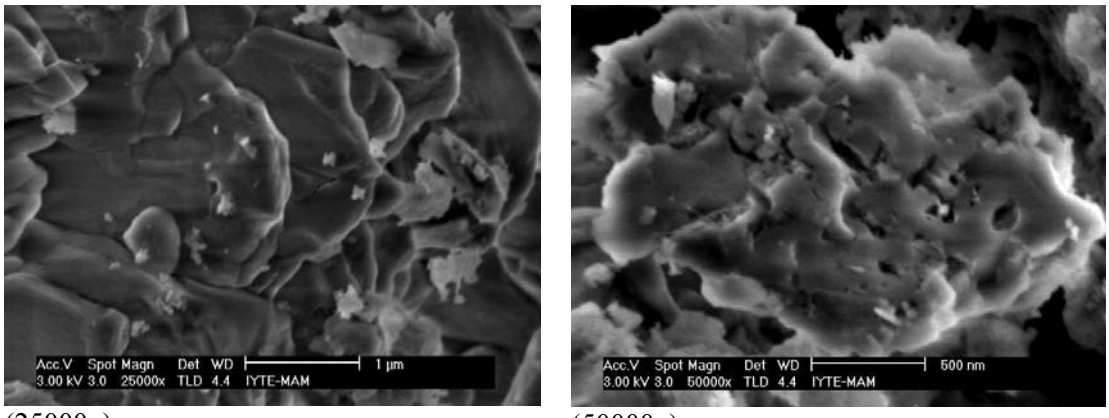

(25000x) (50000x)

Figure 4. 44. SE (secondary electron) images of glassy phases in the amorphous pozzolanic aggregates (RM-1)

The elemental composition analysis of the aggregates by SEM-EDS analyses indicated that they were mainly composed of a high amount of SiO_2, Al_2O_3, Fe_2O_3 and

minor amounts of Na_2O, MgO, K_2O and TiO_2 (Table 4.7). The high amorphous silica content of the aggregates and their high surface area make them reactive substances when in contact with lime.

Table 4. 7. Elemental compositions of fine aggregates used in the Roman mortars

SAMPLES	Fe_2O_3	Na_2O	MgO	Al_2O_3	SiO_2	K_2O	TiO_2
RM-1	9,1±2,3	2,1±0,2	1,4±0,2	5,6±0,1	80,1±2,5	1,0±0,1	0,8±0,5

Chemical composition of white lumps representing the lime used in Roman mortars were determined by SEM-EDS analyses (Figure 4.45). EDS analysis shows that the white lumps are mostly composed of CaO. This analysis indicated that lime used in the perapation of mortars is nearly pure.

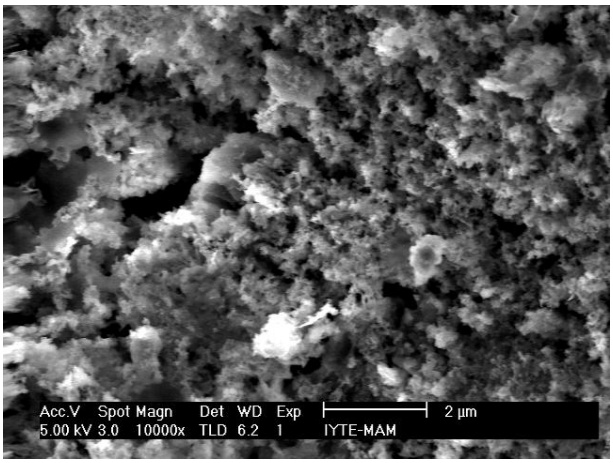

(10.000x)

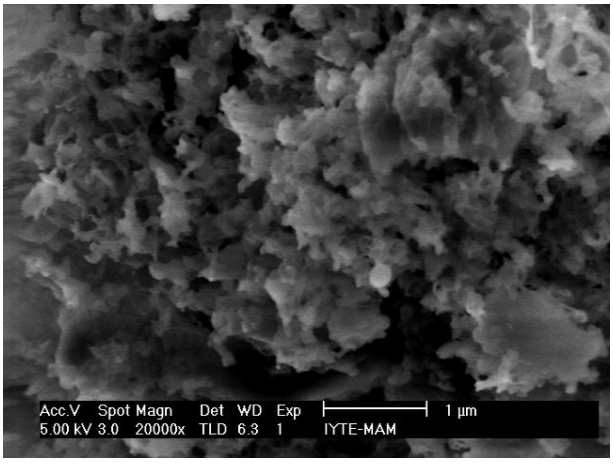

(20.000x)

Figure 4. 45. SE images of white lumps (RM-1)

Microstructural characteristics of mortar matrices with fine aggregates were determined by SEM analysis. The mortar matrices exhibit uniform structure with their fine pores. The fine pores occuped about 30 % of the whole matrices determined by phase analysis by SEM (Figure 4.46). The uniform matrices may show the well mixing process of lime with fine aggregates.

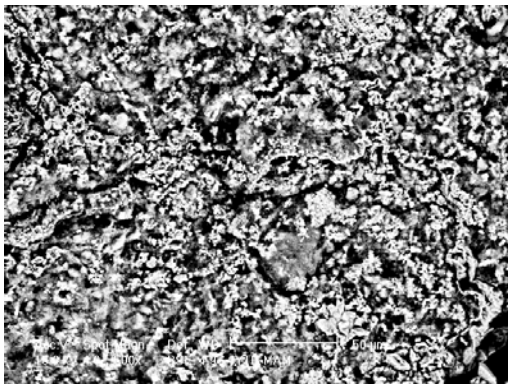

(500x)

Figure 4. 46. BSE image of the mortar matrices with fine aggregates (RM-1)

Gel like formations composed of mainly calcium, silicon and aluminium were observed in the mortar matrices with fine aggregates (Figure 4.47-4.48). This may indicate the formation of hydraulic reaction products (calcium silicate hydrates and calcium aluminate hydrates) formed by the reaction with lime and pozzolanic fine aggregates (Haga et al. 2002). Formation of these compounds provide strong adhesion bonds which make the mortar durable and stiff.

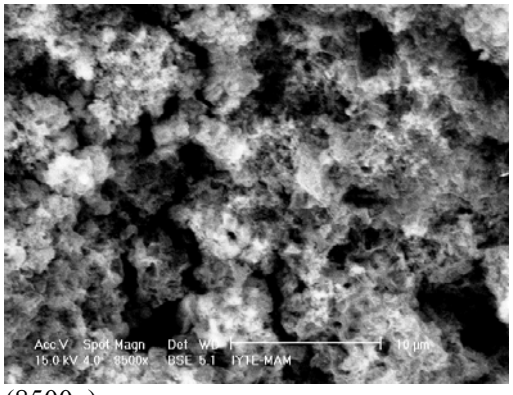

(8500x)

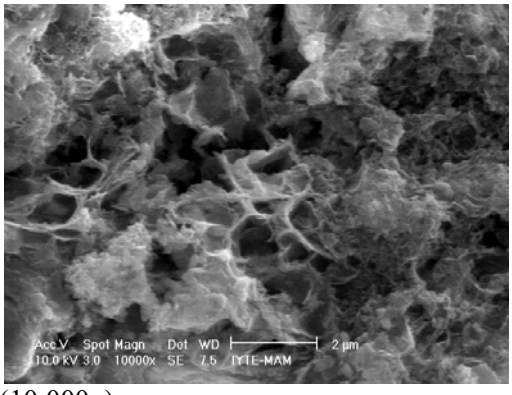

(10.000x)

Figure 4. 47. BSE and SE images of calcium aluminum silicate hydrate crystals in Roman mortar (RM-1)

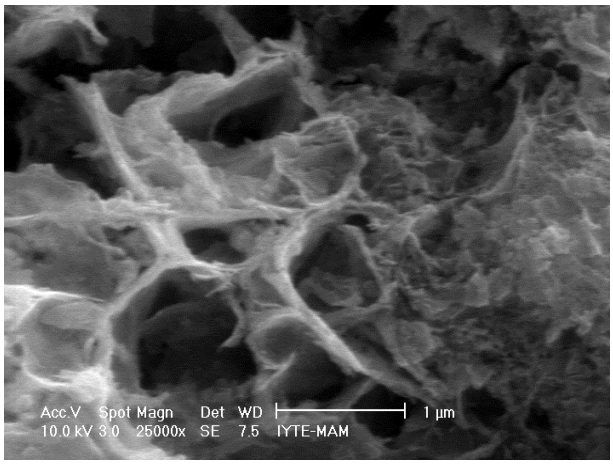

(25.000x)
(A)

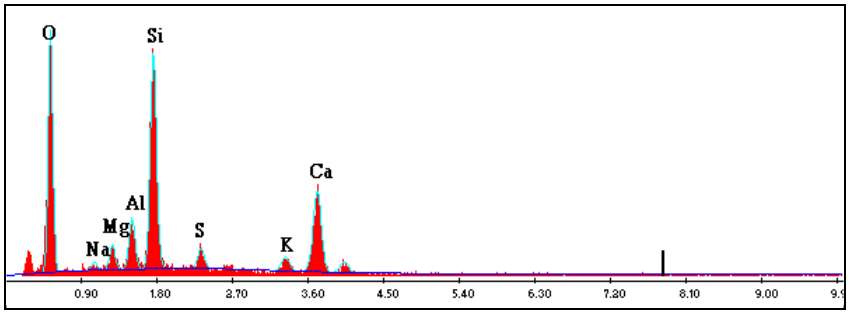

(B)

Figure 4. 48. SE electron image of calcium aluminum silicate hydrate crystals found in Roman mortar (A) and its EDS spectrum (B).

4.3.6. Hydraulicity of Roman Mortars by TGA

For the evaluation of hydraulic characteristic of Roman mortars, thermogravimetric analyses (TGA) were carried out. Percentages of weight losses at temperatures between 200°C and 600°C, and temperatures over 600°C were determined. Weight loss at the temperatures between 200°C and 600°C was mainly due to the loss of structurally bound water (H_2O) of hydraulic reaction products (C-S-H, C-A-H, etc.). Weight loss at the temperatures over 600°C was mainly attributed to the release of carbon dioxide gas (CO_2) during the decomposition of calcium carbonates (Bakolas et al. 1998, Moropoulou et al. 2000b).

Thermal analysis results of several lime mortars from different periods revealed that non-hydraulic lime mortars commonly contain CO_2 over 30 % and structurally bound water (H_2O) lower than 3 %. However, in hydraulic lime mortars, CO_2 content

was less than 30 % and H_2O content more than 3 % (Maravelaki-Kalaitzaki et al. 2002, Moropoulou et al. 2002a, Moropoulou et al. 2000b). Having regard to these results, hydraulicity of lime mortars was commonly evaluated by the ratio of CO_2 / H_2O. This ratio varied between 1 and 10 for hydraulic lime mortars and between 10 and 35 for non-hydraulic lime mortars (Moropoulou et al. 2003, Maravelaki-Kalaitzaki et al. 2002, Moropoulou et al. 2000b).

Roman mortar sample of RM-1 contained structurally bound water of 2.33 % and 6.87 % carbon dioxide (Figures 4.49 and Table 4.8). The CO_2 / H_2O ratio was 2.95. This result indicated that Roman mortars could be regarded as hydraulic lime mortars.

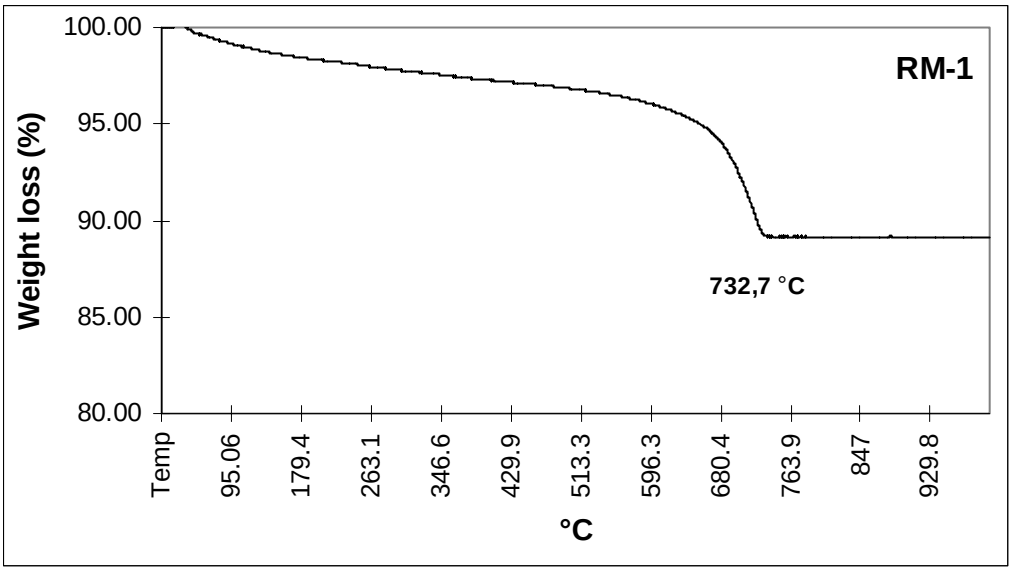

Figure 4. 49. TGA graph of the Roman mortar

Table 4. 8. Structurally bound water (H_2O) percent, carbon dioxide (CO_2) percent and CO_2 / H_2O ratio of Roman mortar.

Sample	H_2O (%)	CO_2 (%)	CO_2/ H_2O
RM-1	2.33	6.87	2.95

4.4. Byzantine Mortars

The Romans used natural pozzolana to produce hydraulic mortars. In the later Roman empire, and especially during the Byzantine times, crushed bricks were also used as artificial pozzolana. In this section, the properties of the Byzantine times mortars used in the Serapis Temple are given and their properties are compared with Roman ones.

4.4.1 Basic Physical and Mechanical Properties of Byzantine Mortars

Byzantine mortars have a stiff and compact appearence like Roman mortars. But, they were slightly less porous and high dense than the Roman mortars. The apparent density of them is about 1.7 gr/cm^3 and the real density value was 2.6 gr/cm^3. The porosity value was 34 % (Figure 4.50).

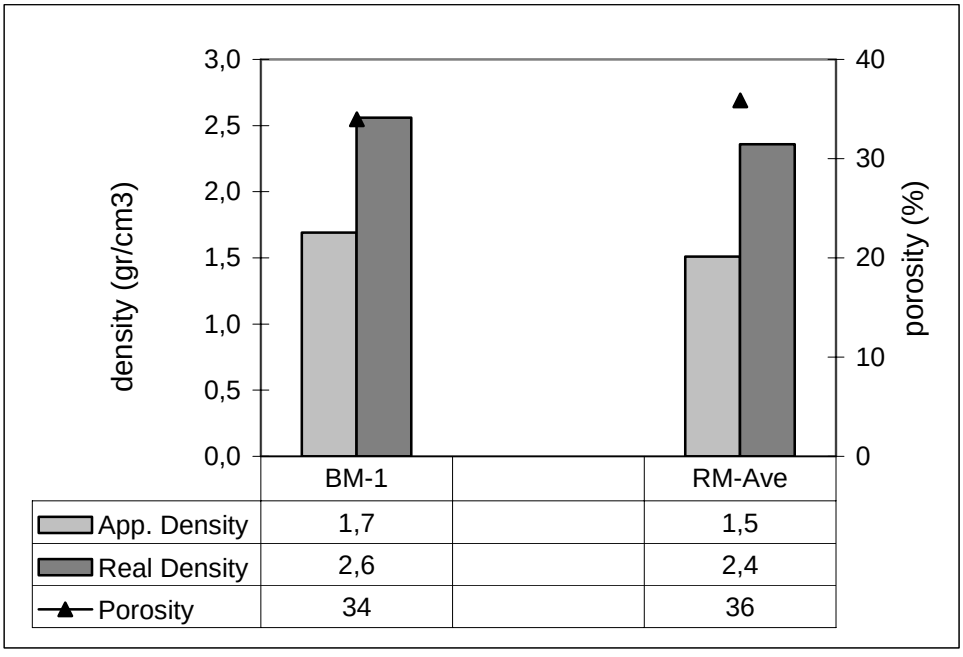

	BM-1		RM-Ave
App. Density	1,7		1,5
Real Density	2,6		2,4
Porosity	34		36

Figure 4. 50. Porosity and density values of Byzantine mortar and average value of Roman mortars.

The 50% adsorbed waters in the saturated mortars evaporate within 15 minutes like roman mortars (Figure 4.51). This indicates that they have mostly macro porous structure.

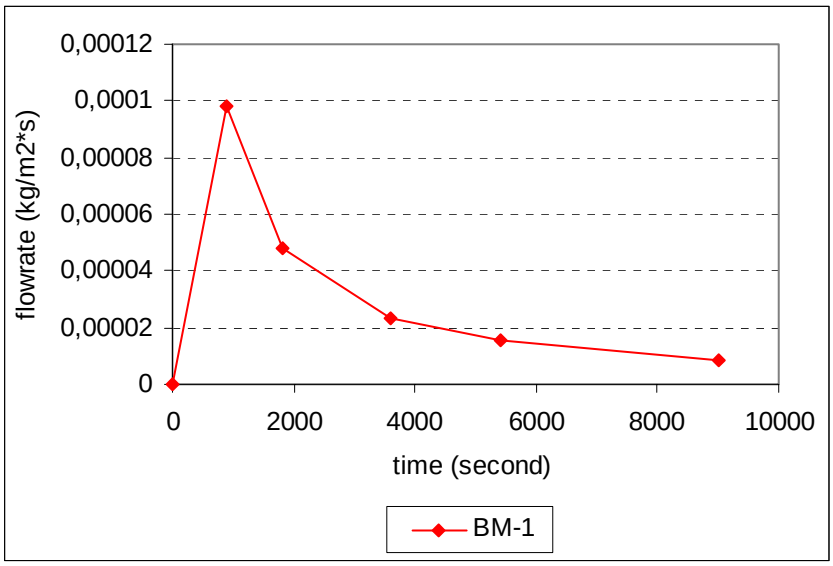

Figure 4. 51. Drying rates of the Byzantine mortars by weight loss versus time and surface area.

Their compressive strength value was found about 6,4 MPa and their modulus of elasticity was found 428.6 Mpa (Table 4.9). These results show that the main physical properties of Byzantine mortars are compatible with the those of Roman ones.

Table 4. 9. Unixial Compressive Strength and Modulus of Elasticity values of Byzantine mortar in dry states.

SAMPLE	COMPRESSIVE STRENGTH (MPA.)	MODULUS OF ELASTICITY (MPA.)
BM-1	6,4 MPa	428.6 MPa

4.4.2 Raw Material Compositions of Byzantine Mortars

Lime/aggregate ratios of Byzantine mortars were found nearly 1: 5 by weight (Figure 4.52). The coarse aggregates (<1180 micrometre) composed the largest fraction of the total aggregates in the mortars (Figure 4.53). This results may show that the manufacturing of Byzantine mortars were nearly the same when considering the lime and aggregate ratios and particle size distribution of the aggregates.

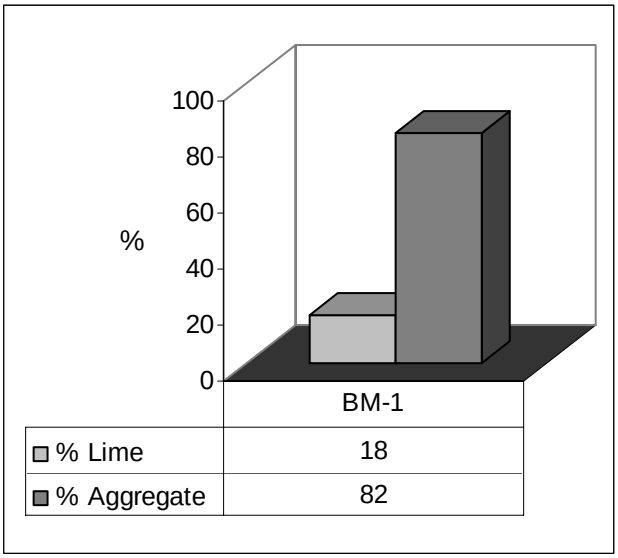

Figure 4. 52. Lime-Aggregate ratios of Byzantine mortars

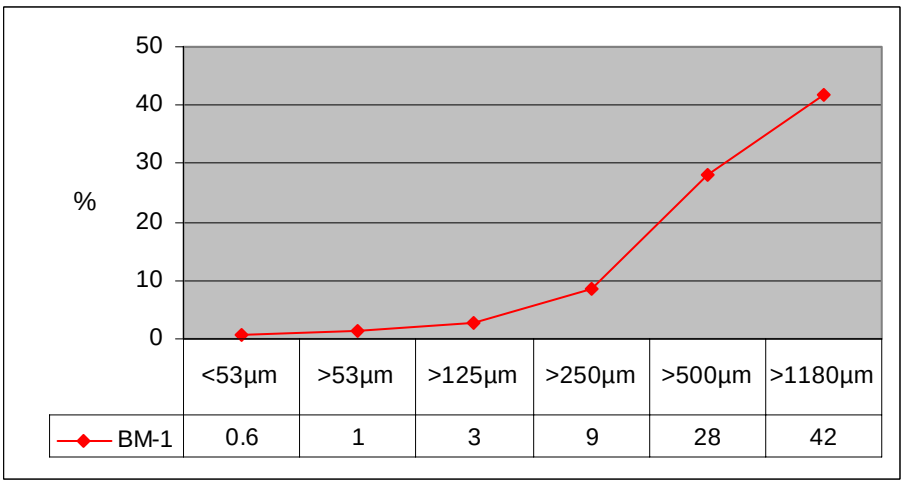

Figure 4. 53. Particle Size Distribution curves of the aggregates used in Byzantine mortars

4.4.3 Pozzolanic Activity of Aggregates of Byzantine Mortars

Brick aggregates as well as sand aggregates were used in Byzantine mortars. The pozzolanic properties of these aggregates were identified separately.

The range of the electrical conductivity value of fine natural aggregates used in lime mortars was found to be 7.72 mS/cm, and the same value was found as 3.23 mS/cm for brick powder (Figure 4.54). These results indicate that natural and artificial aggregates are pozzolanic. However, it is difficult to explain why natural pozzolans as well as crushed bricks with pozzolanic properties had been added to this mortar in the Byzantine Period.

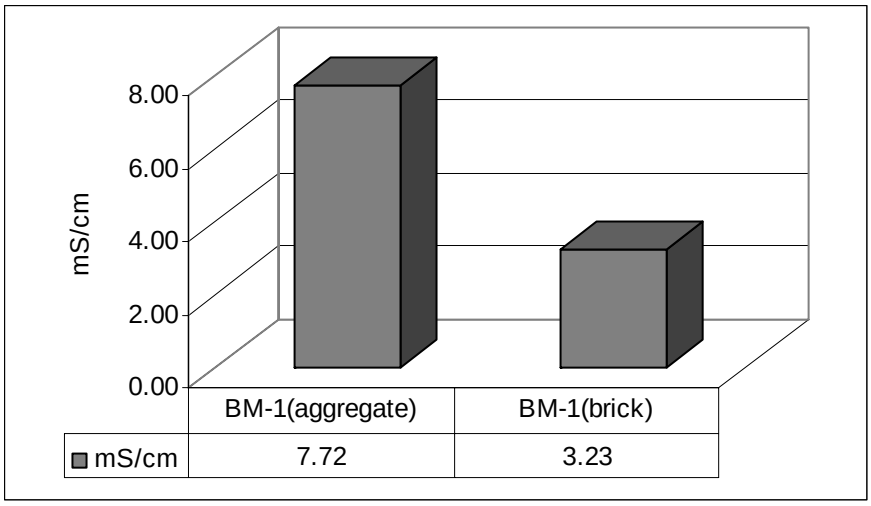

Figure 4. 54. Pozzolanic Activity measurements of fine aggregates and brick aggregates used in Byzantine mortars (less than 53 μm) .

4.4.4 Mineralogical Compositions of the Mortar Matrices and Aggregates of Byzantine Mortars

XRD patterns of the Byzantine Period mortars indicated that they were mainly composed of calcite and quartz (Figure 4.55). Calcite originated from carbonated lime while quartz from aggregates. Although pozzolanic aggregates had been used as in Byzantine mortars, calcium silicate hydrate (CSH) formations were not observed in the XRD patterns. This could be explained by the amorphous characters of the CSH (Haga et al. 2002).

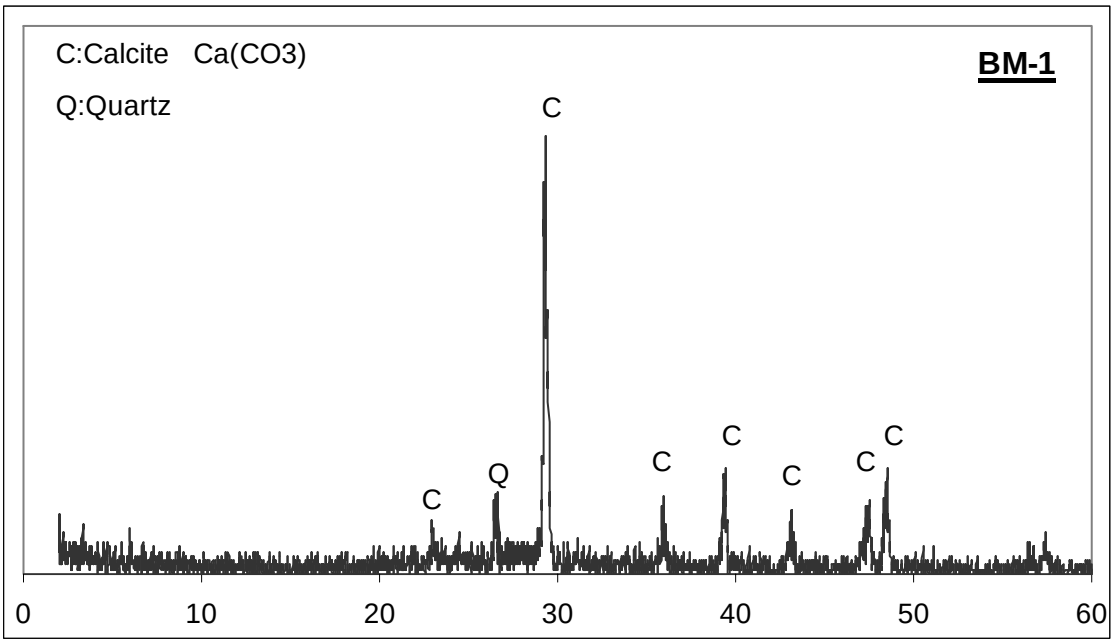

Figure 4. 55. XRD pattern of the Byzantine mortar matrices

The mineralogical compositions of the natural fine aggregates used in the Byzantine Period mortars and those of the brick pieces were identified using XRD (Figure 4.56-4.57).

The XRD patterns of the natural fine aggregates used in the Byzantine Period mortars showed similar XRD patterns to those used in the Roman Period. The XRD patterns of fine aggregates showed that they were mainly composed of albite, K-feldspar, quartz, and muscovite. As observed in the XRD patterns of the Roman Period aggregates (Figure 4.39), a diffuse band between 20-30 degrees was also observed (Figure 4.56). This shows the presence of amorphous substances in their composition.

On the other hand, in the XRD patterns of the brick pieces used as artificial pozzolan, mainly albite, K-feldspar, quartz and muscovite minerals were observed. (Figure 4.57).

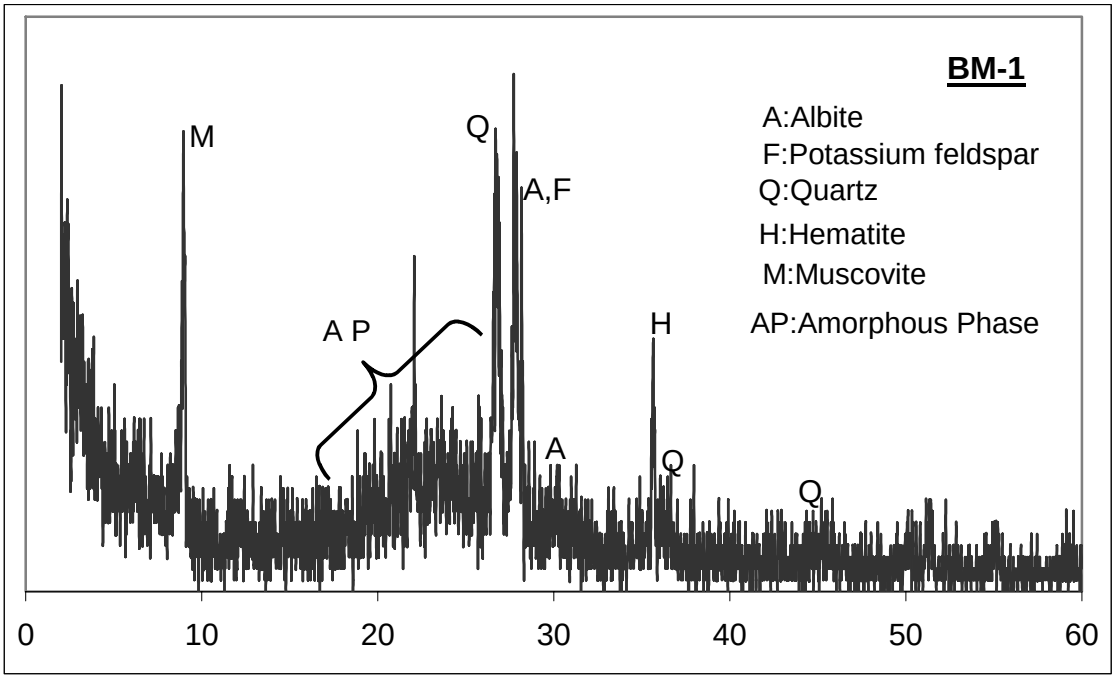

Figure 4. 56. XRD pattern of the fine aggregates used in Byzantine mortar

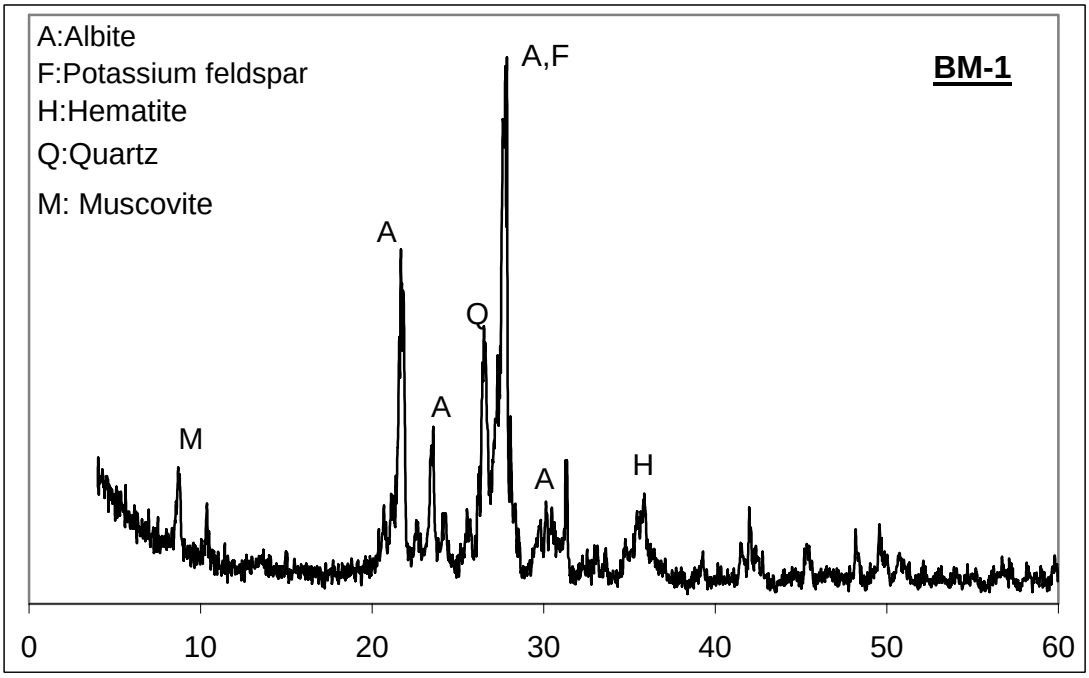

Figure 4. 57. XRD pattern of the brick aggregates used in Byzantine mortar

4.4.5 Elemental Compositions and Microstructural Properties of Byzantine Mortars

Byzantine mortars have stiff and compact apperance like Roman mortars (Figure 4.58). The cohesion between aggregates and lime is strong and their interfaces are generally free from fissures and cracks.

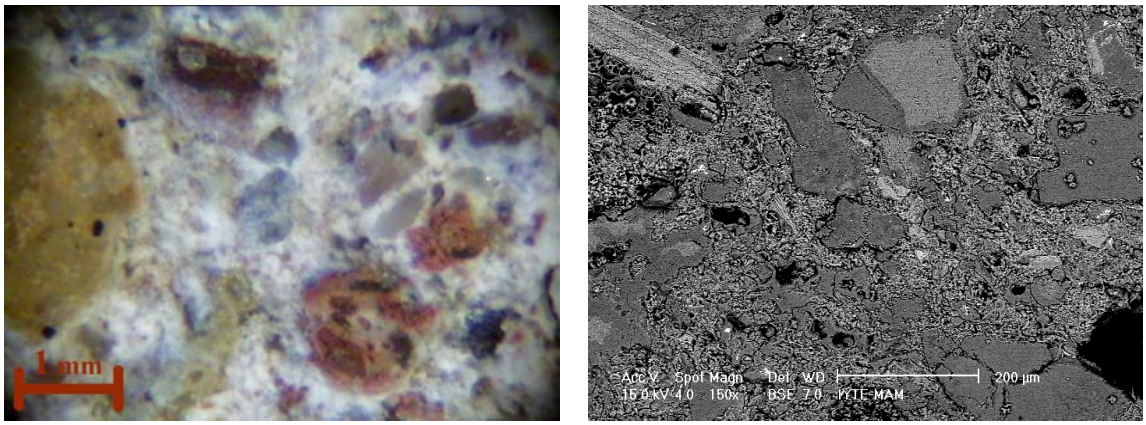

Figure 4. 58. Stereo microscope and BSE image showing good adhsion between aggregates and lime in Byzantine mortar matrix (BM-1).

The natural aggregates used in the mortars were more porous, semi-rounded, soft and easily granulated like Roman ones. They also have a grey color. Their micropores are very fine and irregular (Figure 4.59). Their SEM images show glassy phases in their structure (Figure 4.60-4.62).

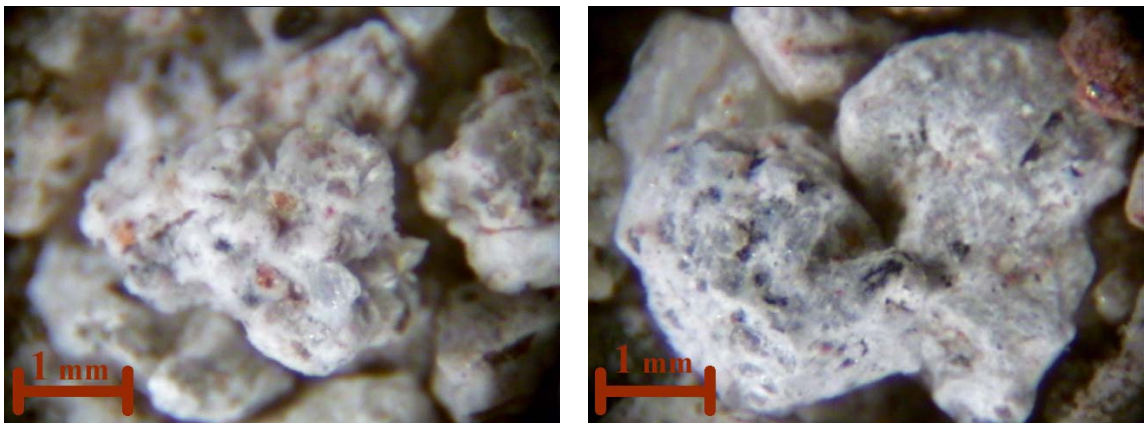

Figure 4. 59. Stereo microscope image of BM-1

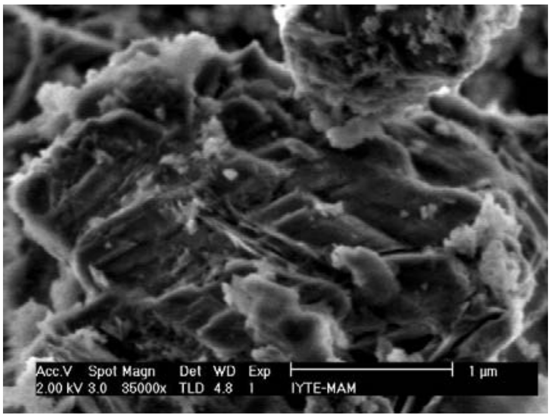

(35.000x)

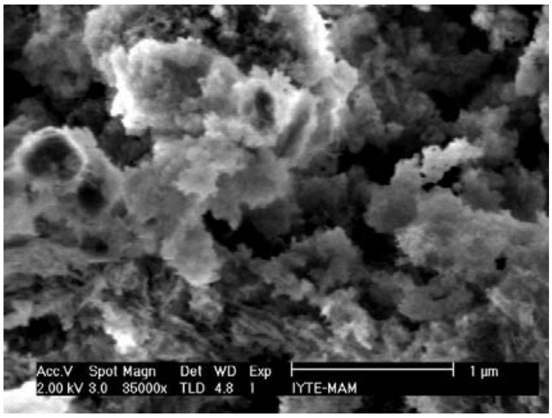

(35.000x)

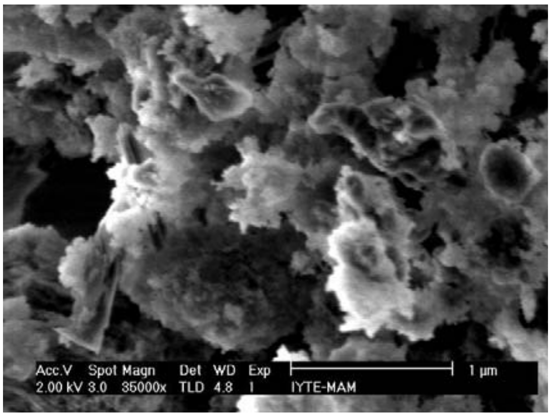

(35.000x)

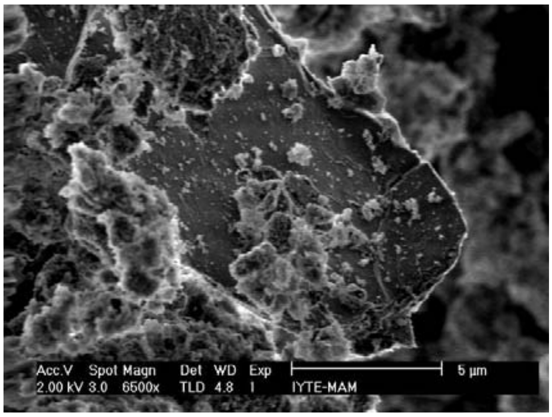

(6.500x)

Figure 4. 60. SE images of glassy phases of the fine aggregates used in the byzantine mortars.

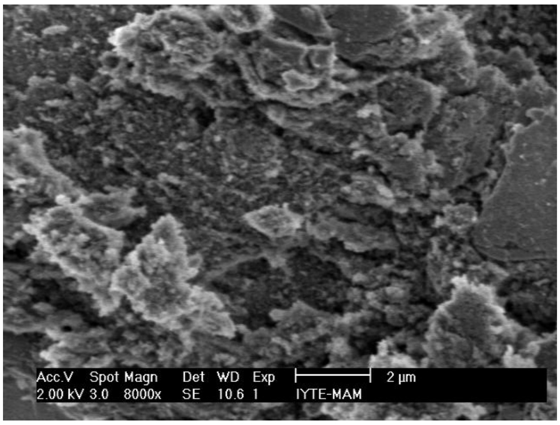

(8.000x)

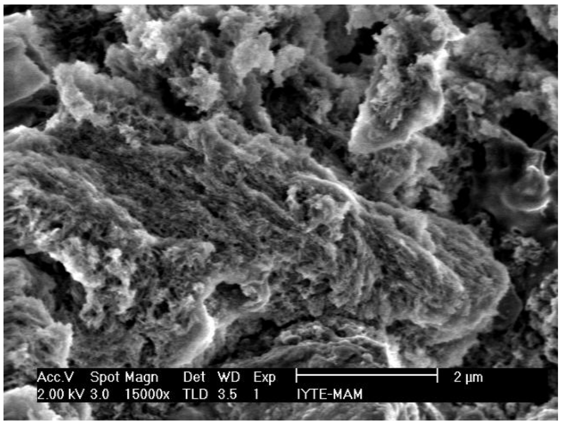

(15.000x)

Figure 4. 61. SE images of amorphous phases in the composition of brick aggregates used in Byzantine mortar.

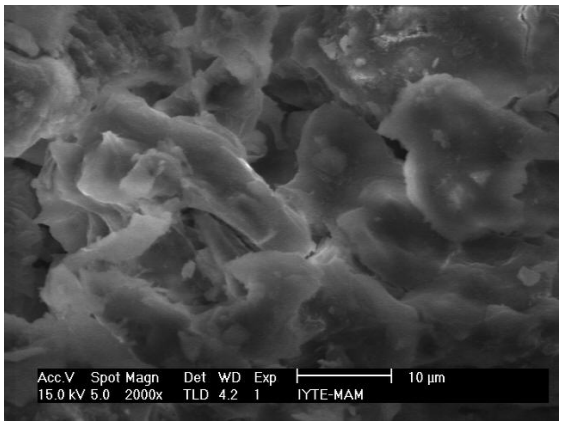

(2.000x)

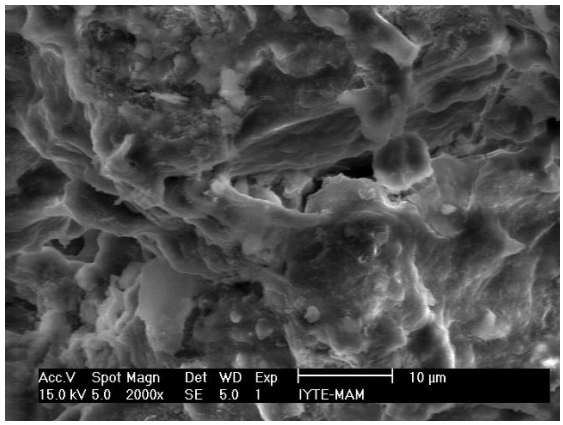

(2.000x)

Figure 4. 62. SE images of glassy phases in the composition of brick aggregates used in Byzantine mortar

The oxide composition analysis of these aggregates carried by EDS indicated that they were mainly composed of a high amount SiO_2, Al_2O_3, Fe_2O_3 and minor amounts of Na_2O, MgO, K_2O and TiO_2. The chemical composition analysis results indicated that they have nearly same oxide composition with the ones used in the roman mortars (Table 4.10).

Table 4. 10. Elemental compositions of natural fine aggregates used in the Roman and Byzantine mortars.

SAMPLES	Fe_2O_3	Na_2O	MgO	Al_2O_3	SiO_2	K_2O	TiO_2
RM-1	9,1±2,3	2,1±0,2	1,4±0,2	5,6±0,1	80,1±2,5	1,0±0,1	0,8±0,5
BM-1	6,8±1,6	1,3±0,3	1,9±0,2	6,6±0,2	81,8±2,1	1,0±0,1	0,7±0,3

In the composition of the brick aggregates used in Byzantine mortars, a high amount of SiO_2, Al_2O_3, and Fe_2O_3 but a little amount of ZnO, K_2O, MgO were identified (Table 4.11).

Table 4. 11. Elemental compositions of brick aggregates used in the Byzantine mortars.

SAMPLES	ZnO	MgO	Al2O3	SiO2	K2O	CaO	Fe2O3
BM-1	1.9±0.7	1.6±0.4	6.7±1.0	50.5±3.2	0.9±0	1.1±0.2	3.9±2.2

Elemental composition of white lumps representing the characteristics of lime used in Byzantine mortars were determined by SEM-EDS analysis. Sparry calcite crystals (~10 μm), which are mainly composed of $CaCO_3$, are observed in the matrices of the white lumps (Figure 4.63). This analysis result indicated that the lime used in the preparation of mortars was nearly pure lime.

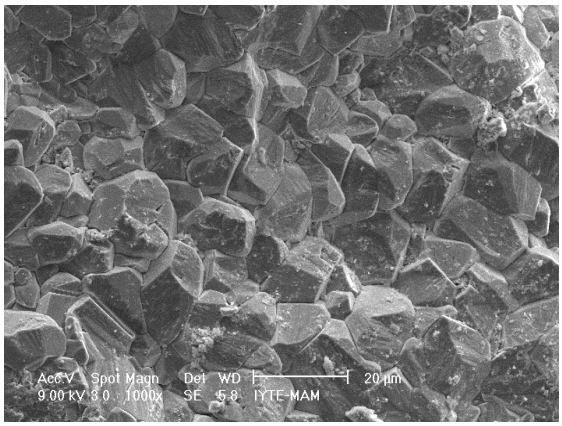

(1.000x)

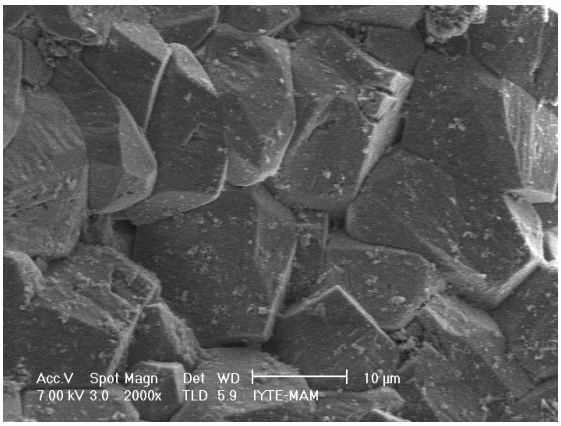

(2.000x)

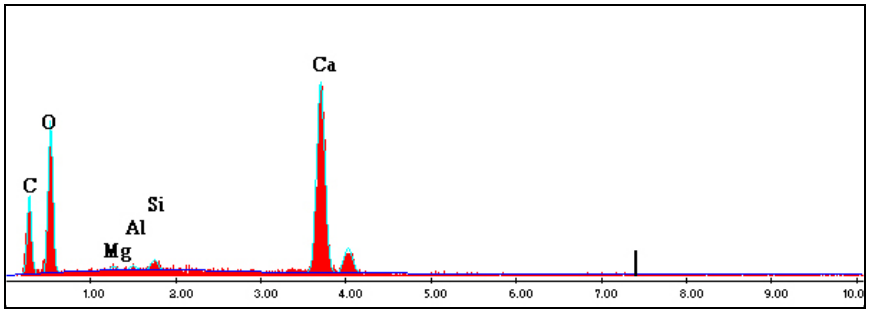

Figure 4. 63. SE images of sparry calcite crystals (~10 μm) and their EDS analysis in the white lumps observed in the Byzantine mortar sample.

The microstructural properties of the mortar matrices were determined by SEM-EDS analyses. Gel like formations composed of mainly calcium, silicon and aluminium were observed in the mortar matrices with fine aggregates (Figure 4.64). This may indicate the formation of hydraulic reaction products (calcium silicate hydrates and calcium aluminate hydrates) formed by the reaction with lime and pozzolanic fine aggregates.

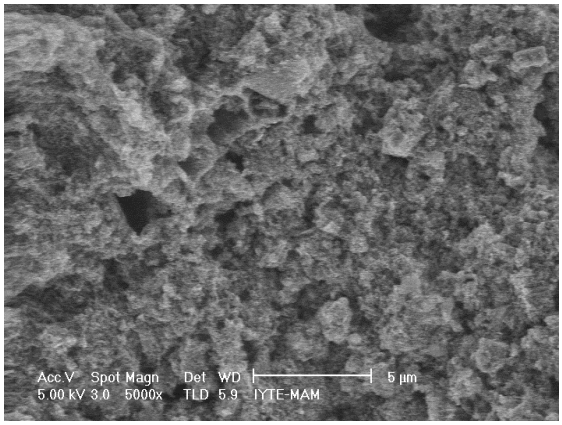

(5.000x)

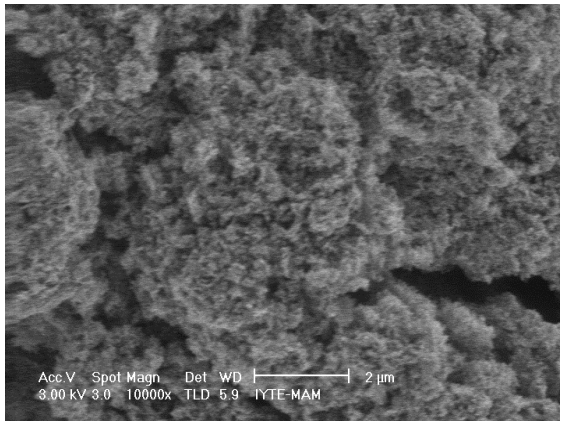

(10.000x)

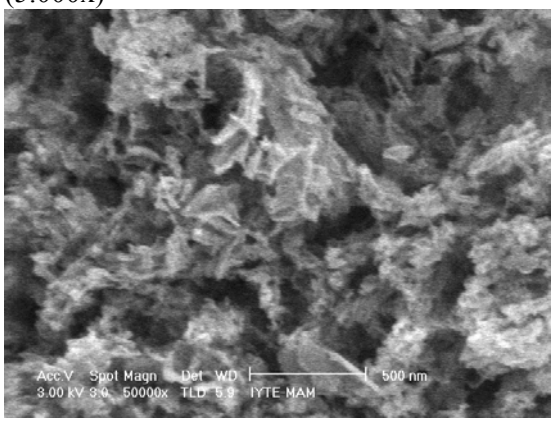

(50.000x)

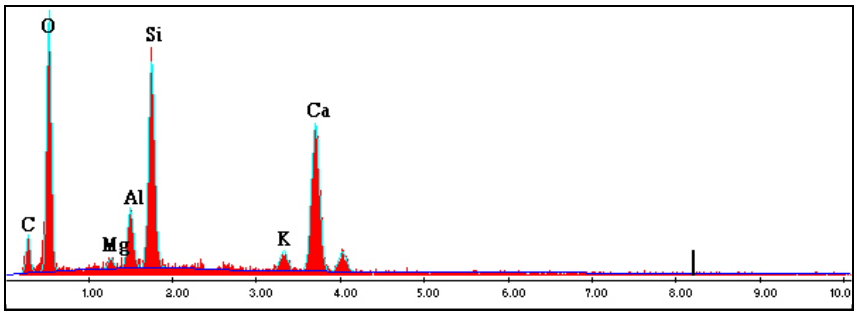

Figure 4. 64. SE images of CSH formation and their EDS spectrum in the Byzantine mortar sample.

4.4.6 Hydraulicity of Byzantine Mortars by TGA

TGA analysis of the Byzantine mortar sample indicated that the weight loss between 200 ºC – 600 ºC was 2.78 % and weight loss over 600 ºC was 13.64 %. CO_2/H_2O ratio was 4.91 (Figures 4.65 and Table 4.12). This result indicated that Byzantine mortars are hydraulic mortars like Roman mortars.

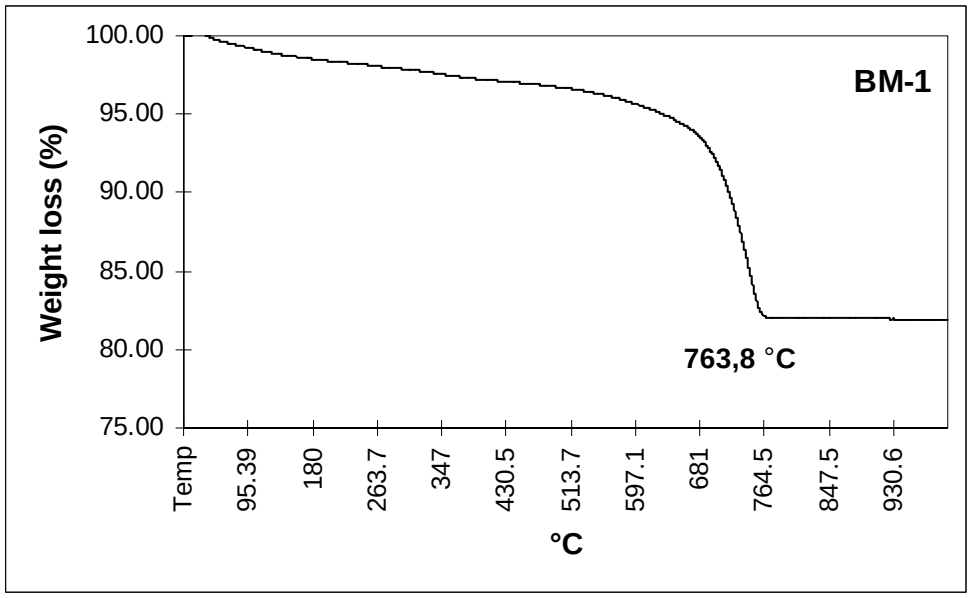

Figure 4. 65. TGA graph of the Byzantine mortar

Table 4. 12. Structurally bound water (H_2O) percent, carbon dioxide (CO_2) percent and CO_2/H_2O ratio of Byzantine mortar.

Sample	H_2O (%)	CO_2 (%)	CO_2/ H_2O
BM-1	2.78	13.64	4.91

4.5. Intervention Mortars

The properties of mortars, which were used in the restoration works in 1940s in Serapis Temple, were analyzed with samples taken from various places of the temple. The aim was to investigate whether they are compatible with the original ones or not.

4.5.1 Basic Physical and Mechanical Properties of Intervention Mortars

Intervention mortars are very weak and easily crumbled by hand. Therefore, their compressive strength could not be measurements.

The porosity values of intervention mortars were in the range of 34 - 40 % , and the average value was 38 % . The real density value was 2.4 gr/cm^3. The apparent density values of mortars varied between 1.4 - 1.6 gr/cm^3 , and the average value was 1.5 gr/cm^3 (Figure 4.66).

Drying rate characteristics of the intervention mortars (IM-2) show that they are dried quickly when compared with orijinal mortar. Basic physical properties of the intervention mortars seem to be compatible with the original Roman and Byzantine mortars. However, the fact that they dry much quicker than the original mortars shows that the large pores they contain have a higher percentage than that of the original ones (Figure 4.67).

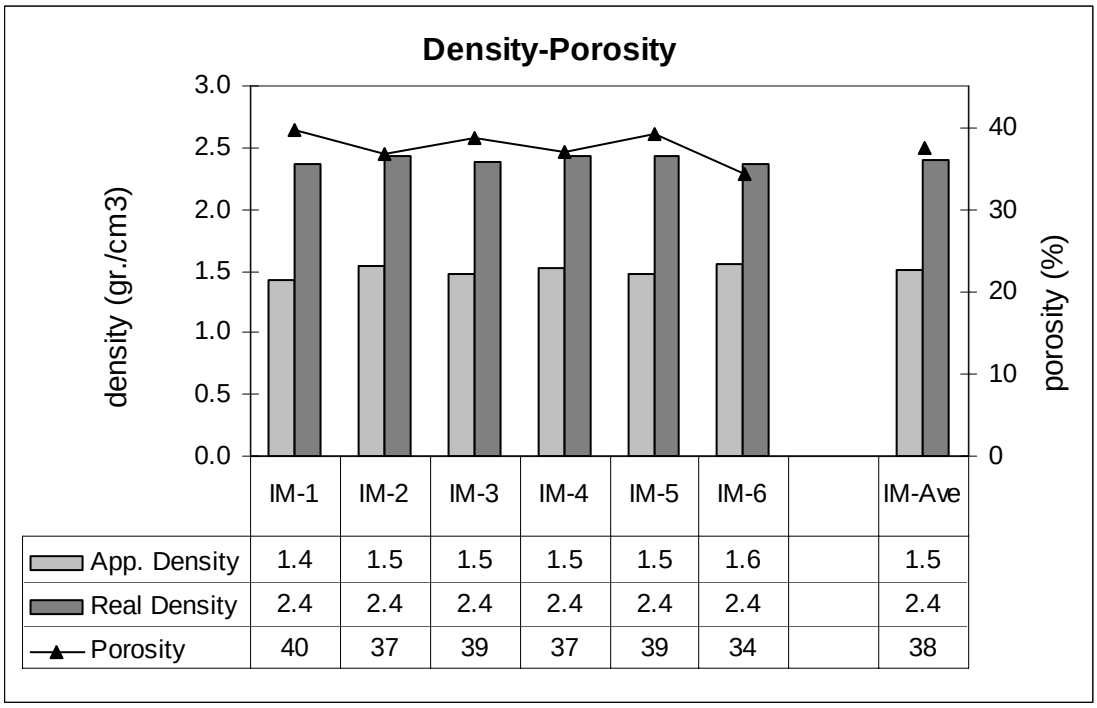

	IM-1	IM-2	IM-3	IM-4	IM-5	IM-6		IM-Ave
App. Density	1.4	1.5	1.5	1.5	1.5	1.6		1.5
Real Density	2.4	2.4	2.4	2.4	2.4	2.4		2.4
Porosity	40	37	39	37	39	34		38

Figure 4. 66. Porosity and density value of intervention mortars

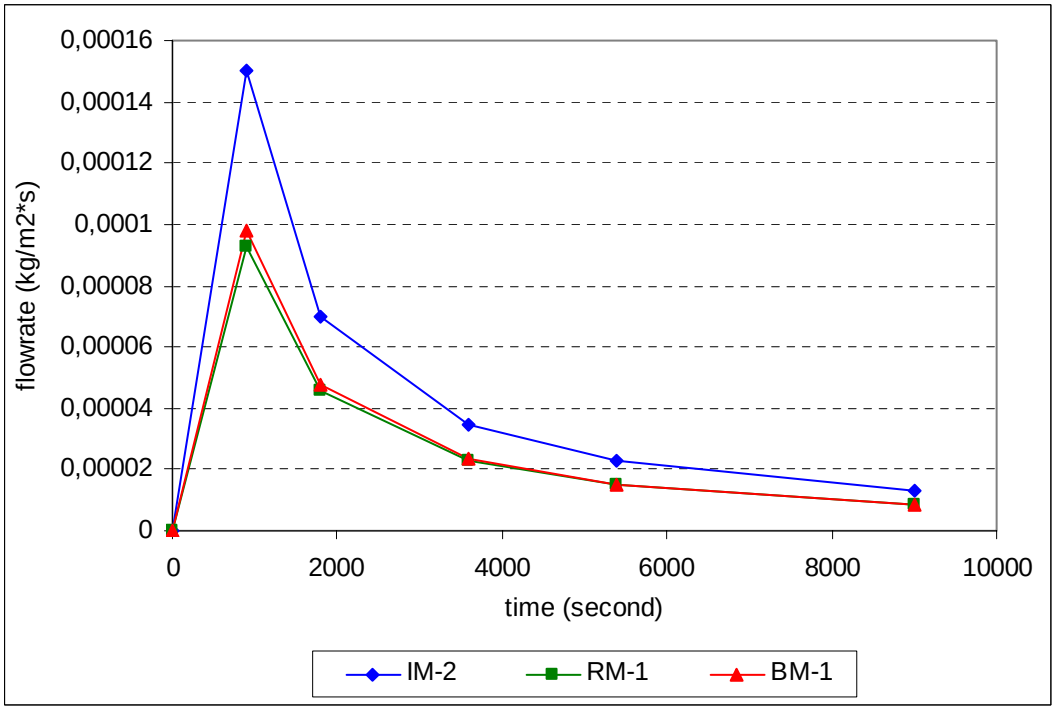

Figure 4. 67. Drying rates of the mortars by weight loss versus time and surface area

4.5.2 Raw Material Composition of Intervention Mortars

Intervention mortars contain low percent lime / aggregate ratios ranging between 1:7 and 1:3 by weight (Table 4.13 and Figure 4.68). These ratios are guite lower than those of Roman and Byzantine mortars. The low percent of lime can be explained by the use of cement together with lime determined by XRD and SEM analyses (Section 4.5.4).

Table 4. 13. Lime-Aggregate ratios of intervention mortars

Sample	Lime/aggregate ratio
ST.IM-1	1 : 4,9
ST.IM-2	1 : 6,1
ST.IM-3	1 : 7,3
ST.IM-4	1 : 3,3
ST.IM-5	1 : 5,7
ST.IM-6	1 : 3,8

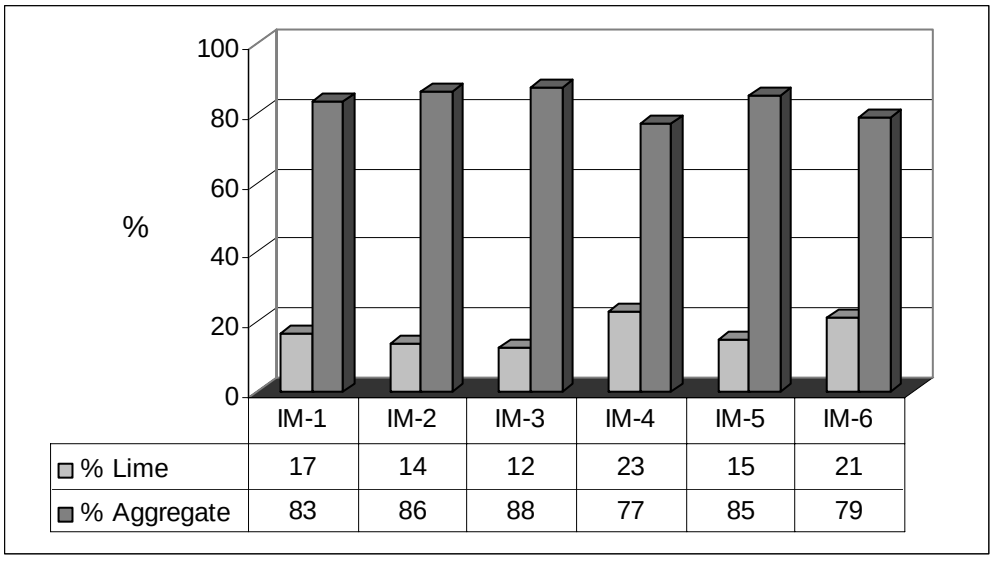

Figure 4. 68. Lime-Aggregate ratios of intervention mortars

Aggregates used in original mortars and intervention mortars had different particle size distributions. Aggregates in original Roman and Byzantine mortars had similar particle size distributions with each other (Figure 4.69). The aggregates with particle sizes greater than µm formed the largest fraction of the total aggregates used in the original mortars, but this value is much lower in intervention mortars, and the greatest fraction is between 750-1180 µm (Figure 4.70). These results indicate that the intervention mortars are not compatible with the original Roman and Byzantine mortars.

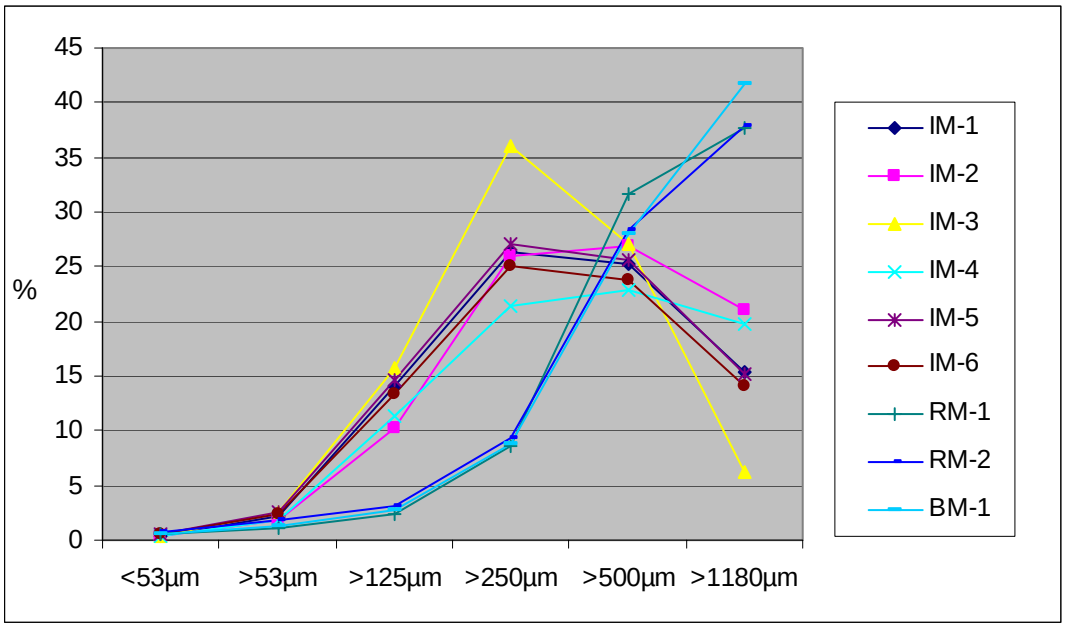

Figure 4. 69. Particle Size Distribution curves of the aggregates used in mortars

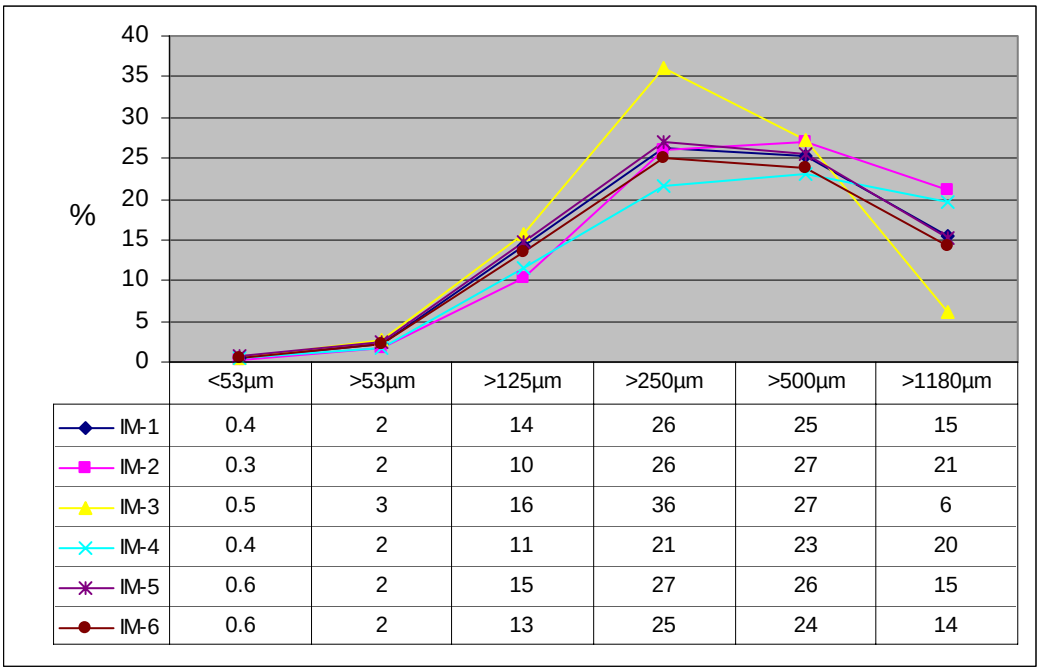

	<53µm	>53µm	>125µm	>250µm	>500µm	>1180µm
IM-1	0.4	2	14	26	25	15
IM-2	0.3	2	10	26	27	21
IM-3	0.5	3	16	36	27	6
IM-4	0.4	2	11	21	23	20
IM-5	0.6	2	15	27	26	15
IM-6	0.6	2	13	25	24	14

Figure 4. 70. Particle Size Distribution curves of the aggregates used in intervention mortars

4.5.3 Pozzolanic Activity of Aggregates Used in Intervention Mortars

The range of electrical conductivity values for the aggregates in intervention mortars are between 1.74 – 2.51 mS/cm. Based on these values, it can be said that the aggregates used in intervention mortars have pozzolanic (Figure 4.71).

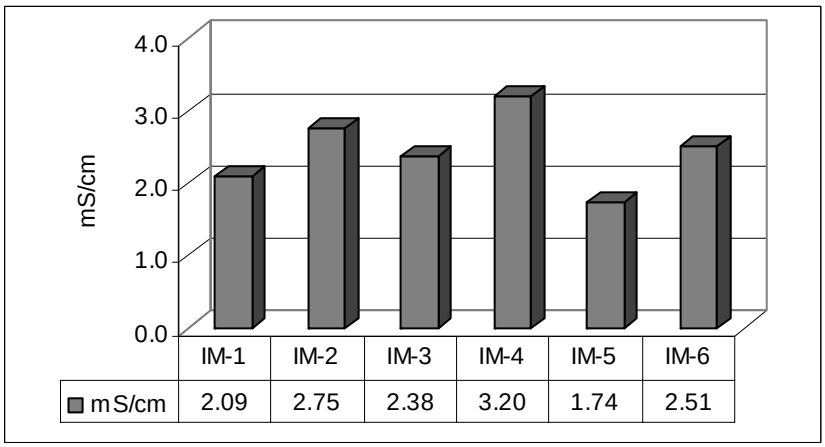

	IM-1	IM-2	IM-3	IM-4	IM-5	IM-6
mS/cm	2.09	2.75	2.38	3.20	1.74	2.51

Figure 4. 71. Pozzolanic Activity measurements of fine aggregates of intervention mortars (less than 53 µm).

4.5.4 Mineralogical Compositions of the Intervention Mortars Matrices and Aggregates

In the XRD pattern of the intervention mortar, calcium aluminum silicate (CAS), calcite (C), quartz (Q), and illite (I) peaks were identified (Figure 4.72). Calcite peaks are those which are observed as a result of the carbonation of lime. Quartz peaks, on the other hand, result from aggregates. The presence of intense calcium aluminum silicate peaks shows that cement had been used in the preparation of intervention mortar.

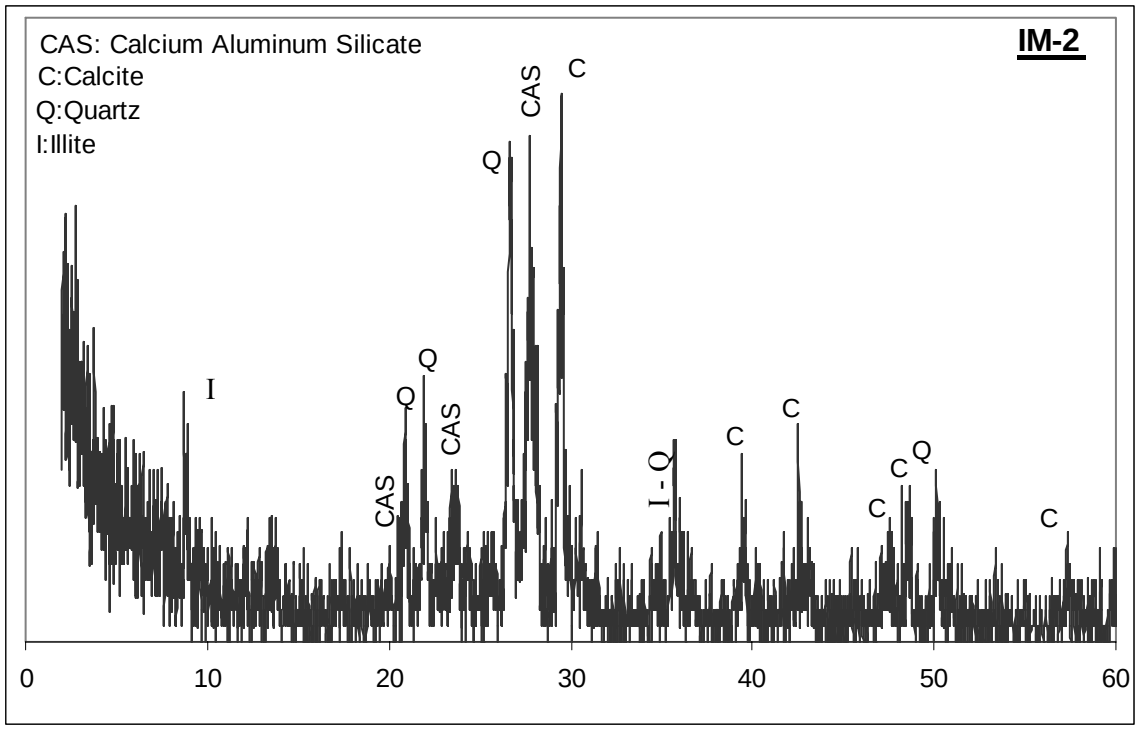

Figure 4. 72. XRD pattern of the intervention mortar matrices

XRD patterns of fine aggregates of intervention mortars indicated that they were mainly composed of potassium feldspar, albite quartz, hematite and amorphous substances (Figure 4.73). The presence of amorphous substances shows the pozzolanic character of the aggregates also confirmed by pozzolanic activity measurements.

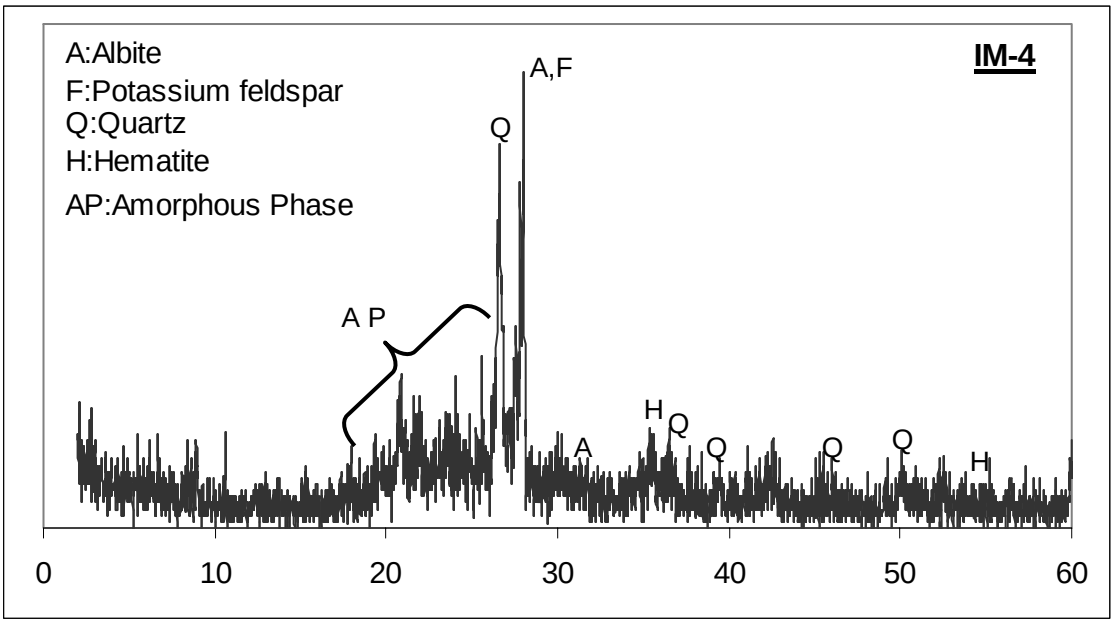

Figure 4. 73. XRD pattern of the fine aggregates used in intervention mortar

3.5.5 Elemental Compositions and Microstructural Properties of the Intervention Mortars Matrices

In the SEM images of intervention mortars, it is seen that lime and aggregates bind weakly and cracks form between them (Figure 4.74-4.75). The compactness and stiffness of the Roman and Byzantine periods mortars are not observed in these mortars.

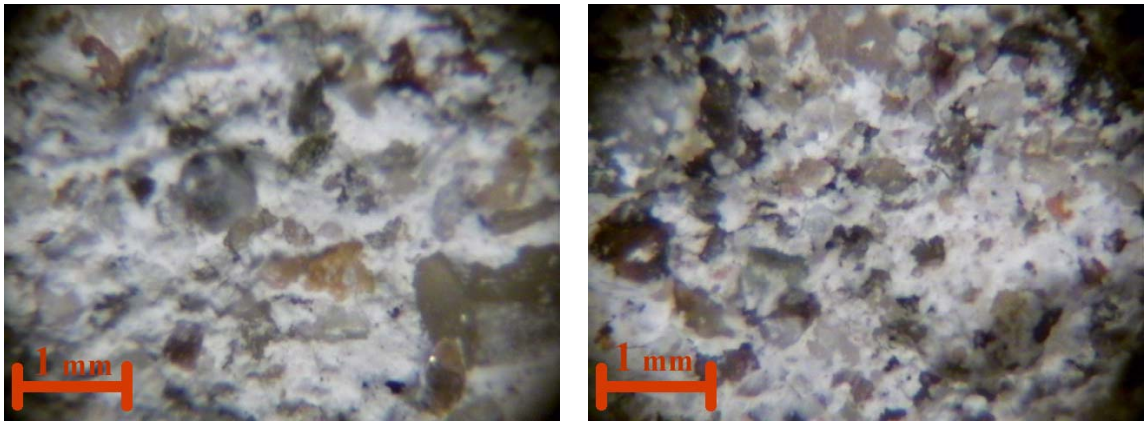

Figure 4. 74. Stereo microscope image showing weak adhesion between binder and aggregates of IM-1

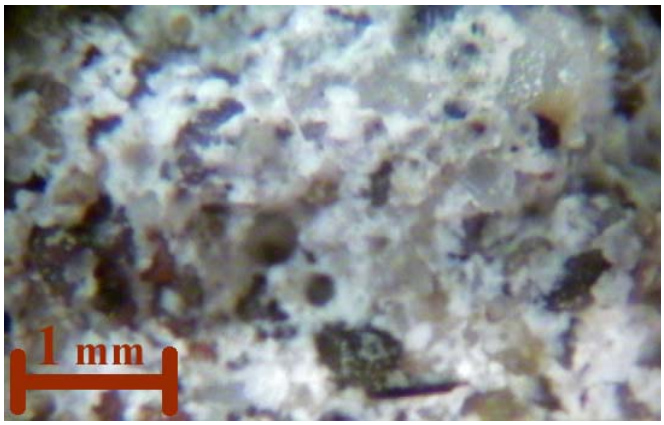

Figure 4. 75. Stereo microscope image showing weak adhesion between binder and aggregates of IM-1**.**

The matrix, which was composed of fine aggregates has a porous structure (Figure 4.76). In the matrix CSH formation is observed due to the use of cement (Figures 6.77 - 6.79).

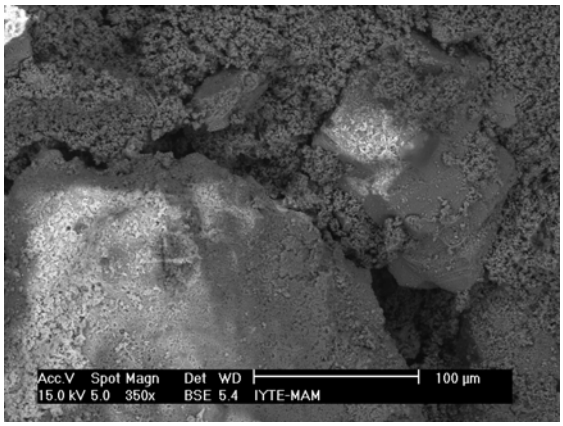

(350x)

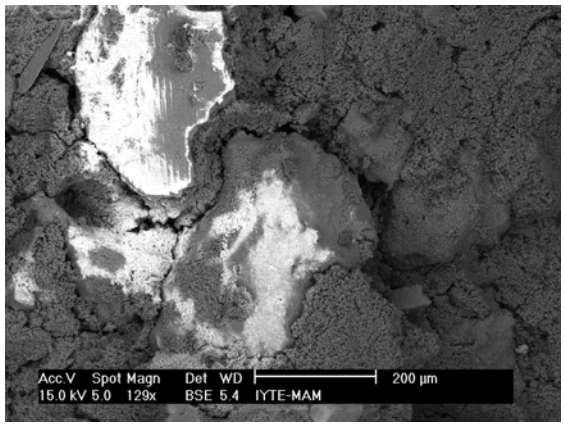

(129x)

Figure 4. 76. BSE images showing cracks between binder and aggregates (IM-2)

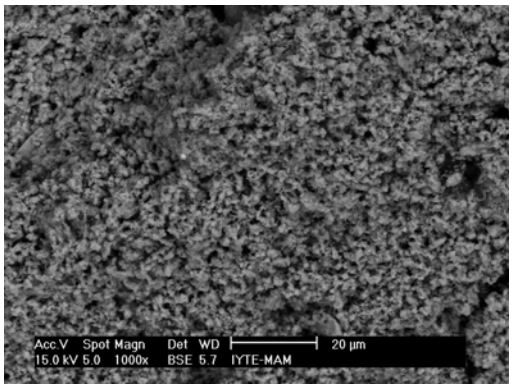

(1000x)

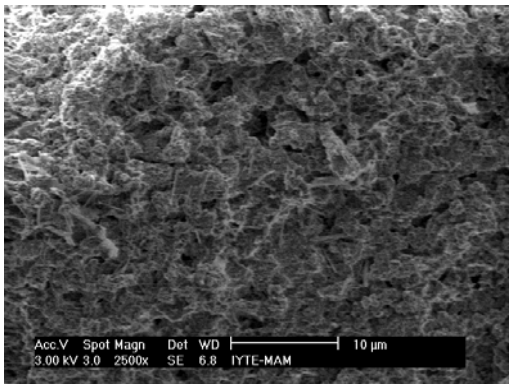

(2500x)

Figure 4. 77. BSE and SE images of the mortar matrix of the intervention mortar. (IM-2)

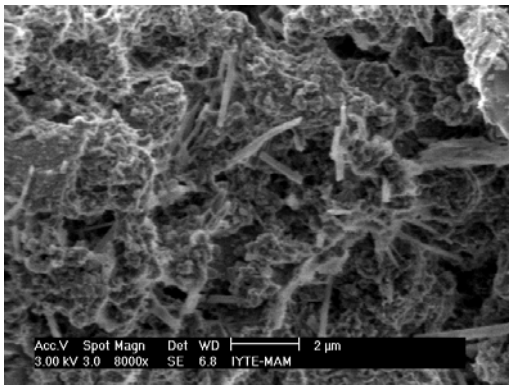

(8.000x)

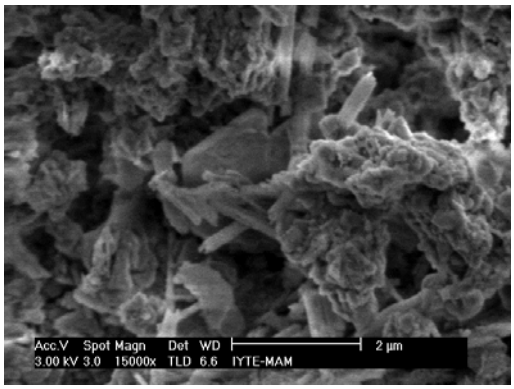

(15.000x)

Figure 4. 78. CSH formation in the intervention mortar matrix being free from coarse aggregates (IM-2)

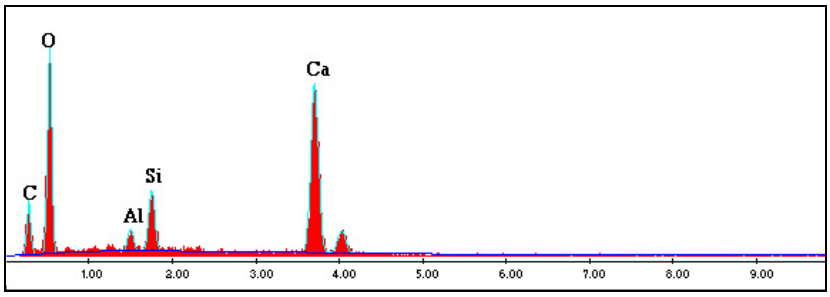

Element	Wt %
C	15.14
O	46.41
Al	1.83
Si	5.36
Ca	31.25

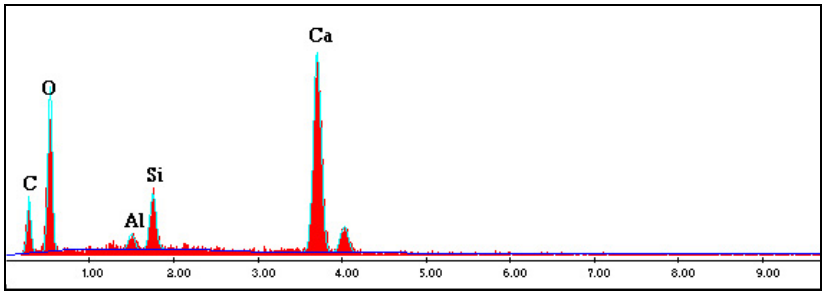

Element	Wt %
C	15.20
O	41.51
Al	1.29
Si	4.83
Ca	37.16

Figure 4. 79. EDX spectrums and elemental compositions (%) of the intervention mortar matrix. (IM-2).

Elemental composition analyses of the fine aggregates used in the intervention mortars were carried out by SEM-EDS analysis (Table 4.14). Aggregates contain a high amount of SiO_2, Al_2O_3, and Fe_2O_3 and a low amount of Na_2O, K_2O, MgO, and TiO. It was found that the amounts of Al_2O_3 and Fe_2O_3 that the aggregates contained were higher than those that the aggregates used in the Roman and Byzantine Periods. This result shows that rather different aggregates had been used in the intervention mortars in comparison with those used in the original mortars.

Table 4. 14. Elemental compositions of fine aggregates used in the intervention mortars

SAMPLES	Fe_2O_3	Na_2O	MgO	Al_2O_3	SiO_2	K_2O	TiO_2
ST. IM-4	15,0±1,6	2,3±0,5	2,6±0,4	11,2±0,8	66,5±2,2	1,5±0,3	0,9±0,2

4.6. Byzantine Plasters

In the inner walls of the temple, brick-lime plasters which are thought to have been made in the Byzantine Period are observed. Differently from the Byzantine mortars, almost all of the aggregates are composed of crushed bricks.

4.6.1 Basic Physical and Mechanical Properties of the Plasters

The values of porosity, density, drying rate, uniaxial compressive strength and modulus elasticity of the plasters collected from Serapis Temple show similarities to the values found in the mortars (Figures 4.80 - 4.81, Table 4.15). These results indicate that plasters are compatible with Roman and Byzantine mortars.

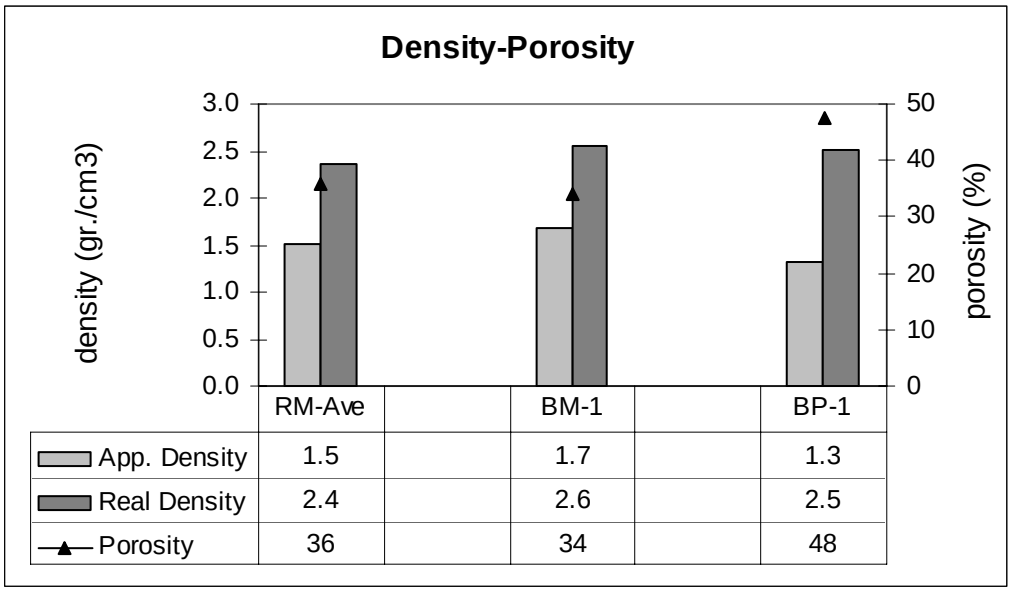

Figure 4. 80. Porosity and density of mortars and Byzantine plaster

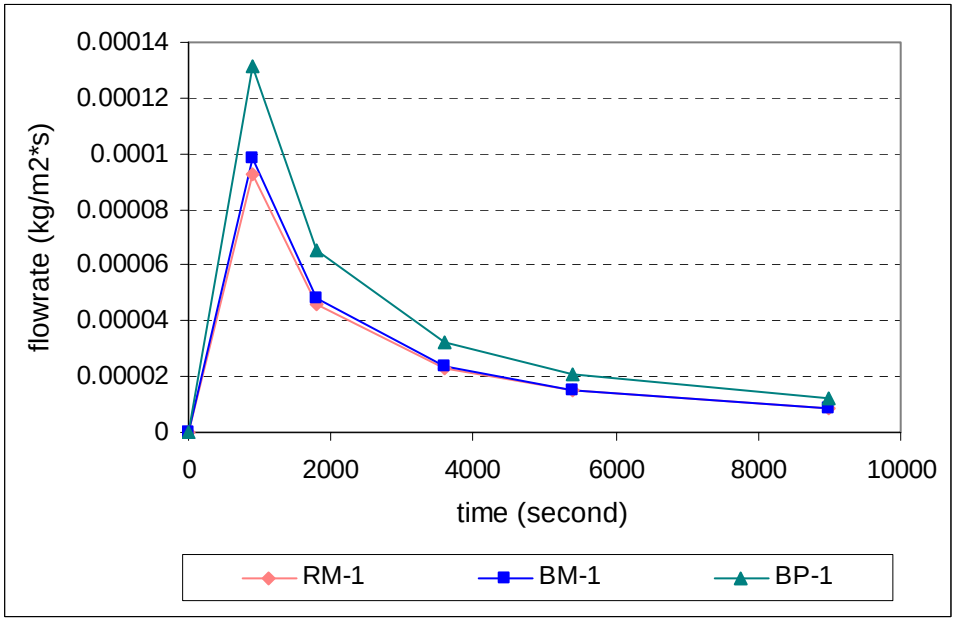

Figure 4. 81. Drying rates of mortars and plaster by weight loss versus time and surface area

Table 4. 15. Unixial Compressive Strength and Modulus of Elasticity values of mortars and Byzantine plaster in dry states.

SAMPLE	COMPRESSIVE STRENGTH (MPA.)	MODULUS OF ELASTICITY (MPA.)
RM-1	6.6 MPa	630.6 MPa
BM-1	6,4 MPa	428.6 MPa
BP-1	3.3 MPa	229.2 MPa

4.6.2 Raw Material Composition of the Plasters

Lime/aggregate ratio of Byzantine plaster was around 1:2,6 (Figure 4.82). This value was guite lower than lime percents of historic horosan plasters which used a lime percent of 50 % by weight (Böke et al. 2004).

The amount of fine aggregates used in plasters are more than the brick-lime (horasan) mortars used in the Byzantine mortars (Figure 4.83). Use of fine aggregates in plasters show similarities to the horasan plasters used in the construction of historic Ottoman baths (Böke et al. 2004).

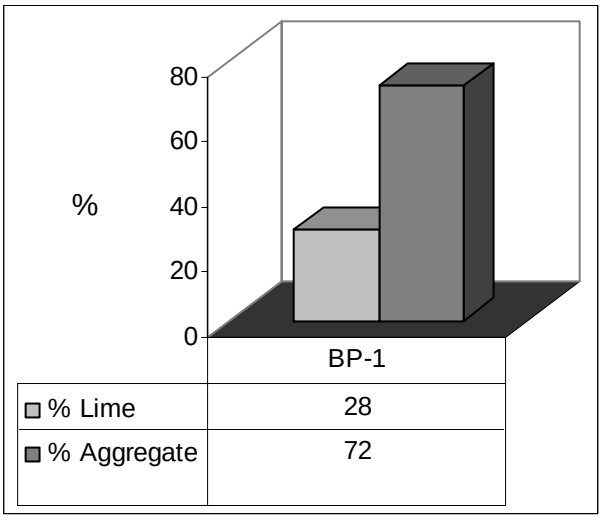

Figure 4. 82. Lime-Aggregate ratios of Byzantine plaster

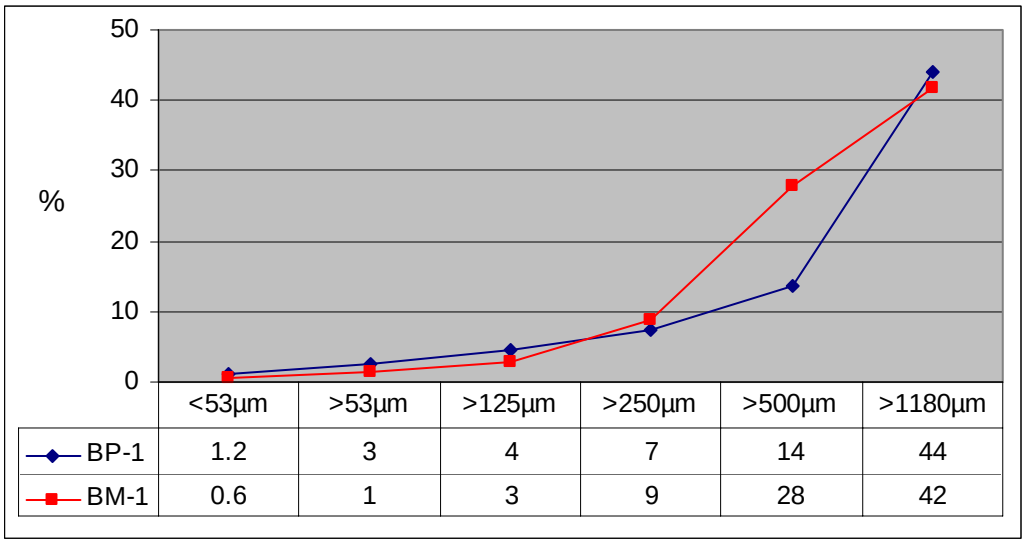

	<53µm	>53µm	>125µm	>250µm	>500µm	>1180µm
BP-1	1.2	3	4	7	14	44
BM-1	0.6	1	3	9	28	42

Figure 4. 83. Particle Size Distribution curves of the aggregates used in Byzantine plaster

4.6.3 Pozzolanic Activity of Brick Aggregates Used in Plasters

The electrical conductivity value of the brick powders used in the plasters was found as 5.90 mS/cm. This value shows that the bricks used as aggregates are good pozzolanic. It also indicates that the bricks had been selected differently from those used for construction, and that the bricks used in plaster making had been specially prepared. Similar results were also derived from some bath structures of the Ottoman Period (Böke et al. 2004, Uğurlu 2005).

4.6.4. Mineralogical Compositions of the Plaster Matrices And Aggregates

The XRD patterns of the Byzantine Period plasters are similar with XRD patterns of the Byzantine Period mortars. Basically, calcite and quartz were observed in the XRD patterns. Calcite originated from carbonated lime while quartz from aggregates (Figure 4.84).

XRD patterns of fine brick aggregates showed that they were mainly composed of albite, K-feldspar, quartz and muscovite (Figure 4.85).

The XRD patterns of natural fine aggregates used in the mortars of the Byzantine Period are similar with patterns of the aggregates used in the Roman Period.

In the XRD patterns of brick aggregates, which are thought to have been used as artificial pozzolan; basically, albite, K-feldspar, quartz, muscovite peaks, and a diffuse band between 20-30 degrees were observed. Observation of a diffuse band shows that brick pieces were rich in amorph materials and had pozzolanic character. This shows that the bricks used as aggregates had been prepared using natural sources, which were high in the amount of clay, and that they had been baked at low temperatures.

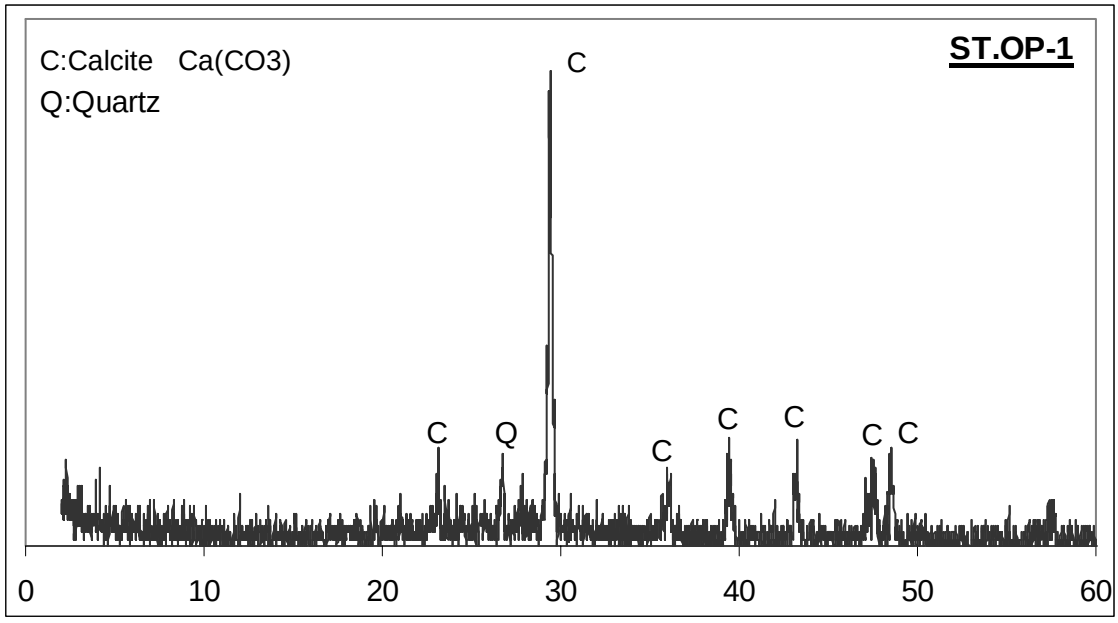

Figure 4. 84. XRD pattern of the Byzantine plaster

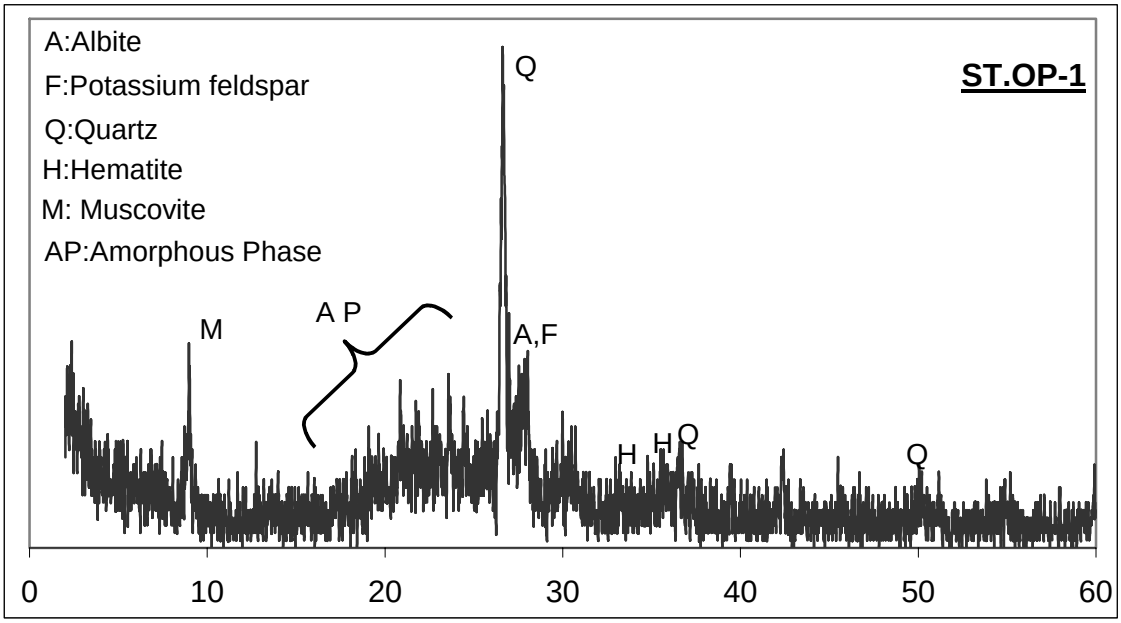

Figure 4. 85. XRD pattern of the brick aggregates used in the Byzantine plasters

4.6.5. Chemical Compositions and Microstructural Properties of the Plasters

Byzantine plasters also have a stiff and compact appearance like Byzantine mortars (Figure 4.86). Brick aggregates are firmly embedded in plaster matrices. This shows the well mixing process of brick aggregates with lime.

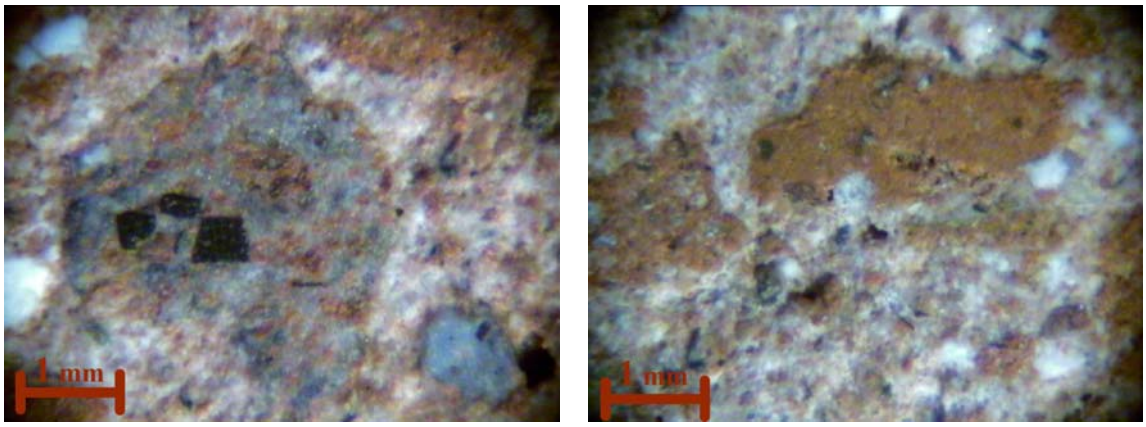

Figure 4. 86. Stereo microscope image showing good adhesion between binder and aggregates of BP-1 sample.

In the composition of the brick aggregates, a high amount of SiO_2, Al_2O_3, and Fe_2O_3 but a little amount of ZnO, K_2O, MgO were identified. The chemical composition analysis results indicated that they have nearly same oxide composition with the brick aggregates used in the Byzantine mortars (Table 4.16).

Table 4. 16. Elemental compositions of brick aggregates used in the Byzantine plaster.

SAMPLES	ZnO	MgO	Al_2O_3	SiO_2	K_2O	CaO	Fe_2O_3
BP-1	2.1±0.4	2.7±0.02	8.8±0.9	43.4±0.8	1.2±0.02	1.6±0.05	6.9±0.6
BM-1	1.9±0.7	1.6±0.4	6.7±1.0	50.5±3.2	0.9±0	1.1±0.2	3.9±2.2

Based on these compositions and SiO_2 - Al_2O_3 - Na_2O phase diagrams, it is possible to say that the glass-forming temperatures of the bricks are in the range of 900 - 1200 °C. From the electron microscope images, it was found that glass-like structure did not form in the brick samples (Figure 4.87 - 4.88). In addition, in the XRD patterns, absence of mullite peaks forming at high temperatures indicates that the temperatures did not exceed 900 °C.

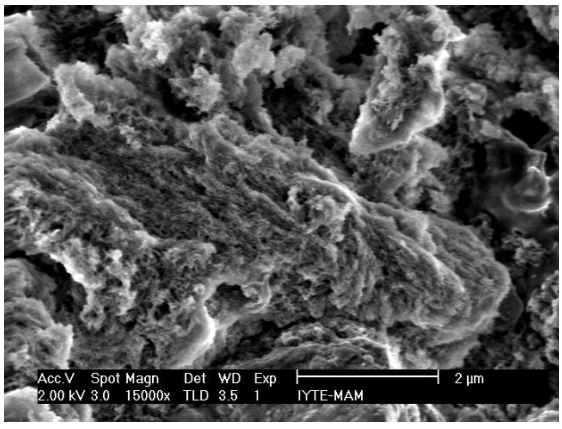

(15.000x)

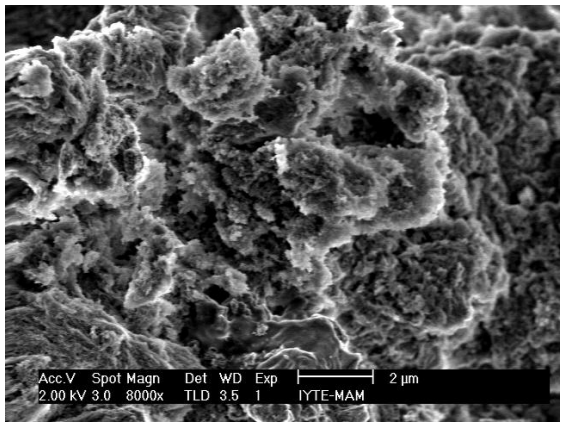

(8.000x)

Figure 4. 87. SE images of amorphous phases in the composition of brick aggregates used in Byzantine plaster.

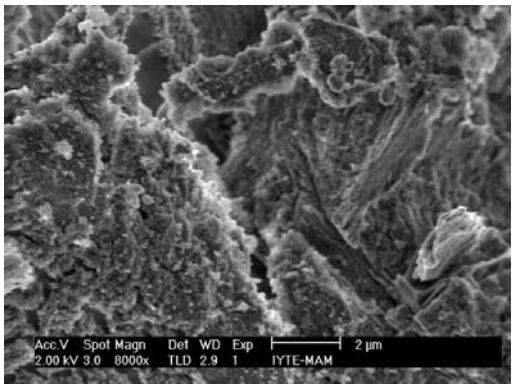

(8.000x)

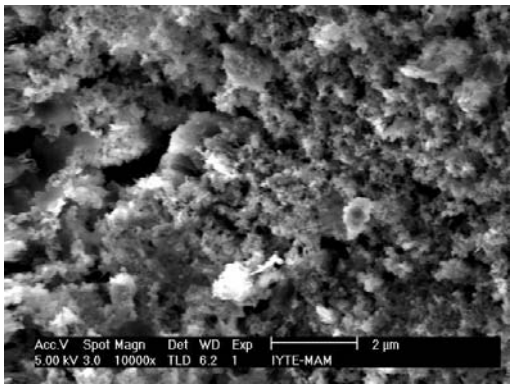

(10.000x)

Figure 4. 88. SE images of brick aggregates used in the Byzantine plaster containing amorphous substances.

Chemical compositions and morphologies of white lumps were determined by SEM analysis as to whether pure lime was used or not in the preparation of the plasters. SEM analysis show that white lumps are composed of micritic calcite crystals which are mainly composed of CaO (Figure 4.89). This result indicates that nearly pure lime was used as binder.

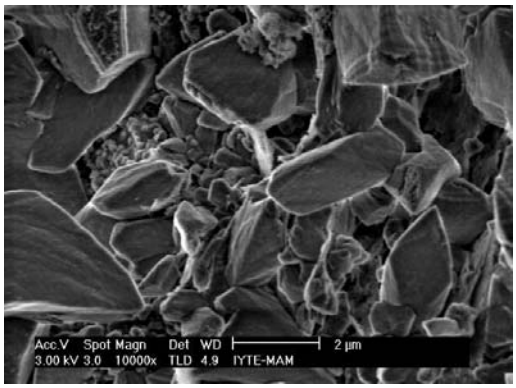

(10.000x)

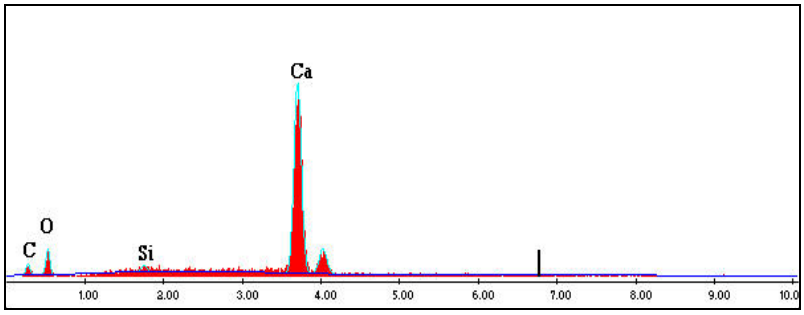

Figure 4. 89. Micritic calcite crystals and their EDS analysis in the white lumps observed in Byzantine plasters.

Active amorphous silicates and aluminates are determined by XRD and EDS analysis in the composition of the brick aggregates. They react with pure lime to produce calcium silicate hydrate and calcium aluminate hydrate. In the plaster matrix, these compounds are observed at the brick lime interface and pores of the bricks. Formation of these products improves the strength and durability of the plaster (Böke and Akkurt 2003).

4.6.6 Hydraulicity of Byzantine Plasters by TGA

TGA analysis of the Byzantine plaster sample indicated that the weight loss between 200 ºC – 600 ºC was 3.42 % and weight loss over 600 ºC was 9.91 %. CO_2/H_2O ratio was 2.90 (Figures 4.90 and Table 4.17). This result indicated that Byzantine plasters are hydraulic.

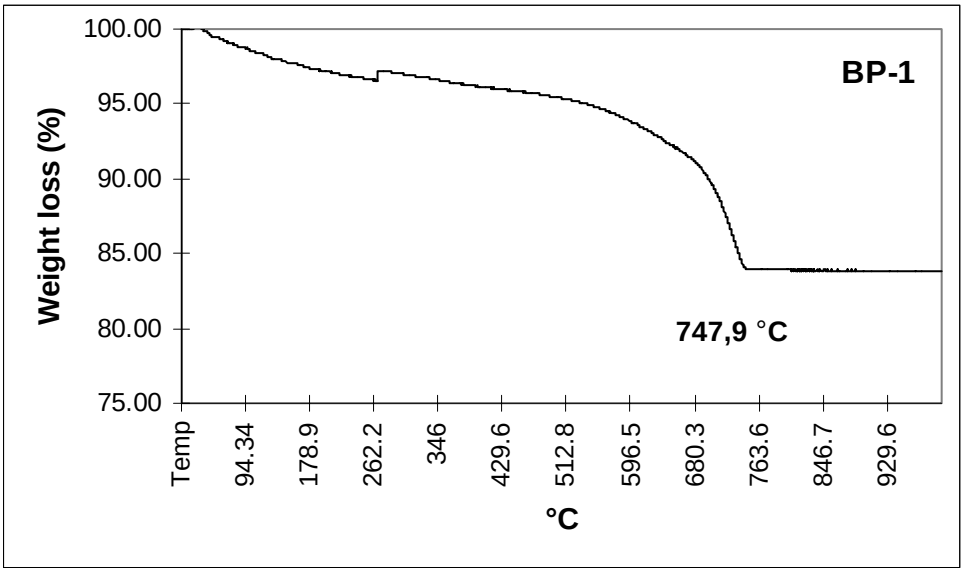

Figure 4. 90. TGA graph of the Byzantine plaster

Table 4. 17. Structurally bound water (H_2O) percent, carbon dioxide (CO_2) percent and CO_2/H_2O ratio of Byzantine plaster.

Sample	H_2O (%)	CO_2 (%)	CO_2/ H_2O
RM-1	3.42	9.91	2.90

4.7. Weathering of Bricks

The determination of weathering signs of the bricks used in the historic buildings is important to describe their conservation works such as cleaning of soluble salts, consolidation, etc. There are some main sources leading to the deterioration of the bricks.

One of the main sources of the brick deterioration is the air pollution. Air-pollution was originated by burning of fossil fuels producing sulphur dioxide. Sulphur dioxide reacts with the minerals of bricks resulting in the formation of gypsum (Lopez-Arce and Garcia-Guinea 2004)

The other main source of brick deterioration is growth of micro organisms on the brick surfaces. They lead to brick deterioration in a number ways:

a) via the decomposition of organic substances
b) via the decomposing minerals procuding organic acids

Soluble salts are also a main source of deterioration of bricks. Their sources are rising damp, marine spray, atmospheric pollution and cement usage in the intervention work of historic buildings.

In this work, soluble salt content in bricks and mortar samples were determined in order to evaluate their deterioration problems. Soluble salt content values of Roman bricks were 1,27 % and 0,46 %. Intervention bricks had low soluble salt contents ranging between 0,68 % - 0,47 % (Figures 4.91).

Soluble salt content values of Roman and Byzantine mortars, Byzantine plaster and intervention mortars ranged between 0,28 % - 0,89 % (Figures 4.92).

Main anion parts of soluble salts in the brick samples were determined to be chloride (CI^-).

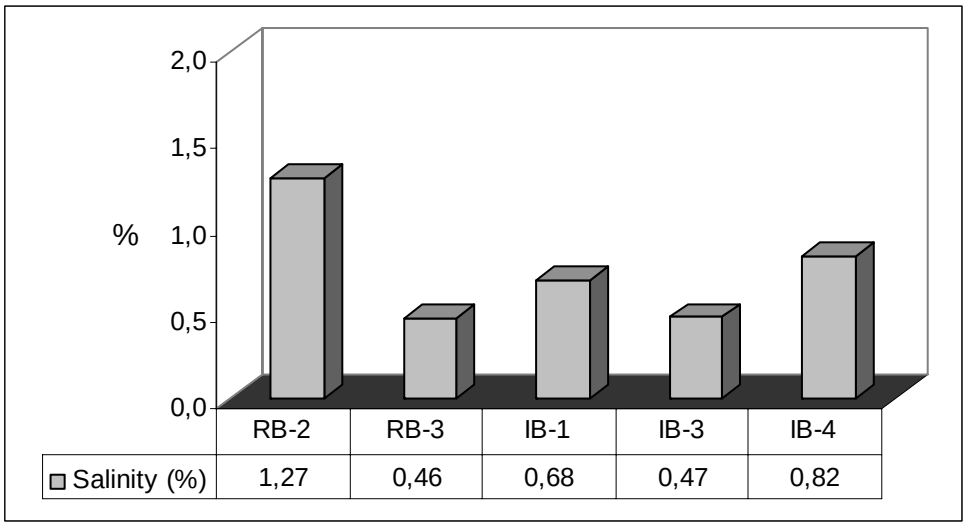

Figure 4. 91. Soluble salt content (%) in original and intervention bricks.

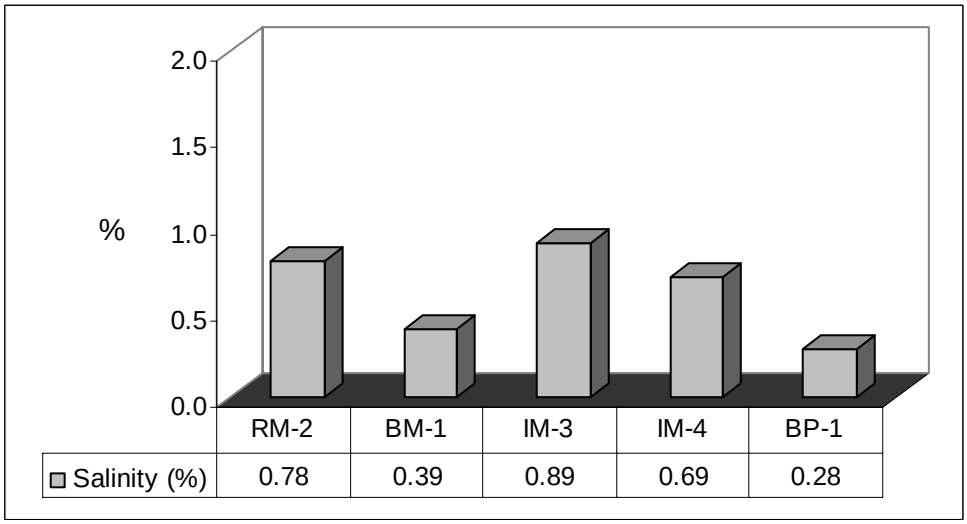

Figure 4. 92. Soluble salt content (%) in original and intervention mortars.

The high percent of soluble salts in the brick samples indicates that the building materials are affected by soluble salts (Figure 4.93-4.99) The source of the soluble salts could be use of cement in the intervention mortars manufactured by using lime and cement as binder.

Figure 4. 93. A view of the north-west elevation of the Serapis Temple – 1986 (Radt 2002).

Figure 4. 94. Growing of micro organisms on the brick surfaces (2004)

Figure 4. 95. The building materials is affected by soluble salts (2004)

Figure 4. 96. Loss of material in the north-east elevation (2004)

Figure 4. 97. Loss of material in the south-west elevation (2004)

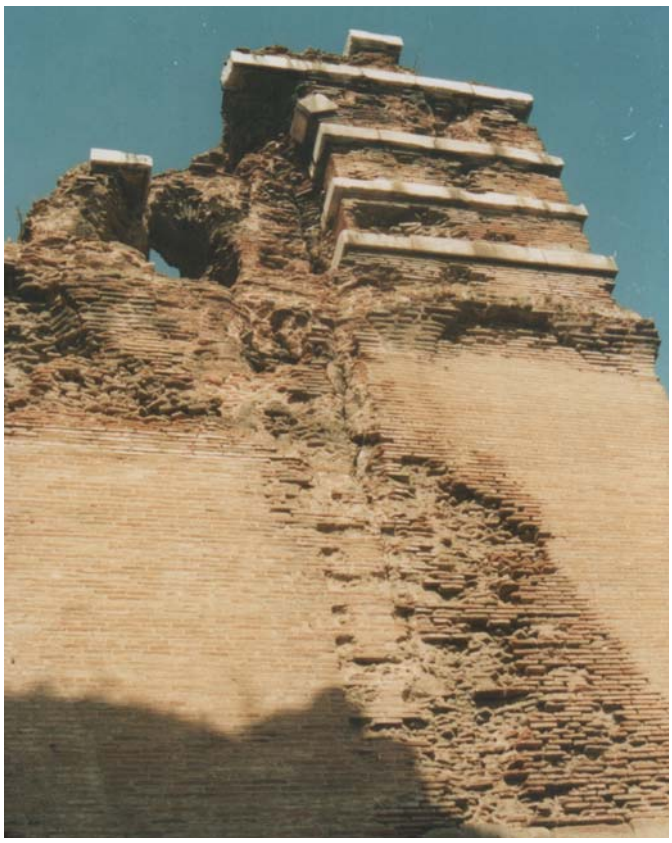

Figure 4. 98. Loss of material in the south-west elevation (2004)

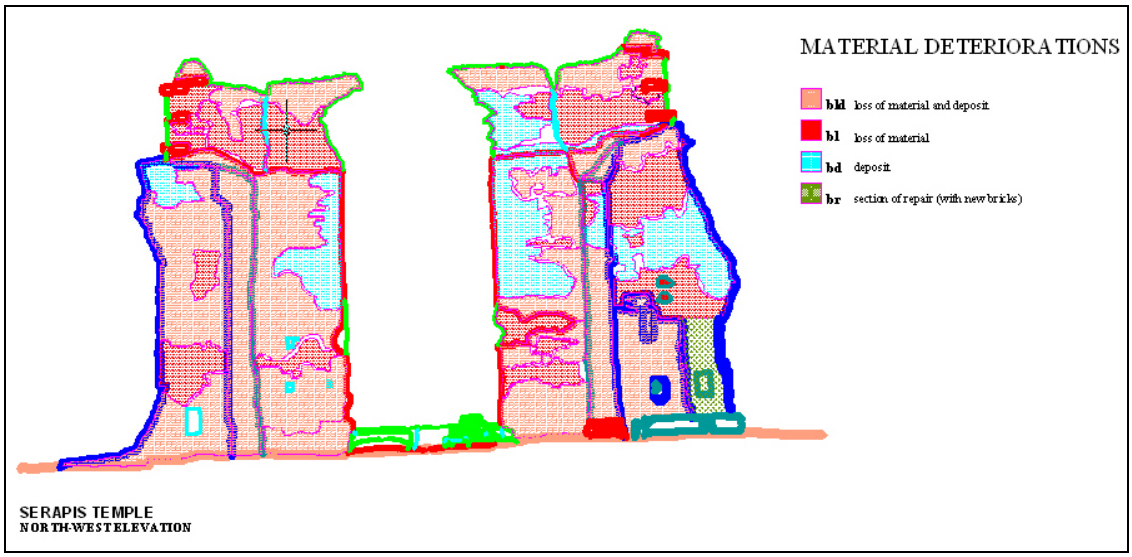

Figure 4. 99. Material deteriorations of north-west elevation of the Serapis Temple.

CHAPTER 5

CONCLUSION

In this study, basic physical, mineralogical, chemical and microstructural properties of the bricks and mortars used in the construction of the Serapis Temple have been determined in order to obtain information on their production technology and to describe the characteristics of compatible intervention materials that will be used in the conservation works of the temple. The general conclusions of the study are presented below.

Basic physical properties (density, porosity, and drying rate) of the original and intervention mortars and plasters used in the structure are similar and they are low dense and high porous materials. The compressive strengths of the original Roman and Byzantine Period mortars and plasters and their values of modulus of elasticity indicate that they can keep their functions as construction materials, and that they are compatible. The new mortars which were used as binder between the intervention bricks have lost their mechanical properties.

Pure lime was used in the preparation of the original Roman and Byzantine mortars. The amount of lime used in the preparation of the mortars is low (% 20-25 weight percent). Use of less amount of lime shows that it had good workability. The plasters which were used in the Byzantine period had been similarly prepared using little amount of lime (~ %30 weight percent). However, cement and lime were used as binder in the conservation works in the Serapis Temple carried out in 1940s. Particle size distributions of the aggregates used in the preparation of the Roman and Byzantine period mortars are similar. The aggregates with particle sizes greater than 1180μm formed the largest fraction of the total aggregates used in the mortars. Fine aggregates were used in the preparation of the plasters. Natural and artificial aggregates (crushed brick) used in the mortars and plasters have pozzolanic characteristics and contain high amount of silicon and low amount of aluminum and iron. Roman and Byzantine mortars and plasters are hydraulic due to the use of pozzolanic aggregates.

New mortars and plasters produced for the conservation work should have similar compositions to those of the original ones in order to keep the structure sound and durable.

Basic physical properties of the original and intervention bricks used in the structure are similar. All bricks have low apparent densities and high porosity values. The compressive strengths and modulus of elasticity values of the original Roman and Byzantine period mortars, bricks, and plasters and the intervention bricks are similar, and this shows that they are compatible.

The calcium poor clays were used as raw materials in the production of all bricks. Roman and intervention bricks are composed of mainly quartz (SiO_2), potassium feldspar ($KAl_2Si_2O_5(OH)_4$), sodium feldspars ($NaAlSi_3O_8$), biotite ($KMg_3AlSi_3O_{10}(OH)_2$). However, brick aggregates in mortars and plasters contain high amounts of amorphous substances originating from the use of high amounts of clay minerals in the production of the bricks. This may show that the bricks used as aggregates in the mortars and plasters were produced differently by using materials of high clay content other than the bricks used in the construction of the temples. All the bricks are mainly composed of a high amount of SiO_2, Al_2O_3 and moderate amount of Fe_2O_3, Na_2O and K_2O (Fig. 11). However, the amounts of Fe_2O_3 in bricks used in the construction are found to be higher than that of all bricks used in mortars and plasters.

The bricks used as aggregates in the mortars and plasters have good pozzolanicity, which is mainly a result of amorphous clay mineral dissociation products. On the other hand, the bricks used in buildings have poor pozzolanicity due to less amounts of amorphous materials. All bricks are little vitrified and don't contain high temperature products like mullite suggesting the low firing temperatures.

The results may indicate that the pozzolanic bricks were particularly chosen for the production of hydraulic mortars and plasters.

The bricks used in the production of new intervention brick-lime mortars and plasters must have a high amount of clay minerals and must be fired at low temperatures of 600 – 900 °C.

A high amount of soluble salts originating from the use of intervention mortars containing cement is one of the reasons of the powdering and crumbling of the bricks and mortars due to cyclic dissolution and crystallization of soluble salts. The soil dust and biological growth are the other causes of the deterioration in the bricks and mortars. Their sources should be controlled in order to prevent further deterioration.

REFERENCES

Adam Jean-Pierre, 1999. *Roman Buildings:Materials and Techniques*, (Routledge, an import of Taylor&Francis Book Ltd.), (ISBN 0-415-20866-1).

Airapetov D., 1986. *Architectural Materials Science*, Translated from the Russian by A.B. Kuznetsov, (Mir Publishers, Moscow), pp. 36-40.

Akman M. S., Güner A., Aksoy İ. H., 1986. "The History and Properties of Khorasan Mortar and Concrete"**,** Turkish and Islamic Science and Technology in the 16th Century, İTÜ Research Center of History of Science and Technology, İstanbul, Vol. I, pp.101-112.

Arnold A., 1983. "Determination of Saline Minerals from Monuments", *GP News Letter*, 4, pp.4-15.

Arseven Celal Esat, 1994. *İsis Sanat Ansiklopedisi*, Cilt: II, İstanbul, p.2410.

Atilla A.Nedim, Öztüre Nezih, 2001. *Parşömen; Gravürler ve Fotoğraflarla Bergama'da Değişim*, (Öztüre Holding Kültür Yayını).

Bakolas A., Biscontin G., Moropoulou A., Zendri E., 1998. "Characterization of structural Byzantine mortars by thermogravimetric analysis", *Thermochimica Acta*, **321**, p.151-160.

Baronio G., Binda L., 1997. "Study of the Puzolanicity of Some Bricks and Clays" *Construction and Building Materials*, volume 11, No.1, p.41-46.

Black C.A., 1965. *Methods of Soil Analysis*, Part 2, American Society of Agronomy, Madison, Wisconsin, USA.

Boynton R.S., 1980. *Chemistry and Technology of Lime and Limestone,* 2nd Edition, (John Wiley & Sons, New York).

Böke H., Akkurt S., 2003. "Ettringite Formation in Historic Bath Brick Lime Plasters", *Cement and Concrete Research*, Vol.33/9, pp.1457-1464.

Böke H., Akkurt S., İpekoğlu B., Uğurlu E., 2004. "Tarihi Yapıların Onarımlarında Kullanılacak Horasan Harç ve Sıvalardaki Puzolanik Malzemelerin Özelliklerinin Araştırılması", TÜBİTAK Projesi, Kod:1021025 (İÇTAG – I607).

Böke H., Saltık E.N., Güçhan Ş., Özgönül N., 1999. "Osmanlı Dönemi Yapılarında Kullanılan Horosan Sıvaların Özelliklerinin Belirlenmesi", AFP projesi, 98.02.01.08, ODTÜ, Ankara.

Cardiano P., Ioppolo S., Stefano C.D., Pettignano A., Sergi S., Piraino P., 2004. " Study and Characterization of the Ancient Bricks of Monastery of 'San Filippo di Fragalá' in Frazzanò (Sicily)", *Analytica Chimica Acta*, **519**, pp. 103-111.

Caron P., Lynch M.F., 1988. “Making Mud Plaster”, *APT Bulletin*, volume 4, pp.7-9.

Cowan Henry J., 1997. *The Master Builders*, (A Wiley-Interscience Publication, New York), ISBN 0-471-02740-5.

Cowper A., 1988. *Lime and Lime Mortars*, (Donhead Publishing Ltd, Dorset, first published in 1927 for the Building Research Station by HM Stationary Office, London).

Çizer Ö., 2005. “Investigation of Lime Mortar Characteristics for the Conservation of the Ottoman Baths in Seferihisar-Urla Region”, M.Sc. Thesis, İzmir Institute of Technology, İzmir.

Davey N., 1961. *Limes and Cements, and Mortar and Concrete*, in A History of Buildings Materials, (Phoenix House, London), pp. 97-127.

Davraz M., Gunduz L., 2005. “Engineering Properties of Amorphous Silica as a New Natural Pozzolan for Use in Concrete”, *Cement and Concrete Research*.

Degryse P., Elsen J., Waelkens M., 2002. “Study of ancient mortars from Sagalassos (TURKEY) in view of their conservation”, *Cement and Concrete Research*, **32**, pp. 1457–1463.

Deubner O., 1977. *Das Heiligtum der AlexandrinischenGottheiten in Pergamon genanat-Kızıl Avlu*, (Berlin), p.227.

Elsen J., Brutsaert A., Deckers M., Brulet R., 2004. “Microscopical study of ancient mortars from Tournai (Belgium)”, *Materials Characterization*, **53**, pp. 289-294.

Güleç A., Tulun T., 1996. “Studies of Old Mortars and Plasters from the Roman, Byzantine and Ottoman period of Anatolia”, *Architectural Science Review*, volume 39.

Güleç A., Tulun T., 1997. “Physico-Chemical and Petrographical Studies of Old Mortars and Plasters of Anatolia”, *Cement and Concrete Research*, Vol. 27, No.2, pp. 227–234.

Haga K., SHIBATA M, HIRONAGA M., TANAKA S., NAGASAKI S., 2002. “Silicate Anion Structural Change in Calcium Silicate Hydrate Gel on Dissolution of Hydrated Cement”, *Journal of NUCLEAR SCIENCE and TECHNOLOGY*, vol.39, No.5, p.540-547.

He C., Bjarne O., Emil M., 1995. “Puzolanic reactions of six principal clay minerals:Activation, Reactivity Assessments and Technological Effects”, *Cement and Concrete Research*, volume 28, No.8, p.1691-1702.

Holmes S., Wingate M., 1997. *Building with Lime*, (Intermediate Technology Publications, London).

Jedrzejevska H., 1981. “Ancient Mortars as Criterion in Analysis of Old Architecture”, in the Proceedings of Symposium on Mortars, Cements and Grouts Used in the Conservation of Historic Buildings, 1981, Rome, pp. 311-329.

Kemertaş Günay, 2000. “Anadolu’da Mısır Tanrılarına Yapılan Tapınaklar”, Yüksek Lisans Tezi, Trakya Üniversitesi-Sosyal Bilimler Enstitüsü, Edirne.

Krumnacher P.J., 2001. “Lime and Cement Technology: Transition from Traditional to Standardized Treatment Methods”, M.Sc. Thesis, Virginia Polytechnic Institute and State University, Blacksburg, Virgina.

Lea F.M., 1940. “Investigations on Pozzolanas”, Building Research, Technical Paper, No.27, pp.1-63.

Lee S., Youn J. K., Hi-Soo M., 1999. “Phase Transformation Sequence from Kaolinite to Mullite Investigated by an Energy-Filtering Transmission Electron Microscope”, *Journal of American Ceramic Society*, volume 10, 5, p.2841-2848.

Lopez-Arce P., Garcia-Guinea J., 2004. “Weathering traces in ancient bricks from historic buildings”, *Building and Environment*.

Luxan M.P., Madruga F., Saavedra J., 1989. “Rapid evaluation of pozzolanic activity of natural products by conductivity measurement”, *Cement and Concrete Research*, **19**, pp. 63-68.

Maravelaki-Kalaitzaki P., Bakolas A., Moropoulou A., 2002. “Physico-chemical study of Cretan ancient mortars”, *Cement and Concrete Research*, **2233**, pp. 1-11.

Massazza F., Pezzuoli M., 1981. “Some Teachings of a Roman Concrete Mortars, Cement and Grouts Used in the Conservation of Historic Buildings”, Proceedings of Symposium in Rome, pp.219-245.

Meir I.A., Freidin C., Gilead I., 2005. “Analysis of Byzantine mortars from the Negev Desert, Israel, and subsequent environmental and economic implications”, *Journal of Archaeological Science*, **32**, pp.767-773.

Middendorf B., Knöfel D., 1990. “Use of Old and Modern Analytical Methods for the Determination of Ancient Mortars in Northern Germany”, in the Proceedings of the 3rd Expert Meeting, Hamburg, NATO-CCMS Pilot Study on Conservation of Historic Brick Structures, Berlin, Germany, pp. 75-92.

Moorehead D.R., 1986. “Cementation by the Carbonation of Hydrated Lime”, *Cement and Concrete Research*, **16**, pp. 700-708.

Moropoulou A., Bakolas A., Bisbikou K., 2000. “Investigation of the technology of historic mortars”, *Journal of Cultural Heritage*, **1**, pp. 45-58.

Moropoulou A., Çakmak A.S., Biscontin G., Bakolas A., Zendri E., 2002. “Advanced Byzantine cement based composites resisting earthquake stresses: the crushed

brick/lime mortars of Justinian' s Hagia Sophia", *Construction and Building Materials*, **16**, pp. 543-552.

Moropoulou A., Polikreti K., Bakolas A., Michailidis P., 2003. "Correlation of physicochemical and mechanical properties of historical mortars and classification by multivariate statistics", *Cement and Concrete Research*, **33**, pp. 891–898.

Pearson G., 1992. *Conservation of Clay and Chalk Buildings*, (Donhead Publishing), ISBN: 1873394004.

Peter N., 1850. *Encylopedia of Architecture*, 2 volumes, (Fry & Co., New York).

Radt Wolfgang, 2002. *Pergamon, Antik Bir Kentin Tarihi ve Yapıları*, (Yapı Kredi Yayınları, İstanbul), pp. 198-207

Riccardi M.P., Duminuco P., Tomasi C., Ferloni P., 1998. "Thermal, microscopic and X-ray diffraction studies on some ancient mortars", *Thermochimica Acta*, 321, pp.207-214.

RILEM, 1980. "Tests Defining the Structure", *Materials and Construction*, 13, p. 73.

Rodriquez-Navarro C., Hansen E., Ginell W.S., 1998. "Calcium Hydroxide Crystal Evolution upon Ageing of Lime Putty", Journal of the American Ceramic Society, volume 81, pp.3032-3034.

Sánchez-Moral S., Luque L., Cañaveras J.C., Soler V., Garcia-Guinea J., Aparicio A., 2004. "Lime pozzolana mortars in Roman catacombs: composition, structures and restoration", *Cement and Concrete Research*.

Snell L.M., Snell B.G., 2000. "The Early Roots of Cement", Concrete International, volume 22, Issue 2, pp.83-85.

Sujeong L., Kim Y.J., Moon H.S., 1999. "Phase transformation sequence from kaolinite to mullite investigated by an energy-filtering transmission electron", J.Am. Ceram. Soc. 10, 2841-2848.

Teutonico J.M., 1988. *Porous Building Materials*, in A Laboratory Manual for Architectural Conservators, (ICCROM Publishing, Rome), pp. 35-68.

Trappmann R.S., 1970. "Tempel Der Agyptıschen Götter in Griechenland und an der Westküste Kleinasiens", Leiden.

Tunçoku S.S., 2001. "Characterization of Masonry Mortars Used in Some Anatolian Seljuk Monuments in Konya, Beyşehir and Akşehir", Ph.D. Thesis, METU, Ankara.

Uğurlu E., 2005. "Investigation of Horasan Plaster Characteristics of the Some Ottoman Baths in İzmir", Unpublished M.Sc. Thesis, İzmir Institute of Technology, İzmir.

WEB_1, 2005. Bergama Resimleri, 27/01/2005. http://www.konak.bel.tr/bergamaresim.htm.

WEB_2, 2004. The Venice Charter, 24/04/2005 http://www.international.icomos.org/e_venice.htm.

WEB_3, 2005. All in One, 25/06/2005. http://petrov.com.ua/Turkey/pages/Bergama_Red_Basilica.htm.

Wissowa G., Kroll W., Witte K., 1914. *Sarapis, Real Encylopadie*, (C.I-A, Stuttgart), pp.2394-2425.

APPENDIX A

BASIC PHYSICAL PROPERTIES OF BRICKS, MORTARS AND PLASTERS

Table A. 1. Density and porosity values of Roman bricks and Intervention bricks.

Sample	Dry weight (g)	Saturated weight (g)	Archimedes weight (g)	Porosity (%)	App. Density (g/cm^3)	Real Density (g/cm^3)
RB-1 a	114,42	139,04	68,67	34.99	1.63	2.50
RB-1 b	111,22	134,97	66,67	34.77	1.63	2.50
RB-1 c	104,66	126,98	63,05	34.91	1.64	2.52
RB-1 d	103,58	126,07	62,02	35.11	1.62	2.49
RB-1 ave.				34.95	1.63	2.50
RB-2 a	107.79	129.14	64.32	32.94	1.66	2.48
RB-2 b	127.03	151.71	76.13	32.65	1.68	2.50
RB-2 ave.				32.80	1.67	2.49
RB-3 a	150.50	178.30	89.22	31.21	1.69	2.46
RB-3 b	132.31	158.30	78.27	32.48	1.65	2.45
RB-3 ave.				31.84	1.67	2.45
IB-1 a	150.73	186.58	86.84	35.94	1.51	2.36
IB-1 b	146.12	180.22	85.96	36.18	1.55	2.43
IB-1 c	149.77	184.40	87.17	35.62	1.54	2.39
IB-1 d	135.43	167.99	80.40	37.17	1.55	2.46
IB-1 ave.				36.23	1.54	2.41
IB-2 a	111.93	139.48	66.06	37.52	1.52	2.44
IB-2 b	115.47	143.49	68.77	37.50	1.55	2.47
IB-2 c	83.11	103.33	48.63	36.97	1.52	2.41
IB-2 ave.				37.33	1.53	2.44

IB-3 a	102.02	125.48	59.98	35.82	1.56	2.43
IB-3 b	116.79	143.46	68.50	35.58	1.56	2.42
IB-3 c	106.19	130.08	61.61	34.89	1.55	2.38
IB-3 d	131.15	162.98	77.13	37.08	1.53	2.43
IB-3 e	125.41	153.67	72.77	34.93	1.55	2.38
IB-3 f	83.38	102.13	48.56	35.00	1.56	2.39
IB-3 ave.				35.55	1.55	2.41
IB-4 a	90.92	112.56	52.69	36.14	1.52	2.38
IB-4 b	85.38	102.45	47.22	30.91	1.55	2.24
IB-4 c	71.93	88.89	41.73	35.96	1.53	2.38
IB-4 ave.				34.34	1.53	2.33

Table A. 2. Density and porosity values of Roman, Byzantine and Intervention mortars.

Sample	**Dry weight (g)**	**Saturated weight (g)**	**Archimedes weight (g)**	**Porosity (%)**	**App. Density (g/cm^3)**	**Real Density (g/cm^3)**
RM-1 a	40.24	50.48	23.88	38.50	1.51	2.46
RM-1 b	112.20	141.36	66.47	38.94	1.50	2.45
RM-1 c	83.28	103.84	49.44	37.79	1.53	2.46
RM-1 d	128.37	160.92	75.90	38.29	1.51	2.45
RM-1 e	55.90	69.63	33.35	37.84	1.54	2.48
RM-1 ave.				38.27	1.52	2.46
RM-2 a	18.94	23.19	10.46	33.39	1.49	2.23
RM-2 b	19.33	23.62	10.86	33.62	1.51	2.28
RM-2 ave.				33.50	1.50	2.26
BM-1 a	94.23	115.97	57.32	37.07	1.61	2.55
BM-1 b	127.33	149.48	77.79	30.90	1.78	2.57
BM-1 ave.				33.98	1.69	2.56

IM-1 a	12.84	16.42	7.40	39.69	1.42	2.36
IM-1 b	15.23	19.42	8.79	39.42	1.43	2.36
IM-1 ave.				39.55	1.43	2.36
IM-2 a	34.23	42.35	20.24	36.73	1.55	2.45
IM-2 b	25.06	31.07	14.69	36.69	1.53	2.42
IM-2 ave.				36.71	1.54	2.43
IM-3 a	30.31	38.01	17.83	38.16	1.50	2.43
IM-3 b	16.05	20.44	9.22	39.13	1.43	2.35
IM-3 ave.				38.64	1.47	2.39
IM-4 a	20.14	24.70	11.81	35.38	1.56	2.42
IM-4 b	12.67	15.94	7.51	38.79	1.50	2.46
IM-4 ave.				37.08	1.53	2.44
IM-5	8.22	10.39	4.84	39.10	1.48	2.43
IM-6 a	10.83	13.36	6.30	35.84	1.53	2.39
IM-6 b	14.11	17.03	8.09	32.66	1.58	2.34
IM-6 ave.				34.25	1.56	2.37

Table A. 3. Density and porosity values of Byzantine plaster.

Sample	**Dry weight (g)**	**Saturated weight (g)**	**Archimedes weight (g)**	**Porosity (%)**	**App. Density (g/cm^3)**	**Real Density (g/cm^3)**
BP-1 a	67.69	91.00	41.02	46.64	1.35	2.54
BP-1 b	70.98	96.52	42.81	47.55	1.32	2.52
BP-1 c	60.23	82.31	36.32	48.01	1.31	2.52
BP-1 d	77.91	106.22	46.94	47.76	1.31	2.52
BP-1 e	88.61	120.73	53.59	47.84	1.32	2.53
BP-1 ave.				47.56	1.32	2.52

Table A. 4. Values of dry, saturated and wet weights of samples.

Sample	mdry	msat	mwet0	mwet1	mwet2	mwet3	mwet4	mwet5	mwet6	mwet7	mwet8	mwet9	mwet10	mwet11	mwet12
RB-1	114.42	139.04	138.52	137.88	137.57	137.06	136.55	135.28	133.81	132.28	125.99	118.06	116.62	116.09	115.94
RB-2	107.79	129.14	128.82	127.78	127.46	126.82	126.22	125	123.35	121.78	114.34	107.91	107.09	106.92	106.91
RB-3	150.50	179.07	179.07	178.1	177.81	177.28	176.84	175.57	173.95	172.13	164.46	153.5	151.49	150.79	150.62
IB-1	150.73	186.89	186.89	185.59	185.06	184.13	183.36	181.6	179.44	177.19	166.69	155.64	153.22	152.08	151.76
IB-2	111.93	139.48	139.08	137.96	137.48	137.08	136.57	135.39	133.87	132.25	124.38	115.26	113.43	112.62	112.41
IB-3	102.02	125.54	125.54	124.08	123.81	123.49	123.04	121.98	120.6	119.22	111.84	104.14	102.64	102.2	102.12
IB-4	85.38	102.45	102	101.32	100.97	100.48	99.98	98.81	97.45	95.99	90.36	87.3	86.35	85.86	85.74
RM-1	128.37	160.92	160.29	159.27	159.04	158.64	158.16	157.02	155.55	154	147.13	140.38	137.6	136.26	135.86
BM-1	127.33	149.48	148.55	147.82	147.34	146.9	146.46	145.43	144.07	142.7	136.64	131.82	130.36	129.75	129.6
IM-2	52.41	64.82	64.82	64.09	63.9	63.63	63.41	63.01	62.18	60.68	55.03	52.76			
BP-1	67.69	91.13	91.13	90.48	90.29	89.95	89.63	88.92	87.98	86.95	81.79	74.11	70.79	69.83	69.62

Table A. 5. Moisture content values of the samples (kg) at the time.

Sample	M1	M2	M3	M4	M5	M6	M7	M8	M9	M10
RB-1	0.000979	0.000953	0.000940	0.00092	0.000899	0.000847	0.000788	0.000725	0.00047	0.000148
RB-2	0.000985	0.000936	0.000921	0.000891	0.000863	0.000806	0.000729	0.000655	0.000307	0.000006
RB-3	0.001000	0.000966	0.000956	0.000937	0.000922	0.000877	0.000821	0.000757	0.000489	0.000105
IB-1	0.001000	0.000964	0.000949	0.000924	0.000902	0.000854	0.000794	0.000732	0.000441	0.000136
IB-2	0.000985	0.000945	0.000927	0.000913	0.000894	0.000852	0.000796	0.000738	0.000452	0.000121
IB-3	0.001000	0.000938	0.000926	0.000913	0.000894	0.000849	0.00079	0.000731	0.000418	0.000090
IB-4	0.000974	0.000934	0.000913	0.000885	0.000855	0.000787	0.000707	0.000622	0.000292	0.000112
RM-1	0.000981	0.000949	0.000942	0.00093	0.000915	0.00088	0.000835	0.000787	0.000576	0.000369
BM-1	0.000958	0.000925	0.000903	0.000884	0.000864	0.000817	0.000756	0.000694	0.00042	0.000203
IM-2	0.001000	0.000941	0.000926	0.000904	0.000886	0.000854	0.000787	0.000666	0.000211	0.000028
BP-1	0.001000	0.000972	0.000964	0.00095	0.000936	0.000906	0.000866	0.000822	0.000602	0.000274

Table A. 6. Density of flow rate (kg / m^2 . s) values.

	Time (s)								
	0	900	1800	3600	5400	9000	16200	25200	81900
	RATE (g1)	**RATE (g 2)**	**RATE (g3)**	**RATE (g4)**	**RATE (g5)**	**RATE (g6)**	**RATE (g7)**	**RATE (g8)**	**RATE (g9)**
	(g 1=M / A x t)								
Samples									
RB-1	0	0.00011	0.00005	0.00003	0.00002	0.00001	0.000005	0.000003	0.0000006
RB-2	0	0.00011	0.00006	0.00003	0.00002	0.00001	0.000005	0.000003	0.0000004
RB-3	0	0.00009	0.00004	0.00002	0.00001	0.00001	0.000004	0.000002	0.0000005
IB-1	0	0.00009	0.00004	0.00002	0.00001	0.00001	0.000004	0.000002	0.0000004
IB-2	0	0.00011	0.00005	0.00003	0.00002	0.00001	0.000005	0.000003	0.0000006
IB-3	0	0.00011	0.00005	0.00003	0.00002	0.00001	0.000005	0.000003	0.0000005
IB-4	0	0.00012	0.00006	0.00003	0.00002	0.00001	0.000005	0.000003	0.0000004
RM-1	0	0.00009	0.00005	0.00002	0.00001	0.00001	0.000005	0.000003	0.0000006
BM-1	0	0.00010	0.00005	0.00002	0.00002	0.00001	0.000004	0.000003	0.0000005
IM-2	0	0.00015	0.00007	0.00003	0.00002	0.00001			
BP-1	0	0.00013	0.00007	0.00003	0.00002	0.00001	0.000007	0.000004	0.0000009

APPENDIX B

BASIC MECHANICAL PROPERTIES OF BRICKS, MORTARS AND PLASTER

Table B. 1. Uniaxial compressive strength values.

Sample	Length (mm)	Width (mm)	A (mm^2)	P (kN)	Compressive strength (MPa)
RB-1 a	41.86	38.97	1631.3	8.97	5.5
RB-3 a	44	41	1804	10.97	6.1
IB-1 c	51.2	49.7	2544.6	24.76	9.7
IB-2 c	47.62	34.98	1665.7	6.63	4
IB-3 a	45	38	1710	15.03	8.8
IB-4 a	33.75	41.81	1411.1	8.15	5.8
RM-1 d	47.3	40.01	1892.5	12.44	6.6
BM-1 b	47	44	2068	13.29	6.4
BP-1 e	48.81	38.52	1880.2	6.28	3.3
IM-2	59	38.55	2274.45	0.89	0.4

Table B. 2. Modulus of elasticity values of bricks.

Sample	Stroke (mm)	Load (kN)	ΔStroke (mm)	ΔLoad (kN)	ΔLoad/ΔStroke (kN/ mm)	Modulus of elasticity (MPa)
RB-1 a	0.0150	0.00375	0.0039	0.00181	0.4641	464.1
	0.0111	0.00194				
RB-3 a	0.0497	0.00409	0.0048	0.00203	0.4229	422.9
	0.0449	0.00206				
IB-1 c	0.04208	0.009	0.00341	0.00228	0.6686	668.6
	0.03867	0.00672				
IB-2 c	0.01813	0.0036	0.00112	0.00034	0.3036	303.6
	0.01701	0.00326				
IB-3 a	0.01489	0.00412	0.0062	0.00307	0.4952	495.2
	0.00869	0.00105				
IB-4 a	0.02162	0.00511	0.00092	0.00044	0.4783	478.3
	0.0207	0.00467				

Table B. 3. Modulus of elasticity values of mortars and plaster.

Sample	Stroke (mm)	Load (kN)	ΔStroke (mm)	ΔLoad (kN)	ΔLoad/ΔStroke (kN/ mm)	Modulus of elasticity (MPa)
RM-1 d	0.02263	0.00481	0.00314	0.00198	0.6306	630.6
	0.01949	0.00283				
BM-1 b	0.03732	0.00332	0.00294	0.00126	0.4286	428.6
	0.03438	0.00206				
IM-2	0.13597	0.00023	0.00809	0.00004	0.00494	4.94
	0.12788	0.00019				
BP-1 e	0.03005	0.00178	0.00288	0.00066	0.2292	229.2
	0.02717	0.00112				

APPENDIX C

LIME/AGGREGATE RATIOS OF MORTARS AND PLASTER AND PARTICLE SIZE DISTRIBUTIONS OF AGGREGATES

Table C. 1. Lime/aggregate ratios and particle size distributions of aggregates used in mortars and plaster.

Sample	Lime (%)	Aggregate (%)	Aggregate size distribution (%)					
			≥1180µm	500µm	250µm	125µm	53µm	<53µm
RM - 1	81.55	18.45	37.73	31.59	8.57	2.37	1.17	0.53
RM - 2	80.19	19.81	37.89	28.27	9.30	3.14	1.79	0.74
BM - 1	82.45	17.55	41.62	27.95	8.72	2.73	1.34	0.58
IM - 1	83.17	16.83	15.41	25.19	26.36	14.12	2.21	0.44
IM - 2	86.07	13.93	20.99	26.96	25.96	10.32	1.78	0.30
IM - 3	87.58	12.42	6.17	27.13	36.11	15.74	2.58	0.45
IM - 4	77.04	22.96	19.73	22.95	21.49	11.42	1.84	0.37
IM - 5	85.34	14.66	15.27	25.53	27.05	14.62	2.50	0.63
IM - 6	78.75	21.25	14.12	23.87	24.98	13.41	2.32	0.60
BP - 1	72.27	27.73	43.93	13.61	7.28	4.45	2.59	1.21

APPENDIX D

POZZOLANIC ACTIVITY OF BRICKS AND AGGREGATES

Table D. 1. Pozzolanic activity measurements of Roman and intervention bricks.

Samples	Electrical conductivity of $Ca(OH)_2$ (mS/cm)	Electrical conductivity of $Ca(OH)_2$ mixed with with brick (mS/cm)	Difference in electrical conductivity (mS/cm)
RB-1	8.17	7.56	0.61
RB-2	8.13	8.10	0.03
RB-3	8.20	8.13	0.07
IB-1	8.22	7.96	0.26
IB-2	8.22	7.93	0.29
IB-3	8.16	7.80	0.36
IB-4	8.16	8.06	0.10

Table D. 2. Pozzolanic activity measurements of fine aggregates used in mortars and plaster.

Samples	Electrical conductivity of $Ca(OH)_2$ (mS/cm)	Electrical conductivity of $Ca(OH)_2$ mixed with fine aggregate (mS/cm)	Difference in electrical conductivity (mS/cm)
RM-1	8.11	2.08	6.03
RM-2	7.96	0.26	7.70
BM-1	8.18	0.464	7.72
IM-1	8.05	5.96	2.09
IM-2	8.20	5.45	2.75
IM-3	8.00	5.62	2.38
IM-4	8.13	4.93	3.20
IM-5	8.12	6.38	1.74
IM-6	8.06	5.55	2.51
BP-1	8.24	2.34	5.90

APPENDIX E

CHEMICAL COMPOSITIONS OF BRICKS AND AGGREGATES

Table E. 1. Elemental compositions of Roman and intervention bricks

SAMPLES	Fe2O3	Na2O	MgO	Al2O3	SiO2	K2O	CaO
RB-1	11,4±2,3	2,4±0,3	3,9±0,1	17,6±0,3	57,5±2,7	3,3±0,5	3,8±0,4
RB-2	9,7±1,5	3,4±0,4	3,1±0,5	17,8±0,1	58,1±1,3	3,6±0,5	4,4±0,7
RB-3	11,2±2,4	3,0±0,4	4,0±0,5	17,0±0,4	56,0±2,1	4,6±0,4	4,2±0,4
IB-1	9,8±1,5	1,9±0,4	2,6±0,3	20,4±0,3	59,7±1,8	3,7±0,6	2,0±0,1
IB-2	8,1±0,8	1,9±0,2	2,3±0,1	19,3±0,7	63,0±2,0	3,5±0,2	1,9±0,3
IB-3	11,3±2,0	2,2±0,3	2,8±0,3	20,9±0,2	57,3±2,0	3,9±0,4	1,6±0,1
IB-4	10,6±1,7	2,3±0,4	2,5±0,2	20,5±0,5	58,2±2,1	4,1±0,3	2,0±0,3

Table E. 2. Elemental compositions of fine aggregates used in the mortars and plaster.

SAMPLES	Fe2O3	Na2O	MgO	Al2O3	SiO2	K2O	TiO2
RM-1	9,1±2,3	2,1±0,2	1,4±0,2	5,6±0,1	80,1±2,5	1,0±0,1	0,8±0,5
BM-1	6,8±1,6	1,3±0,3	1,9±0,2	6,6±0,2	81,8±2,1	1,0±0,1	0,7±0,3
IM - 4	15,0±1,6	2,3±0,5	2,6±0,4	11,2±0,8	66,5±2,2	1,5±0,3	0,9±0,2
BP-1	8,5±1,4	1,5±0,1	2,4±0,1	7,6±0,4	77,4±0,8	1,5±0,2	1,1±0,2

APPENDIX F

SOLUBLE SALTS IN BRICKS, MORTARS AND PLASTER

Table F. 1. Percent soluble salts in Roman and intervention bricks.

Sample	Conductivity (µS/cm)	Salinity (%)
RB-2	398	1.27
RB-3	143	0.46
IB-1	214	0.68
IB-3	146	0.47
IB-4	256	0.82

Table F. 2. Percent soluble salts in mortars and plaster.

Sample	Conductivity (µS/cm)	Salinity (%)
RM-2	245	0.78
BM-1	123	0.39
IM-3	279	0.89
IM-4	217	0.69
BP-1	86	0.28

Table F. 3. Anion parts of soluble salts in bricks.

Sample	Soluble salts				
	SO_4^{-2}	Cl^-	NO_3^-	CO_3^{-2}	PO_4^{-3}
RB-2	-	+	-	-	-
RB-3	-	+	-	-	-
IB-1	-	+	-	-	-
IB-3	-	-	-	-	-
IB-4	-	+	-	-	-

Table F. 4. Anion parts of soluble salts in mortars and plaster.

Sample	Soluble salts				
	SO_4^{-2}	Cl^-	NO_3^-	CO_3^{-2}	PO_4^{-3}
RM-2	-	-	-	-	-
BM-1	-	-	-	-	-
IM-3	-	-	-	-	-
IM-4	-	-	-	-	-
BP-1	-	-	-	-	-